T.R.
VAN YUZUNCU YIL UNIVERSITY
INSTITUTE OF NATURAL AND APPLIED SCIENCES
DEPARTMENT OF PHYSICS

SOME PHYSICAL PROPERTIES OF $LiPaO_3$ COMPOUND: AN AB INITIO STUDY

M.Sc. THESIS

PREPARED BY :Khalat Ezzulddin HUSSEIN
SUPERVISOR :Assoc. Prof. Dr. Emel KILIT DOĞAN

VAN-2022

T.R.
VAN YUZUNCU YIL UNIVERSITY
INSTITUTE OF NATURAL AND APPLIED SCIENCES
DEPARTMENT OF PHYSICS

SOME PHYSICAL PROPERTIES OF $LiPaO_3$ COMPOUND: AN AB INITIO STUDY

M.Sc. THESIS

PREPARED BY: Khalat Ezzulddin HUSSEIN

VAN-2022

ACCEPTANCE and APPROVAL PAGE

This thesis entitled "SOME PHYSICAL PROPERTIES OF $LiPaO_3$ COMPOUND: AN AB INITIO STUDY" presented by Khalat Ezzulddin HUSSEIN under supervision of Assoc. Prof. Dr. Emel KILIT DOGAN in the department of Physics has been accepted as a M. Sc. thesis according to Legislations of Graduate Higher Education on 06/06/2022 with unanimity / majority of votes members of jury.

Chair: Doç. Dr. Hakan GÜNDOĞMUŞ	Signature:
Member: Doç. Dr. Sinem ERDEN GÜLEBAĞLAN	Signature:
Member: Doç Dr. Emel KİLİT DOĞAN	Signature:

This thesis has been approved by the committee of The Institute of Natural and Applied Science on ..……../........../…..….. with decision number ....

Signature
……………..………..
Director of Institute

THESIS STATEMENT

All information presented in the thesis obtained in the frame of ethical behavior and academic rules. In addition, all kinds of information that does not belong to me have been cited appropriately in the thesis prepared by the thesis writing rules.

Khalat Ezzulddin HUSSEIN

ABSTRACT

SOME PHYSICAL PROPERTIES OF $LiPaO_3$ COMPOUND: AN AB INITIO STUDY

HUSSEIN, Khalat Ezzulddin
M.Sc. Thesis, Department of Physics
Supervisor: Assoc. Prof. Dr. Emel KILIT DOĞAN
June 2022, 115 pages

In this study, the structural, electronic and elastic properties of $LiPaO_3$ crystal have been investigated by using ABINIT computer programme. ABINIT programme is based on the Density Functional Theory. Density Functional Theory has some approximations to calculate the pseudopotentials such as Generalized Gradient Approximation and Local Density Approximation. Here, both approximations were used for all calculations in order to compare all our results under these approximations.

In order to do those calculations, first we made the cut-off energy and k-point optimizations. Afterwards we performed the volume optimization. In this level we investigated the structural properties of $LiPaO_3$ crystal. We also obtained the sketch of unit cell, bonds and the bond lengths by using VESTA computer programme. Then, we investigated the electronic structure of $LiPaO_3$ crystal by calculating and plotting the electronic band structure, the density of states of $LiPaO_3$ and the partial density of states. We also investigated the optic properties of $LiPaO_3$ crystal. Last of all, we focused on the elastic properties of $LiPaO_3$ and we noticed that this crystal is mechanically stable and very elastic material.

We believe that this thesis study will help to the researchers' future studies on $LiPaO_3$ crystal.

Keywords: ABINIT, Density functional theory, Density of states, Elastic properties, Electronic properties, $LiPaO_3$, Optic properties.

ÖZET

$LiPaO_3$ BİLEŞİĞİNİN BAZI FİZİKSEL ÖZELLİKLERİ: BİR TEMEL İLKELER ÇALIŞMASI

HUSSEIN, Khalat Ezzulddin
Yüksek Lisans Tezi, Fizik Anabilim Dalı
Tez Danışmanı: Doç. Dr. Emel KİLİT DOĞAN
June 2022, 115 sayfa

Bu çalışmada, ABINIT bilgisayar programı kullanılarak $LiPaO_3$ kristalinin yapısal, elektronik ve elastik özellikleri araştırılmıştır. ABINIT programı, Yoğunluk Fonksiyonel Teorisine dayanmaktadır. Yoğunluk Fonksiyonel Teorisi, psödopotansiyelleri hesaplamak için Genelleştirilmiş Gradyan Yaklaşımı ve Yerel Yoğunluk Yaklaşımı gibi bazı yaklaşımlara sahiptir. Burada, tüm sonuçlarımızı bu yaklaşımlar altında karşılaştırmak için tüm hesaplamalar için her iki yaklaşım da kullanılmıştır.

Bu hesaplamaları yapabilmek için öncelikle kesme enerjisi ve k noktası optimizasyonlarını yaptık. Daha sonra hacim optimizasyonunu gerçekleştirdik. Bu seviyede $LiPaO_3$ kristalinin yapısal özelliklerini araştırdık. VESTA bilgisayar programını kullanarak birim hücre, bağ ve bağ uzunluklarının taslağını da elde ettik. Daha sonra, $LiPaO_3$'ün elektronik bant yapısını, durum yoğunluğunu ve kısmi durum yoğunluklarını hesaplayıp çizerek $LiPaO_3$ kristalinin elektronik yapısını araştırdık. Ayrıca $LiPaO_3$ kristalinin optik özelliklerini araştırdık. Son olarak, $LiPaO_3$'ün elastik özelliklerine odaklandık ve bu kristalin mekanik olarak kararlı ve çok elastik bir malzeme olduğunu fark ettik.

Bu tez çalışmasının araştırmacıların $LiPaO_3$ kristali ile ilgili gelecekteki çalışmalarına yardımcı olacağına inanıyoruz.

Anahtar kelimeler: ABINIT, Durum yoğunluğu, Elastik özellikler, Elektronik özellikler, $LiPaO_3$, Optik özellikler, Yoğunluk fonksiyoneli teorisi.

ACKNOWLEDGMENT

In the present world of competition there is a race of existence in which those are having will to come forward succeed. Project is like a bridge between theoretical and practical working. With this willing, I joined this kind of theoretical project.

First of all, I would like to thank the supreme power the almighty God who is obviously the one has always guided me to work on the right path of life and letting me through all the difficulties, without his grace this project could not become a reality.

The research has been given to me as a part of the curriculum in 2 years master degree in solid state. I have tried my best to present this information as clearly as possible using basic terms that I hope will be comprehended by the widest spectrum of researchers, analysts and students for future studies.

I have completed this study under the able guidance and supervision of (Assoc. Prof. Dr. Emel KILIT DOĞAN), I would like to acknowledge and giving my warmest thanks to my honorable dear Assoc. Prof. Dr. Emel for her supervision throughout the working time who made this work possible, she helped me a lot sharing her invaluable knowledge with me and carried me through all the stages of writing my project. I would also like to give special thanks to my husband (Amanj) who has always helped me to complete this project, my children (Taman and Meer) and my family as a whole for their continuous support and understanding when undertaking my research and writing my project. their prayer for me was what sustained me this far. Finally, I am highly obliged in taking the opportunity to sincerely thanks to all the staff members of the department of physics for their generous attitude and friendly behaviors. At last, but not the least I am thankful to all my teachers and friends who have been always helping and encouraging me throughout the year. I have no valuable words to express my thanks, but my heart is still full of the favors received from every person.

2022
Khalat Ezzulddin HUSSEİN

TABLE OF CONTENTS

Page

ABSTRACT i
ÖZET ………………………………………………………………………..………....iii
ACKNOWLEDGMENT .... ……..…v
TABLE OF CONTENTS vii
LIST OF TABLES xi
LIST OF FIGURES xiii
SYMBOLS AND ABBREVIATIONS xvii
1. INTRODUCTION 1
2. LITERATURE REVIEW 3
3. THEORETICAL BACKGROUND 7
    3.1. Classification of Solids 7
    3.2. Crystal Structure 8
    3.3. Types of Crystal Structures and Bravais Lattice 9
        3.3.1. One dimensional crystal 9
        3.3.2. Two dimensional crystal 10
        3.3.3. Three dimentional crystal 11
    3.4. Diffraction in Crystals 13
    3.5. Bragg’s Law of X-ray Diffraction 15
    3.6. Receprocal Lattice 16
    3.7. Brilllouin Zone 18
    3.8. Miller Indices 20
    3.9. Band Structure in Crystals 23
        3.9.1. Transition from atomic levels to bands 23
        3.9.2. Energy band formation in solids 24
    3.10. Optical Properties 26
        3.10.1. Optical constants 27
    3.11. Elastic Properties 30

Page

3.11.1. Elastic constants 31

3.12. Perovskite Definition 34

3.12.1. Properties of perovskite mineral.. 35

3.13. The Multi-Particle Problem 36

3.13.1. Born-Oppenheimer (adiabatic) approach 39

3.13.2. Hartree method and self-consistent field.. 40

3.13.3. Hartee-Fock method 41

3.13.4. Slater determinant and change energy.. 43

3.13.5. Correlation energy.. 44

3.13.6. Thomas-Fermi theory and dirac change energy...................................... 45

3.13.7. Density functional theory (DFT).. 46

3.13.8. Hohenberg-Kohn’s theorems 47

3.13.9. Kohn-Sham equations 49

3.13.10. Local density approximation (LDA) 51

3.13.11. Generalized gradient approach (GGA).. 52

3.13.12. Pseudopotential method 53

4. RESULTS AND DISSCUSION.. 55

4.1. LiPaO$_3$ Crystal 55

4.2. Structural Properties of LiPaO$_3$ Crystal 55

4.2.1. Cut-off energy.. 56

4.2.2. Number of k-points.. 57

4.2.3. Volume optimization 59

4.2.4. Lattice parameters of LiPaO$_3$ crystal 63

4.2.5. Unit cell of LiPaO$_3$ crystal.. 65

4.3. The Electronic Properties of LiPaO$_3$ Crystal 65

4.3.1. Electronic band structure 66

4.3.2. Density of states (DOS) 69

4.3.3. Partial density of states (PDOS) 71

4.4. The Optical Properties of LiPaO$_3$ Crystal.. 74

Page

4.5. The Elastic Properties of $LiPaO_3$ Crystal 78

5. CONCLUSION 81

REFERENCES 83

EXTENDED TURKISH SUMMARY 89

CURRICULUM VITAE.. 115

LIST OF TABLES

Table **Pages**

Table 3.1. The 2D five crystal system and their Bravais lattices (Oura et al., 2003; Galsin, 2019). 10

Table 3.2. The seven crystal systems and their Bravais lattices (Ott-Borchardt, 1995; Hammond, 2015).. 12

Table 4.1. The calculated elastic stiffness constants of $LiPaO_3$ under GGA and LDA…78

Table 4.2. Some elastic modulus and constants of LiPaO3 crystal under GGA and LDA approximations 79

LIST OF FIGURES

Figure **Page**

Figure 3.1. Atomic structure of each type of Monocrystalline (single crystalline), Polycrystalline and Amorphous solid according to the theory periodicity (Alajlani et al., 2018) 8

Figure 3.2. Two-dimensional crystal lattice which contains space lattice and basis (Mello and Cavalcanti, 2020).. 8

Figure 3.3. Five types of planar 2D lattices (Grundmann, 2016; Oura et al., 2003). 11

Figure 3.4. 14 Bravais lattices classified according to their lattice system (Solyom, 2007; Reventos et al., 2012; Hammond, 2015). .... …13

Figure 3.5. Diffraction patterns of X-rays from crystal planes in accordance with Bragg's law (Tilley, 2006; Nasir, 2018).. 15

Figure 3.6. Brillouin zone for the different type of two-dimensional reciprocal lattice (a) rectangular lattice (b) hexagonal lattice (Grenier and Ballou, 2012)…………………………………………………………………..18

Figure 3.7. Brillouin zones of the square lattice in two dimensions are seen here (Doitpoms, 2021) 19

Figure 3.8. Semiconductor band structure (Valence and Conduction bands, 2021)……25

Figure 3.9. Schematic conduction band (CB) and Valence band (VB) for (a) Metals (b) Insulators (c) Semiconductors (Rioult, 2015). 26

Figure 3.10. ABX_3 perovskite structure (Luo and Daoud, 2015). 34

Figure 3.11. Electron quantum configuration of lithium (Li).. 43

Figure 3.12. Representation scheme of the Hohenberg and Kohn theorem. 48

Figure 3.13. Represent the Kohn and Sham approach which is H-K theorem applied to the non-interacting problems. 50

Figure 3.14. Schematic illustration of the pseudo wave function, pseudopotential with the all-electron wave function, and all-electron potential.. 54

Figure 4.1. The change in total energy with respect to cut-off energy for $LiPaO_3$ under GGA 56

Figure **Page**

Figure 4.2. The change in total energy with respect to cut-off energy for $LiPaO_3$ under LDA 57

Figure 4.3. Total energy with respect to Monkhorst-Pack grids under GGA approximation for $LiPaO_3$.. 58

Figure 4.4. Total energy with respect to Monkhorst-Pack grids under LDA approximation for $LiPaO_3$.. 59

Figure 4.5. Total energy vs. volume graph of $LiPaO_3$ crystal under GGA.. 60

Figure 4.6. Total energy vs. volume graph of $LiPaO_3$ crystal under LDA…………….60

Figure 4.7. Total energy vs. pressure graph of $LiPaO_3$ crystal under GGA. 61

Figure 4.8. Total energy vs. pressure graph of $LiPaO_3$ crystal under LDA.. 62

Figure 4.9. Pressure vs. volume graph of $LiPaO_3$ crystal under GGA.. 62

Figure 4.10. Pressure vs. volume graph of $LiPaO_3$ crystal under LDA.. 63

Figure 4.11. Total energy vs. lattice parameter graph of $LiPaO_3$ crystal under GGA.. . 64

Figure 4.12. Total energy vs. lattice parameter graph of $LiPaO_3$ crystal under LDA. ... 64

Figure 4.13. The unit cell of the $LiPaO_3$ crystal (Momma and Izumi, 2011)................ 65

Figure 4.14. Electronic band structure of $LiPaO_3$ under GGA. The red line is the fermi energy level.. 66

Figure 4.15. Electronic band structure of $LiPaO_3$ under GGA. The red line is the fermi energy level.. 67

Figure 4.16. Electronic band structure of $LiPaO_3$ between -4 and 6 eV energy values under GGA.. 68

Figure 4.17. Electronic band structure of $LiPaO_3$ between -4 and 6 eV energy values under LDA.. 69

Figure 4.18. Density of states graph of LiPaO3 crystal under GGA …………………...70

Figure 4.19. Density of states graph of $LiPaO_3$ crystal under LDA……………………70

Figure **Page**

Figure 4.20. The partial density of states (PDOS) graph of Li atom under (a) GGA and (b) LDA approximations.. 71

Figure 4.21. The partial density of states (PDOS) graph of Pa atom under (a) GGA and (b) LDA approximations.. 72

Figure 4.22. The partial density of states (PDOS) graph of O(1) atom under (a) GGA (b) LDA, O(2) atom under (c) GGA, (d) LDA, O(3) atom under (e)GGA and (f) LDA approximations.. 73

Figure 4.23. (a) The real and (b) the imaginal components of complex dielectric function of $LiPaO_3$ crystal under GGA.. 74

Figure 4.24. (a) The real and (b) the imaginal components of complex dielectric function of $LiPaO_3$ crystal under LDA... 75

Figure 4.25. (a) Reflectivity, (b) Refractive index, (c) Extinction coefficient, (d) Effective number of valence electrons per unit cell, (e) Energy loss function for surface and (f) Energy loss function for volume of $LiPaO_3$ crystal under GGA.. 76

Figure 4.26. (a) Reflectivity, (b) Refractive index, (c) Extinction coefficient, (d) Effective number of valence electrons per unit cell, (e) Energy loss function for surface and (f) Energy loss function for volume of $LiPaO_3$ crystal under GGA.. 77

SYMBOLS AND ABBREVIATIONS

Some symbols and abbreviations used in this study are presented below, along with descriptions.

Symbols	**Description**
Li	Lithium
Pa	Protactinium
O	Oxygen
$\mathbf{E_{cut}}$	Cut-off energy
$\mathbf{E_g}$	Energy Gap
$\mathbf{E_{HF}}$	Hartree-Fock energy
$\mathbf{E_0}$	Ground state energy
$\mathbf{E_f}$	Fermi energy
$\mathbf{C_{ij}}$	Elastic stiffness constant
ABINIT	Program using pseudo-potential method based on density functional theory
DFT	Density functional theory
DOS	Density of states
LDA	Local density approximation
GGA	General gradient approximation
$\mathbf{LiPaO_3}$	Lithium Protactinium Oxide

1. INTRODUCTION

There are many theories related to physical science and engineering, during many decades, this information that we know about the materials and the ways to describe, analyze and controlling the properties of them is due to many years of research, keep looking into the fields to get a perfect result and understandable reasons (Kohanoff, 2006).

We have taken a crucial decision to restrict the scope of DFT, the idea of this is the energy is a system can show in an electron probability (Atkins and Friedman, 2005).

Because of the success of the DFT study, it quickly became a significant and effective approach for many materials modeling in the fields of physics, chemistry, solid state, material science and in many engineering areas. Understanding and regulating the physical characteristics of material at the level of individual atoms and molecules is critical to scientific and technological improvement in many domains of physical sciences and engineering. Density functional theory is a remarkably effective way to discovering solutions to the Schrodinger equation, which describes the quantum behavior of atoms and molecules in real frameworks (Sholl and Steckel, 2009).

As we know from the periodic table, 90% are stable and as a reason of high efficiency and high absorption coefficient, they can be used in a perovskite-based structure (Roque-Malherbe, 2010), perovskite materials are those materials which are easy to use and give an excellent result properties (Zhou and Wang, 2020) and it can be used in many application areas such as material science, chemistry and advanced physics (Tejuca and Fierro, 1993).

In this work, we have used a perovskite-based oxide which is lithium protactinium oxide, $LiPaO_3$, to understanding some properties like structure, electronic, elastic and optical properties based DFT method using Generalized Gradient Approximation (GGA) and Localized Density Approximations (LDA) within the help of ABINIT software program. We also sketched the unit cell structure by using the programme VESTA. Additionally, by using this programme, we calculated the bonds and bond lengths of $LiPaO_3$.

We have given all our results on $LiPaO_3$ with tables, graphs and detailed discussions. We also compared all of the results obtained by LDA and GGA and we saw almost all of them in a good agreement with each other. This is the first study in the literature on $LiPaO_3$, so, the results could not be compared with the literature. Since all the results are compatible within this study, I believe that this study will be very useful for the future studies on the $LiPaO_3$ crystal.

2. LITERATURE REVIEW

To predict the physical properties of the materials, researchers use density functional theory as a way to achieving and understanding well-known the behavior and structure of the materials, this approach is an excellent way to guess the characteristics of materials without doing any experimental work.

Rahaman et al. (2019) have worked on a new compound material which is $LiCuBiO_4$, they have investigated mechanical, electronic, optical and thermodynamic properties by DFT calculations using GGA method. The structural parameters with compare to experimental results are in good geometry. Elastic properties show the mechanical stability of that compound and about the optical properties the LCBO is selected as an optoelectronic device especially in the visible and ultraviolet region.

Wang et al. (2019) have worked on $LiBeF_3$ to calculate thermodynamic and optical properties by DFT, as it is clear in their work, above 260 K, the $LiBeF_3$ has a good structural stabilization and the calculated electronic properties has an indirect band gap that can be used in optical lithography steppers in semiconductor industry.

Benmhidi et al. (2016) reported the electronic structure, elastic and transport properties for $LiBeF_3$ cubic compound Fluoroperovskite structure investigated for the first time which is based on DFT study within LDA. The electronic structure of that compound has indirect band gap which has a good arrangement with the theoretical principles.

Javid et al. (2018) investigated structural, electronic and optical properties for $LiNbO_3$ (lithium niobate) with direct band gap DFT study using LDA and GGA. As a result, the calculated parameters were very close to the experimental results which have a widely use in the optoelectronics and the optical properties of $LiNbO_3$ that is very important material for holographic memories.

Cabuk. (2010) has investigated electronic and optical properties for two kind of perovskite materials which are $LiNbO_3$ and $LiTaO_3$ ferroelectrics with DFT study using LDA. They had indirect band gap structure, LiNbO3 is 3.39 eV and LiTaO3 is 3.84 eV which is 15% and 14% is lower than the experimental values that the experimental values are 4.0

eV and 3.93 eV, respectively, at standard temperature. The symmetry of both structure is the same and the chemical bond of them is covalent bond.

Su et al. (2021) examined two different perovskite structures which are $LiNbO_3$ and $LiSbO_3$ under high pressure with DFT theory, as a result, the mechanical and ferroelectric properties have improved under high pressure, it means that at high pressure the ferroelectric stability is promoted for both of those perovskite materials. The elastic coefficient for both of them becomes larger by increasing pressure and finally it is noticed that Ln-$LiSbO_3$ is a high efficiency ferroelectric photocatalytic material that absorbs ultraviolet light.

Zhou and Zhao. (2016) focused to understand the relation between microstructure and composition of four perovskite materials ($LiBiO_3$, $NaBiO_3$, $KBiO_3$ and $AgBiO_3$). Their structural, electronic and optical properties were investigated. In their present work, they showed that the compounds have the same structural compositions. The structure and optical properties are close with the experimental data. The micro-structural properties lead to stronger interaction between bismuth and oxygen and these properties are important benefit to photocatalyst applications for energy carriers.

Jia et al. (2018) used DFT to calculate electronic structure and optical properties of $LiBiO_3$ with different amount of doped V, Nb and Ta. As it is shown, the covalent interaction is stronger with the doped material than the original one, thus it is caused a good photocatalytic performance. It means that the photocatalytic property of $LiBiO_3$ is effectively improved with a moderate on concentration doping.

Van Troeye et al. (2014) tested hexagonal $LiIO_3$ lithium iodate-based density functional theory using GGA and LDA to calculate structural, electronic and optical properties. According to this, and to comparison with the experimental value it is underestimate and it is going from reasonable to excellent prediction, which is depends on the property of the compound, the lattice parameters and microscopic dielectric constants are fair enough to compare with the experimental data within 2%, and also the electronic structure is predicted.

Erum and Iqbal (2017) tried to understand some physical phenomenon for $KPaO_3$ and $RbPaO_3$ like structural, electronic, elastic and optical properties based on DFT using LDA and GGA. From this work, they focused to calculate some quantities such as lattice constants, ground state energy and according to them we can say that protactinium-based oxide is mechanically stable and the electronic state has direct band gap, so it is a semiconductor compound.

Lal and Kapila (2017) used DFT theory within LDA and GGA for $BaPaO_3$ and $BaUO_3$ to calculate structural, optical, electronic and mechanical properties. They changed the second cation to see the different distribution of electron density and chemical bonding of those perovskite compounds. In conclusion, according to the electronic state, both of them have a narrow direct band gap, these are semiconductors and they supposed that those perovskite compounds have an important character in reduction to tiny size technology.

Khandy et al. (2018) worked on some physical properties based on DFT method for $BaPaO_3$ under pressure. 0 to 30GPa used, Bulk modulus increased as a contrast the lattice constant decreased and they suggest the elastic and mechanical properties ductile and elastic behavior for this perovskite compound at 0 k and 0 GPa.

From the literatures, we have understood the DFT study is the effective way to calculate the physical properties, especially for perovskite materials according to the elastic parameters, they are more stable and according to the optical properties they are useful as an optoelectronic device. In this work, I have used $LiPaO_3$ to investigate structural, electronic, elastic and optical properties based on DFT using GGA and LDA approximations because lithium ions have widely study in solid state potential applications such as electronic devices like cell phone batteries, computers and cameras and protactinium already used with different cation to see the optical and other physical properties and it gives a good enough agreement. I have searched many times to find the physical properties of $LiPaO_3$, but I achieved only band gap, density and crystal system which is available in the materials project which is an open access database for materials properties (Jan et al., 2013) which are related to my work. I found that Xiang Li and his coworkers (2019) (Li et al., 2019) calculated the formation energies of a large number of perovskite materials within $LiPaO_3$ with the transfer learning model. Balachandran and his team (2018) (Balachandran et al., 2018) applied machine learning methods to many of perovskites to construct new perovskite materials and possible new cubic perovskites within $LiPaO_3$.

In this work, I am trying to find out the structural, electronic, elastic and optic properties of $LiPaO_3$ perovskite compound by the DFT theory using ABINIT software program. I also focused on the unit cell structure, bonds and bond lengths by using the VESTA computer programme.

3. THEORETICAL BACKGROUND

3.1. Classification of Solids

It is necessary to list all the equilibrium locations of the atoms for determining the structures of solids (Kazmerski, 1980). Crystallography is the study of the long-range organization of crystals and the arrangements of their constituent atoms. Many of a material's chemical and physical characteristics are determined by its crystal structure (Tilley, 2006). Since the physical characteristics of elements are classified based on their electronic structures, the electronic structure of the atoms is very important (Myers, 2009). The macroscopic features of matter may now be explained using quantum physics and the electrostatic interactions between electrons and ionic nuclei (Kasap, 2006). All atom's neighbors in all solid-state materials are organized in the same manner as they would be in a molecular structure. This property is referred to as short-range and long-range order (Enderlein and Horing, 1997).

The most essential property of the crystalline form of matter is the periodic ordering of its properties. While certain solid-state materials are amorphous, their internal structure is not regularly organized. The aggregate state of matter of all substances may be divided into solid states, liquids, and gases (Hoffmann, 2020). Many substances exist in a non-crystalline state owing to their production process, which does not show crystallinity in all solids (Kasap, 2006).

In addition to the two types of crystals, atoms in crystals are arranged into finite, regular patterns in space (Myers, 2009) such as single crystal and poly crystal. To distinguish between single and poly crystals, which both have long-range order and are separated by boundaries, we may look at the grain border, which is where the crystal orientation changes when it crosses the grain boundary (Tilley, 2006; Solyom, 2007; Hoffmann, 2020). It is assumed that the periodicity continues to infinity, which implies that the regular array of atoms is not disturbed by the existence of actual surfaces (Kasap, 2006).

Since perfect crystals are characterized by their precise structure but an amorphous solid cannot be specified with the same level of accuracy (Kazmerski, 1980). This kind of material is not crystallized because it lacks a crystal structure (long-range order) (Kasap, 2006) (Figure 3.1).

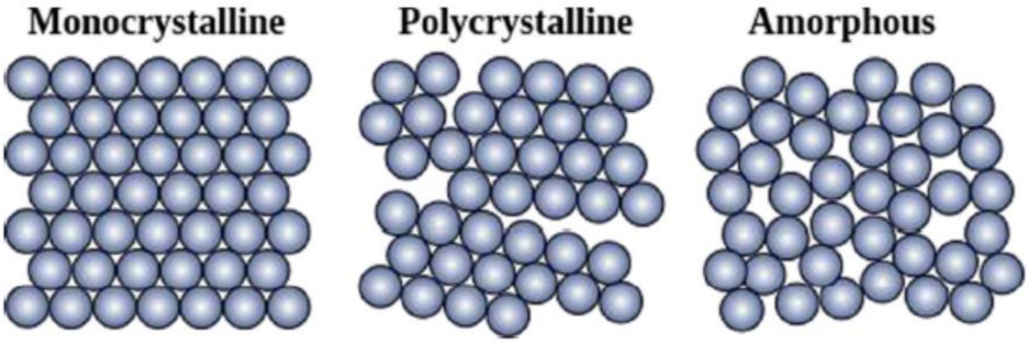

Figure 3.1. Atomic structure of each type of Monocrystalline (single crystalline), Polycrystalline and Amorphous solid according to the theory periodicity (Alajlani et al., 2018).

3.2. Crystal Structures

A lattice and a basis may be used to describe any crystal. Without the presence of atoms, a lattice is an endless periodic arrangement of geometric points. At each lattice point, we get the crystal structure if we insert an identical collection of atoms or molecules termed a basis. The crystal is therefore a lattice plus a basis (Kasap, 2006).

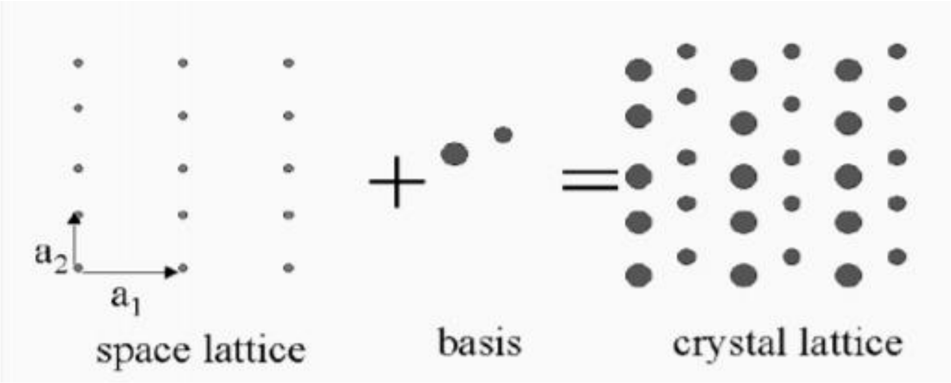

Figure 3.2. Two-dimensional crystal lattice which contains space lattice and basis (Mello and Cavalcanti, 2020).

In order to describe a crystal's structure, one must know the least amount of information necessary to identify a unit cell, which is the smallest volume of material that may be used to build a crystal (Kasap, 2006). The length of the cubic unit cell is known as the lattice parameter of the crystal structure (Kasap, 2006). The axial vectors a, b, and c are commonly assumed to be parallel to the unit cell's edges (Tilley, 2006).

3.3. Types of Crystal Structures and Bravais Lattices

For a given crystal structure, there can be a variety of unit cells (Tilley, 2006), and a crystal system defines the geometry of crystals and crystal structures (Kasap, 2006). 1D, 2D, and 3D crystal structures are all subsets of one another.

3.3.1. One dimensional crystal structures

One-dimensional crystal structures are made by periodic distributions of atoms or groups of atoms in one direction along a straight line, and the same structure is obtained by translating an infinite structure by the vector. The atomic arrangement in the crystal structure is the same from any point in the lattice; all lattice points have the same places in the crystal structure (Szwacki and Szwacka, 2010).

$$\mathbf{P} = u\mathbf{a} \tag{3.1}$$

Here, P is the lattice point, a is the basis vector and u is the positive and negative integer number.

A force operating on an atom wants to return it to its equilibrium position. Various atoms move concurrently because of the interaction between them, therefore we must take into account the mobility of all of the lattices. For simplicity, we assume that the force between atoms in the lattice is proportional to the relative displacements from equilibrium position. This is known as the harmonic approximation, which holds well provided that the displacements are small, one might think of the atoms in the lattice as interconnected by elastic springs (Tsybal, 2021).

3.3.2. Two-dimensional crystal

In two dimensions, we may access to a greater variety of atom configurations than we have in one dimension. Two-dimensionally, a unit cell is a reference surface (Cleland, 2003).

$$\mathbf{P} = u\mathbf{a} + v\mathbf{b} \tag{3.2}$$

Here P is the lattice point, a and b are the basis vectors, u and v are the positive and negative integer numbers.

There have only been two orientations in which the surface structure is periodic (Oura et al., 2003). There are five primary varieties of planar crystal structures, together referred to as two-dimensional Bravais lattice (Oura et al., 2003).

A Bravais lattice is the name given to each group or symmetry class. The simple square Bravais lattice is the simplest two-dimensional Bravais lattice, whereas the rectangular Bravais lattice is identical to the simple square but contains two distinct lattice spacings (Cleland, 2003). The number of Bravais lattices in two dimensions are five as given in Table 3.1 and Figure 3.3 (Cleland, 2003).

Table 3.1. The 2D Five crystal system and their Bravais lattices (Oura et al., 2003; Galsin, 2019)

Crystal system	Crystal lengths	Crystal angles
Oblique lattice	$a \neq b$	$\gamma \neq 90^{\circ}$
Rectangular lattice	$a \neq b$	$\gamma = 90^{\circ}$
Centered rectangular lattice	$a \neq b$	$\gamma = 90^{\circ}$
Square lattice	$a = b$	$\gamma = 90^{\circ}$
Hexagonal lattice	$a = b$	$\gamma = 120^{\circ}$

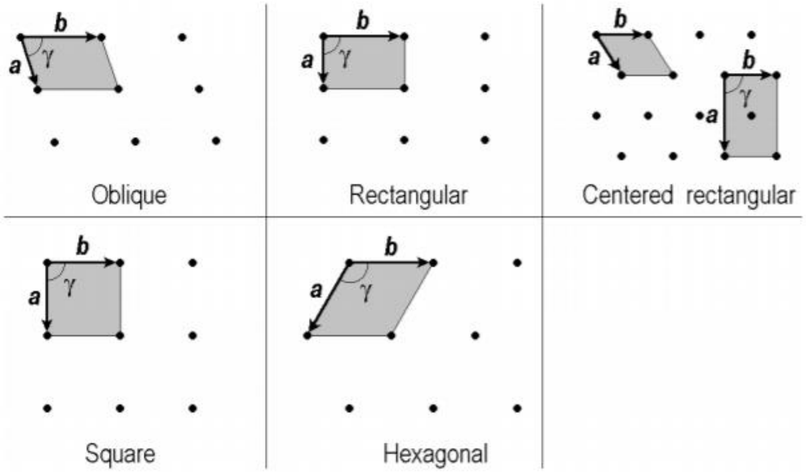

Figure 3.3. Five types of planar 2D lattices (Oura et al., 2003; Grundmann, 2016).

3.3.3. Three-dimensional crystal

There are a variety of three-dimensional Bravais lattice types that might result from a given Bravais group and the connection between the Bravais cell's lattice parameters. There are certain three-dimensional Bravais lattices in which the primitive cell does not display the symmetry of the underlying lattice, but a big Bravais cell may be selected that demonstrates the point group symmetry of the lattice. This is similar to the two-dimensional example. There are three vectors in the Bravais cell such as a, b and c (Solyom, 2007).

$$\mathbf{P} = u\mathbf{a} + v\mathbf{b} + w\mathbf{c} \tag{3.3}$$

where P is the lattice point, a, b and c are the basis vectors, u, v and w are the positive and negative integer numbers.

Crystallographers have enlarged the categorization to include seven crystal systems, which are called based on the connection between the axes and the inter-axial angles (Tilley, 2006). Each spot in three-dimensional space may be arranged in any one of fourteen possible forms, all of which are similar in their surrounds. The Bravais lattices are a set of fourteen arrays (Myers, 2009).

When the lattice invariance under the point symmetry group is applied to a three-dimensional crystal, it gives 14 Bravais lattices (translational groups) and 32 crystallographic point groups. In addition, it has been determined that there are 230 different spaces groups that may be used. Figure 3.4 shows the seven translational groups and 14 Bravais lattices that are compatible with each other (Galsin, 2019).

Table 3.2. The seven crystal systems and their Bravais lattices (Ott-Borchardt, 1995; Hammond, 2015)

Crystal system	Crystal lengths	Crystal angles	Number of Bravais lattices	Bravais lattices	Characteristic symmetry
Cubic	a = b = c	α = β = γ = 90º	3	Primitive Body centered Face centered	4-fold
Orthorhombic	a ≠ b ≠ c	α = β = γ = 90º	4	Primitive Body centered Face centered Base Centered	2-fold
Trigonal	a = b = c	α = β = 90º , γ = 120º	1	Primitive	1-fold
Tetragonal	a = b ≠ c	α = β = γ = 90º	2	Primitive Body centered	4-fold
Triclinic	a ≠ b ≠ c	α ≠ β ≠ γ ≠ 90º	1	Primitive	3-fold
Monoclinic	a ≠ b ≠ c	α = γ = 90º ≠ β ≥ 90º	1	Primitive Base centered	2-fold
Hexagonal	a = b ≠ c	a = β = 90º, γ = 120º	1	Primitive	6-fold

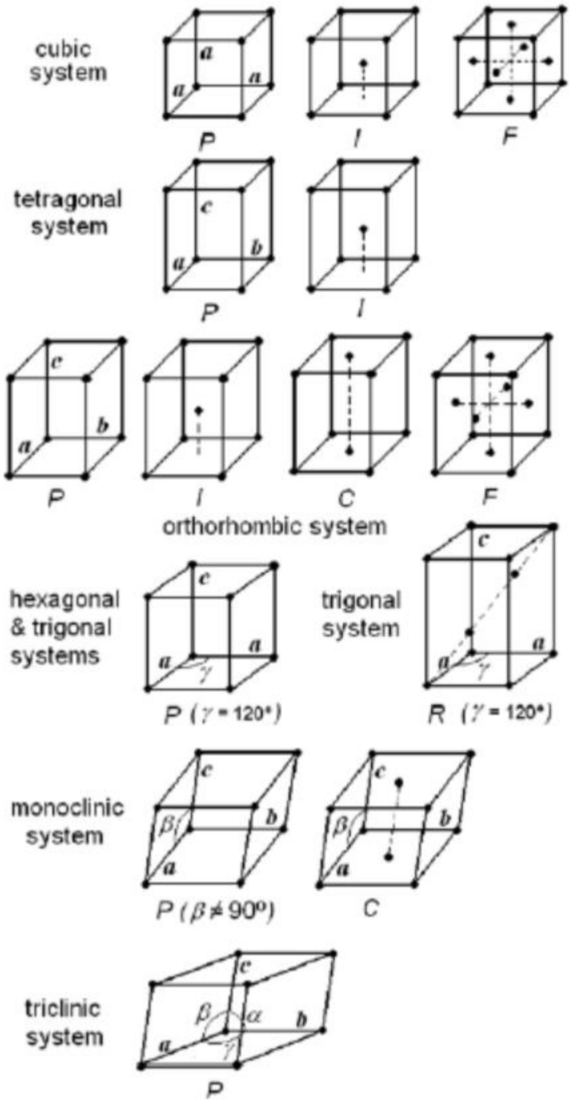
cubic system
a
a
a
P
I
F
tetragonal system
c
a
b
P
I
c
a
b
P
I
C
F
orthorhombic system
hexagonal & trigonal systems
c
a
a
γ
P (γ = 120°)
trigonal system
c
a
a
γ
R (γ = 120°)
monoclinic system
c
β
b
a
P (β ≠ 90°)
c
β
b
a
C
triclinic system
c
β
α
b
a
γ
P

Figure 3.4. 14 Bravais lattices classified according to their lattice system (Solyom, 2007; Reventos et al., 2012; Hammond, 2015).

3.4. Diffraction in Crystals

It's possible to learn about the crystal structure of materials by using X-rays of the order of lattice constant wavelengths and shorter ones (Hommond, 2015). When a crystal is hit by radiation, it is dispersed in a number of ways. It is called diffraction when the scattering occurs when the wavelength of the radiation is close to the atom spacing in the crystal, and it produces a pattern of distinct beams organized in a certain geometry. There is a correlation between diffracted beam locations and intensities and other characteristics, such as the atomic number of an object, when X-ray diffraction occurs. It is possible to derive the arrangement of atoms and their chemical type by recording the locations and intensities of the diffracted beams (Tilley, 2006).

Most crystal structures are determined by the use of an X-ray diffractometer, with the addition of neutron and electron diffractometers, which provide more information than an X-ray diffractometer. Three distinct portions make up the subject matter. Diffracted beam locations may first be used to estimate the material's unit cell size. The intensity of the diffracted beams must be calculated and correlated with the crystal structure in a second step. Lastly, the crystal structure must be reconstructed utilizing the information in the diffraction pattern (Tilley, 2006).

The crystal structure may be studied in great detail by diffraction. If one is hoping to see the crystal's reflections, one must have an oscillating wave of the right frequency, which is on the order of a few Angstroms. By comparison, the interatomic spacing in crystalline materials is just a few thousand angstroms, hence visible light cannot be utilized to determine the structure of crystals (Galsin, 2019).

The periodic arrangement of atoms in a crystalline solid might meet the diffraction requirement for X-rays, according to Max Von Laue. W. Friedrich and P. Knipping produced the most significant discovery in solid state physics in 1912, according to his recommendation. They demonstrated that X-rays interfere with each other as they go through a crystal. This was the first evidence that X-rays were waves and that a crystal had a space lattice. Thus, the atomic theory of crystals and the wave theory of X-rays were born. Laue scattering, developed by Max Von Laue, marked the beginning of scattering investigations from crystals. When William Henry Bragg and his son William Lawrence Bragg researched the structure of rock salt crystals in 1913, it was the first time this had ever been done (Galsin, 2019). A diffraction pattern is formed on a screen due to the periodic lattice scattering rays. The rules of Bragg and Von Laue, which govern constructive interference pattern, are discussed (Aharony and Entin-Wohlman, 2019).

3.5. Bragg's Law of X-ray Diffraction

Each set of parallel planes of atoms in the crystal functions as a three-dimensional grating rather than a plane grating utilized in optics in crystalline solids. What makes Bragg's work so appealing is that it provides an easy-to-follow formula for X-ray diffracting from certain parallel planes of crystal. Parallel X-ray beams fall on the crystal and are reflected off the parallel planes of the rectangular lattice illustrated in Figure 3.5. An angle of incidence where all of the beam's X-rays are parallel and constructively interact with each other results in a brilliant spot on the photosensitive plate. As stated in Bragg's law, the path difference between two intersecting parallel planes of a given set may be constructively interfered with if the path difference is an integer multiple of lambda. This is

$$2d \, \mathrm{Sin}\theta = n\lambda \tag{3.4}$$

where n is an integer, d is the distance between neighboring planes, and θ is an angle established by an incident X-ray beam with one of the crystal's planes Figure 3.5. It is significant to mention that d may or may not be equal to the crystal lattice value (Kittle, 2005; Galsin, 2019).

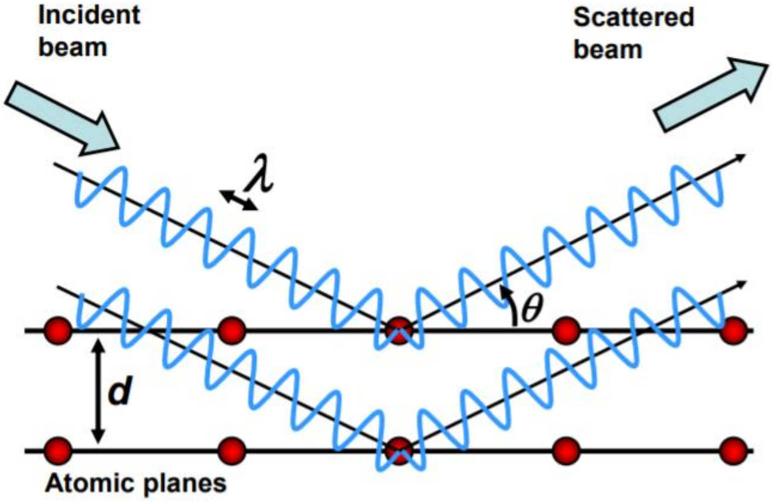

Figure 3.5. Diffraction patterns of X-rays from crystal planes in accordance with Bragg's law (Tilley, 2006; Nasir, 2018).

Radiation of a certain kind may travel through the crystal without diffraction, but at a certain Bragg angle for a certain combination of planes (hkl), some energy will be diverted into another beam, which can be used for further study. It's difficult to get a comprehensive picture of what occurs when radiation hits a genuine crystal since there are so many planes that might diffract the radiation simultaneously. This may be done using a simple graphical structure initially proposed by Ewald.

Finally at the point of view, there are many advantages of going diffraction, because we are able to relate what we see in the micrographs to the crystallography. Using the diffraction pattern, we can answer many questions for example, whether the specimen is crystalline or amorphous. From the diffraction pattern we can also tell the orientation of the crystal, and obtain the specimens crystal graphic characteristics such as lattice parameter and symmetry. And also, by looking at the shape of the diffraction pattern we can find the fold of symmetry whether it is rectangular or cubic. Electron beam interacts with the material to give rise to diffraction patterns, so we can view that by looking at the wave vectors.

3.6. Reciprocal Lattice

When doing structural studies using diffraction methods, the reciprocal lattice notion is quite helpful (Oura et al., 2003) which is a fundamental principle. X-ray and electron diffraction patterns and electron behavior in crystals may both be simplified geometrically using reciprocal space, which is equal to (k-space) (Hammond, 2015). This section introduces the notion of the reciprocal lattice, which has the same point-group symmetry as the crystal lattice (direct lattice) and plays an essential role in the understanding of the physical characteristics of crystalline materials. In an ideal infinite crystalline material, the electrostatic potential generated by all charges is periodic with the periodicity of the crystal lattice. This will serve as the basis for the introduction of reciprocal lattice (Szwacki and Szwacka, 2010).

An X-ray or neutron diffraction pattern occurs in a reciprocal space, which has dimensions that are equal to the length of the diffraction pattern. As a result, one must first establish a reciprocal lattice in order to comprehend the X-ray diffraction pattern and then link it to the crystal (direct) space. The reciprocal lattice was first postulated by Ewald in 1921 and investigated by Bernal in 1927. Think of a reciprocal space Bravais lattice that has three basic translation vectors, each with a value of b_1, b_2 and b_3. It is possible to create a reciprocal by making the direct space's basic vectors orthogonal to those of the reciprocal (Galsin, 2019).

The reciprocal space and reciprocal lattice concepts are relevant here since electron motion in a crystal is often represented in both real and momentum space (or k-space). Like any periodic time-varying function, the spatial features of a periodic crystal may be characterized by the sum of its Fourier components in the frequency domain or its reciprocal space. Perfect crystals have an infinite periodic three-dimensional array of points with spacings that are in inversely proportional to the distance between lattice planes of the Bravais lattice. These features are intimately linked to their geometric structure by the reciprocal lattice geometric architecture, which is based on reciprocal geometry. The reciprocal lattice idea may be used to understand several essential physical, electrical, and optical aspects of semiconductors and metals (Li, 1993).

There are certain X-ray diffraction occurrences that cannot be explained by the Bragg's rule, but the law can explain the vast majority of them. The non-Bragg angle diffuse scattering is an example of this. A more broad theory of diffraction employing the vector representation is needed for this purpose. The reciprocal lattice idea is very useful for dealing with all of the diffraction phenomena. Diffraction phenomena by crystals may be studied using the reciprocal-lattice model of diffraction, which is universally applicable. The crystal or rea-space lattice, as opposed to the reciprocal lattice, is the standard collection of three-dimensional atomic coordinates (Waseda et al., 2011).

$$b_1 = 2\pi \frac{a_2 \times a_3}{a_1 . a_2 \times a_3} \tag{3.5}$$

$$b_2 = 2\pi \frac{a_3 \times a_1}{a_1 . a_2 \times a_3} \tag{3.6}$$

$$b_3 = 2\pi \frac{a_1 \times a_2}{a_1 . a_2 \times a_3} \tag{3.7}$$

where b_1, b_2, b_3 are vectors in reciprocal space. Because they occupy the same amount of space, reciprocal lattices may be thought of as just another kind of lattice. There are three basic vectors that define it. In the direct lattice unit cell, these vectors point in a direction perpendicular to the end faces. In other words, direct axes and reciprocal axes are perpendicular if they are labeled differently. Triclinic, monoclinic, orthorhombic, or any other form of direct lattice gives a reciprocal cell of the same type (triclinic, monoclinic, orthorhombic, etc.). The cubic face centered direct lattice's reciprocal lattice is a cubic base centered, while the cubic base centered lattice's reciprocal lattice is a cubic face centered (Tilley, 2006).

3.7. Brillouin Zone

The first Brillouin zone refers to the core cell of the reciprocal lattice, which is particularly significant in solids theory. Brillouin zones are defined as the smallest volumes that are encompassed by the perpendicular bisectors of the reciprocal lattice traced from the origin, (Kittle, 2005). In the 2D, the perpendicular bisectors are lines but in the 3D is plane.

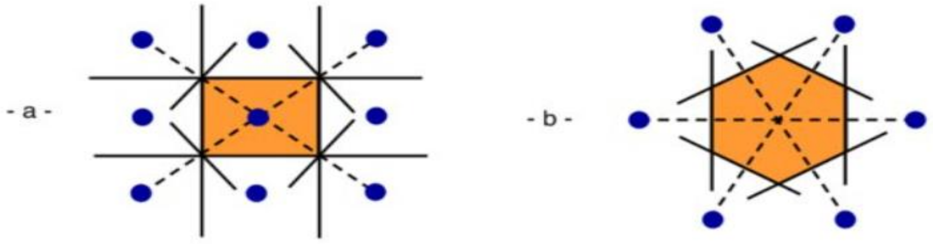

Figure 3.6. Brillouin zone for the different type of two-dimensional reciprocal lattice (a) rectangular lattice (b) hexagonal lattice (Grenier and Ballou, 2012).

There is a Wigner Seitz cell regarding those reciprocal Brillouin points Figure 3.6 that is the innermost area you will discover if you do that. To go to the first Brillouin zone from the origin of reciprocal space, you don't need to traverse any Bragg planes. To produce the second Brillouin zone, repeat this procedure for the vectors that connect the origin with its next closest neighbors (Aharonu and Entin-Wohlman, 2019). The 3rd Brillouin zone is the region in the reciprocal space that you can access by making sure that you cross two Bragg planes but don’t cross 3rd Bragg plane in the given direction. Finally nth Brillouin zone cross (n-1) Bragg planes.

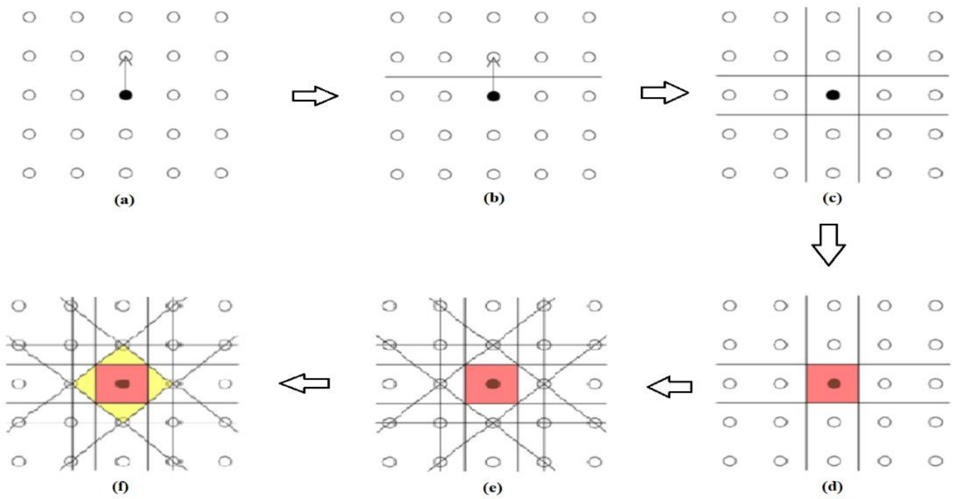

Figure 3.7. Brillouin zones of the square lattice in two dimensions are seen here (Doitpoms, 2021).

The Brillouin zone which come from the periodic structure of the material and the wave information which come from the electrons that are valuable in the material and all of this information have to be put together then we will get the information about the bands and band gaps. When studying crystal electronic energy band structures, the Brillouin zone notion is critical (Oura et al., 2003). There hasn't been much mention of the Brillouin zone in X-ray diffraction terminology until recently, yet the zones are critical to understanding crystal electronic energy band structures citation (Kittle, 2005).

The important of Brillouin zone is that we complete characteristic of the Bloch function which can be defined in the first Brillouin zone itself because of that Brillouin zone is easier to understand the diffraction patterns, as well as crystallographic characteristics, the most often employed in solid state science, if we constructed the reciprocal lattice. the

Brillouin zone started by saying that it is simple the Winger Seitz cell about the reciprocal lattice point, then we said look Wigner Seitz cell the boundaries of the Wigner Seitz cell are the Bragg planes. The reciprocal lattice vectors' perpendicular to bisector planes. Wave vector has the direction of propagation of the wave and its value is 2π/λ which is of theory of wave propagation in crystalline systems. If the wave vector terminates on the boundaries of the Brillouin zone, then they will be satisfying the Bragg's law and we will get the condition of diffraction pattern (Oura et al., 2003; Kittle, 2005; Aharony and Entin-Wohlman, 2019).

3.8. Miller Indices

Miller indices is useful to distinguish between different directions in crystals, to identify them using some indices and to identify the crystallographic planes using indices (hkl) (Tilley, 2006). So miller indices is a standard method which is been used for this purpose (Grundmann 2016; Hoffmann, 2020). The Miller indices were developed by British mineralogist and crystallographer William Hollowes Miller in 1839 as a three-number system to represent the crystal orientation of a planar set of parallel planes of atoms (Hoffmann, 2020). It is possible that the crystal lattices might be specified using Miller indices, which are used to identify the crystal faces in a systematic way as well as to denominate lattice planes. In the context of a collection of planes, we are referring to the distance between the two parallel plane is (d) and the plane has (hkl) as a result we identify the distance (d) has (d_{hkl}). In the Braggs law state ($n\lambda=2d_{hkl}\sin\theta$) d is the distance in Angstron (A^{o}) unit and the indices (hkl) indicated the plane designation of planes. There will be an exact match between the number of indices and crystal dimensions. In 1D there will be 1 index, in 2D there is 2 indices and in 3D there will be 3 indices and etc.

Miller indices is used for two different purposes;

1. All the lattice points of the same lattice are in different direction from the origin, in this case miller indices are used to indicate the direction of a lattice point from the origin or from the reference point.

2. A lattice consists of several planes all these planes occur in a different orientation, in this case miller indices are used to specify the orientation of lattice or crystal plane.

Different brackets used for a different purpose; for a direction of lattice point it is denoted in a square bracket [hkl] particular direction, <hkl> it is denoted by the member of family and {hkl}denoted by the family of plane. If we write the miller indies of the planes, we denoted in the round bracket (hkl). (hkil) is miller Bravais indices.

For example

Family of direction	Members in family
<110>	[100], [010], [001], [$\bar{1}$00], [0$\bar{1}$0], [00$\bar{1}$]

Family of plane	Members in family
{100}	(100), (010), (001), ($\bar{1}$00), (0$\bar{1}$0), (00$\bar{1}$)

If any plane passing through the origin, we have to consider another plane parallel to this, all the parallel planes have the same miller indices. Sometimes like in the case of miller Bravais indicates for hexagonal lattices and crystals addition indices are used to high light the symmetry of the structure. In the case of the miller Bravais indices for hexagonal (hkil)-4 indices are used in 3D space. The use of such redundant indices brings out the equivalence of the members of a family (Tilley, 2006).

For a crystallographic axis, a1, a2, a3 and c are needed to define the hexagonal lattice, this is the reason that to specify its plane not 3 but 4 indices are required, and these 4 indices are called miller Bravais indices (hkil) (Oura et al., 2003).

The geometry relationship between h, k, and l is

i = -(h+k)

a1 related to h, a2 related to k, a3 related to I and c related to l.

Miller indices and miller Bravais indices can be converted to each other

Miller indices	Miller Bravais indices i= -(h+k)
(110)	(11$\bar{2}$0) or (11.0)

$(\bar{1}10)$	$(\bar{1}100)$ or $(\bar{1}1.0)$
(124)	$(12\bar{3}4)$ or (12.4)

How to find miller indices, (hkl)?
h is s number of intercept per unit length along x axis
k is s number of intercept per unit length along y axis
l is s number of intercept per unit length along z axis

We need to know the crystallographic point directions and planes. Point coordinate is specified in terms of its coordinates as fractional multiple of unit cell length, they are not separated by comma. To a crystallographic directions of miller indices, we need to instruct some condition as follows (Hammond, 2015; Hoffmann, 2020).

1. Find the coordinates of two points that are in the same direction using the right-handed coordinate system.
2. In order to get the number of the lattice parameters that moved in a certain direction, subtract the coordinates of the heady point from the coordinates of the heady point.
3. Remove all fractions and reduce them to the smallest integers possible.
4. if a negative (-) sign produces, replace the negative (-) sign with a bar over the number.

And to find the crystallographic miller indices for plane, we have to instruct some step as follows (Hammond, 2015; Hoffmann, 2020).

1. Lattice parameters may be used to determine where the plane intersects with the x, y, and z coordinates on the plane. It is necessary to shift the origin of the unit cell if the planes are intersecting at that point.
2. Take reciprocals of the intercepts
3. Clear fractions but do not reduce to lowest integer
4. When writing negative (-) numbers, write the number with a bar above it in parentheses (hkl).

Using the plane's 1, 2, 3, the reciprocals would be 1/1, 12, 1/3; the fewest three numbers that share this ration are 6, 3, 2.

3.9. Band Structure in Crystals

In terms of crystal structure, there is a vast range of options. We prefer to categorize materials into three broad groups based on the periodic table of elements. These elements include metals, nonmetals, and a tiny number of elements that we designate as semiconductors. An understanding of electrons in materials is critical to determining conductivity, and band theory is a factor in determining conductivity, for example, some metals are much more conductive than others and some nonmetals are excellent insulators because they don't conduct electricity at all (Vainshtein et al., 2000).

Atoms in matter are made up of a nucleus and a number of electrons that circle the nucleus in distinct shells. A compound is formed when atoms from different elements combine to create a single molecule. A micro electron volt is the maximum amount of energy that may be transferred to an electron in this kind of conduction.

When the two atoms are brought close together to form an interact system, the energy of two electron system will no longer be same, when they are far a part of each other, isolated from each other, the energy of these two electrons will be same, it means that their energy levels have it is own things, but if the atoms start to get closer, their electron wave functions start to overlap, they interact each other. The energy of these two electrons will no longer be the same, because of Pauli’s exclusion principle which state that no two electrons in a given interacting system may share the same quantum state and hence same energy (Razeghi, 2002; Galsin, 2019).

3.9.1. Transition from atomic levels to bands

In a band, there are lots of energy levels that are all quite near to each other. It is important to remember that the electrons of an isolated nucleus reside in a "atomic orbital," which is defined as an energy level distinct from the rest of the nucleus. The atomic orbitals combine to form the molecular orbitals, which are distinct from the individual orbitals. As more atoms are bought together, the molecular orbitals extended larger and the energy levels of the molecular will become increasingly dense. Eventually the collection of atoms forms a band structure combining the properties of individual atoms (Razeghi, 2002).

The wavefunctions define how electrons behave in a periodic system. The Bloch theorem is one of the techniques we use to deal with solids mathematically. To prove Bloch's theorem, it is necessary to know how the crystalline structure excites itself in terms of lattice vibrations, electron states and spin waves. The Schrödinger equation for a crystalline solid with a periodic potential may therefore be solved using (Singleton, 2001; Roque-Malherbe, 2010).

$$V(r) = V(r+T) \tag{3.8}$$

$$E\Psi(r) = -\frac{\hbar^2}{2m}\nabla^2\,\Psi(r) + V(r)\Psi(r) \tag{3.9}$$

3.9.2. Energy band formation in solids

In physics we know that a matter can convert its state and this gives rise to various different properties that we see around us. The state of a matter is completely covered by the energy that keeps stabilization. Matter possesses a spectrum of energies that might have been described by its electronic band structure.

The valence band and conduction band are the two basic kinds of energy bands in a material. If you look at the valence and conduction band Figures 3.8, you'll see that in the valence band, the valence electrons are all in one molecular orbital, and the valence band's maximum energy level is at the top of the band. In contrast, the conduction band is a delocalized band of energy levels in a crystal that is responsible for electrical conductivity. In order for an electron to go from the valence band to the conduction band, it must have a minimal quantity of energy. In absolute zero, the highest occupied molecular orbital at the middle of the valence and conduction band is referred as the fermi level, and the particles in that state have their own quantum states and normally do not interact with one other (Razeghi, 2002; Kittle, 2005).

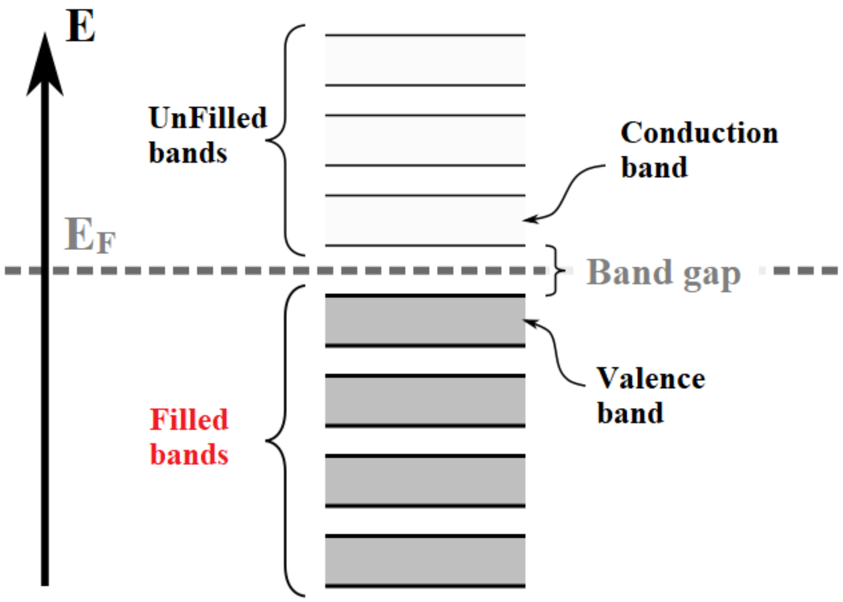

Figure 3.8. Semiconductor band structure (Valence and Conduction bands, 2021).

Figure 3.9 (a) shows a conduction band that overlaps the valence band, thus any electrons that exist in the valence band are automatically in the conduction band; in other words, the outermost electrons are free to conduct. As in Figure 3.9 (a), all insulators have valence and conduction bands. However, a significant prohibited gap prevents electrons in the valence band from crossing across to the conductivity band. However, the forbidden gap between the two is considerably smaller than that between an insulator and a semiconductor Figure 3.9 (b,c) because an electron must pass from the valence band into the conduction band to get energy.

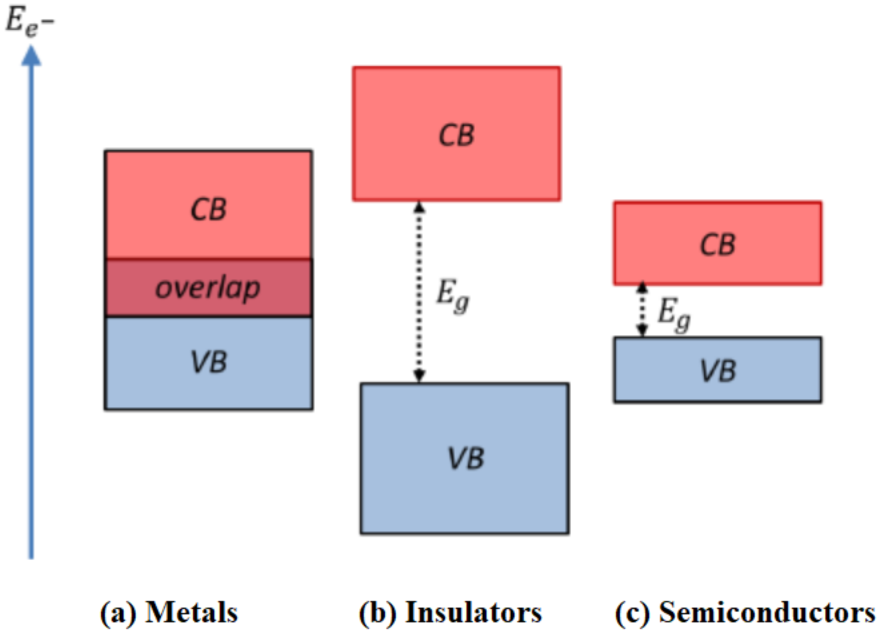

Figure 3.9. Schematic Conduction band (CB) and Valence band (VB) for (a) Metals (b) Insulators (c) Semiconductors (Rioult, 2015).

3.10. Optical Properties

When a light fall onto a material, (like a semiconductor material) reflection, refraction, absorption and transmission phenomenon are take place, which is because of the interaction of the light with the electrons in the atoms. Some factors are affecting the phenomenon such as the band gap of the material, the arrangement and also the intensity of the light. The response of the materials with the electromagnetic waves, the electronic excitation of the spectrum is determined by the dielectric function which is depend of the frequency of light. The complex dielectric function of a material consists of two parts, which are real and imaginary parts.

$$\mathcal{E}(\omega) = \mathcal{E}_1(\omega) + i\mathcal{E}_2(\omega) \tag{3.10}$$

$\varepsilon_1(\omega)$ is the real part of the dielectric function, $\varepsilon_2(\omega)$ is the imaginary part of the dielectric function.

Kramer-Kronig relation tells us that dispersive and absorptive properties of the dielectrics are not independent, it means if we know the imaginary part of the dielectrics, we can calculate the dispersive spectrum of the real part.

$$\varepsilon_1(\omega) = 1 + \frac{2}{\pi} P \int_0^\infty \frac{\acute{\omega}\varepsilon_2(\acute{\omega})}{\acute{\omega}^2 - \omega^2} \, d\acute{\omega} \tag{3.11}$$

$$\varepsilon_2(\omega) = -\frac{2\omega}{\pi} P \int_0^\infty \frac{\varepsilon_1(\acute{\omega}) - 1}{\acute{\omega}^2 - \omega^2} \, d\acute{\omega} \tag{3.12}$$

With the complex dielectric function, we can get many properties of the materials like reflection, absorption, refractive index (Lucarini et al., 2005; Stenzel, 2016; Azam et al., 2019).

3.10.1. Optical constants

Refractive index (n): Whenever a beam of light passes through a medium and into another medium, its direction is reversed. This occurs as a result of the fact that the speed of light differs across various mediums. Since the densities of the substances varies, the quantity of refraction that occurs is affected. For example, when light travels through a thick material such as glass, it slows down because the angle of refraction is lower than the angle of incidence, and the light bends towards the normal. When light passes through a less dense medium, the speed of the light increases and the rays bend away from the regular path.
Index of refraction measures how much light bends as it passes from one material to another. By using the dielectric function of real and imaginary components, we can calculate the refractive index as follows.

$$n(\omega) = \left[\frac{\sqrt{\mathcal{E}_1{}^2(\omega) + \mathcal{E}_2{}^2(\omega)}}{2} + \frac{\mathcal{E}_1(\omega)}{2}\right]^{1/2} \tag{3.13}$$

Extinction coefficient (damping coefficient or absorption coefficient) (k): This kind of coefficient is related to the absorption of electromagnetic radiation into the crystal structure, it means that this coefficient determines how much quantity of light decreases when it pass into a media, by using the real and imaginary components of the dielectric function, we can calculate the damping coefficient.

$$k(\omega) = \left[\frac{\sqrt{\mathcal{E}_1{}^2(\omega) + \mathcal{E}_2{}^2(\omega)}}{2} - \frac{\mathcal{E}_1(\omega)}{2}\right]^{1/2} \tag{3.14}$$

Reflection coefficient (R): This coefficient shows the rate of the returning electromagnetic wave which is coming form the crystal to the media. By the refractive index and damping coefficient, we can calculate the reflection of coefficient by the relation of:

$$R(\omega) = \frac{(1-n)^2 + k^2}{(1+n)^2 + k^2} \tag{3.15}$$

And also, by using the complex dielectric function, we can again calculate the reflection coefficient as follows.

$$R(\omega) = \left|\frac{1 - \sqrt{\mathcal{E}(\omega)}}{1 + \sqrt{\mathcal{E}(\omega)}}\right|^2 \tag{3.16}$$

Energy loss function (L): This function refers the value of energy that loses by fast moving the electrons between energy bands as they pass through the surface and the volume of the matter, which we can calculate it by the real and imaginary dielectric function (Khan et al., 2015; Azam et al., 2019).

$$L(\omega) = Im\left(-\frac{1}{\varepsilon(\omega)}\right) \tag{3.17}$$

The energy lose function is denoted by L_S (ω) for the surface and L_V(ω) for the volume.

$$L_S(\omega) = \frac{\varepsilon_2}{{\varepsilon_1}^2 + {\varepsilon_2}^2 + 2\varepsilon_1 + 1} \tag{3.18}$$

$$L_V(\omega) = \frac{\varepsilon_2}{{\varepsilon_1}^2 + {\varepsilon_2}^2} \tag{3.19}$$

Effective number of valence electrons (N_{eff}): This gives the information about the effective number of valence electrons per unit cell. We can use effective number of valence electrons to get the information about the absorption process in the crystal structure.

$$N_{eff}(E) = \frac{2m\varepsilon_0}{\pi\hbar^2 e^2 Na}\int_0^{\varepsilon_0} \varepsilon_2(E)E dE \tag{3.20}$$

here, ε_0 , m, e and Na are permeability of space, mass of electron, charge of electron, density of the atom, respectively.

Effective optical dielectric constant (ε_{eff}): It is the second rule of the dielectric constant to determine the contribution of transitions between bands in the range between 0 to ε_0 to give the information about the absorption process (Lucarini et al., 2005).

$$\varepsilon_{eff}(E) = 1 + \frac{2}{\pi}\int_0^{\varepsilon_0} \varepsilon_2(E)E^{-1}dE \tag{3.21}$$

In this thesis study we studied effective number of valence electrons instead of effective optical dielectric constant.

3.11. Elastic Properties

Elastic characteristics are necessary in determining the hardness and mechanical stability of a material, as well as the bond strengths between the atoms that make up the structure. Except in cases when the elastic limit is exceeded, the compression or stretching of a solid is proportional to the force applied to its surface. If an object can not regain its original shape after being deformed by a force is referred to as elastic deformation, which means the change in shape or size of the body. The force that deforms an object is referred to the deforming force. The ability of an object to regain its original shape after being deforming by a force is referred to as the elasticity of an object. When you apply a deformation force to a material, inside the material there is a force called Restoring force which is simply a force that tends to restore a deformed body to its original form.

The force which is applied to a sample tried to compress or stretch the sample is represented as the stress. Strain means the change in dimensions per unit of the original dimensions under amount of force (stress). In an elastic deformation, the stress is experienced by a body is directly proportional to the strain.

Every material has specific elastic limit, that depends on the deforming force applied on the object and the properties of the material. When a sample is more compressed or stretched further than a certain point which is the elastic limit, the sample will get permanently deformed and if we keep increasing the force which is applied to the sample, it will break the bonds in atoms of the sample. This type of deformation force is called as plastic deformation.

$$Elasticity = \frac{stress}{strain} \tag{3.22}$$

$$E = \frac{\sigma}{\varepsilon} \tag{3.23}$$

Stress and strain have two basic categories, which are normal (perpendicular) and shear. Each of them has two sub categories which are Tensile and compressive (Martin, 2004; Beer and Maina, 2008; Wang, 2012; Slola-Valim, 2015).

3.11.1. Elastic constants

Stress and strain are key terms that characterize condensation states. Some of the group of constants that we called elastic modules play an important role in the characteristic of the material. The elastic constants are given in the following.

Elastic stiffness constants (C_{ijkl}) is the ratio between stress and the strain ($\sigma_{ij} = C_{ijkl}\varepsilon_{kl}$) and the elastic compliance constants are (S_{ijkl})are the ratio between the strain and the stress ($\varepsilon_{ij} = S_{ijkl}\sigma_{kl}$). Both of them are rank four tensors but using a matrix notation they can be written with two indices (C_{ij} and S_{ij}). These elastic stiffness and elastic compliance constants are important to calculated the following elastic properties.

Bulk modulus: Bulk modulus shows the reaction of a body to stress that changes the volume, without changing in shape. That is

$$B = -V \frac{\triangle P}{\triangle V} \tag{3.24}$$

B is the Bulk moduli, V is the Volume and $\frac{\triangle P}{\triangle V}$ change in pressure with respect to volume. Bulk modules are calculated with Voight, Reuss and Hill approaches. The Voight approach can be calculated as

$$9B_V = (C_{11} + C_{22} + C_{33}) + 2(C_{12} + C_{23} + C_{31}) \tag{3.25}$$

The Bulk modulus with Reuss approach;

$$1/B_R = (S_{11} + S_{22} + S_{33}) + 2(S_{12} + S_{23} + S_{31}) \tag{3.26}$$

The Hill approach is the average value of Voight and Reuss approaches,

$$B_H = (B_V + B_R)/2 \tag{3.27}$$

Young modulus: It is the ratio of the longitudinal stress divided by the longitudinal strain, longitudinal refers to change in length

$$E = \frac{F/_A}{\triangle L/_L} = \frac{F\ .\ L}{A\ .\ \triangle L} \tag{3.28}$$

here E is young's module, F is the force applied to a sample, L is the original length, A is the cross-sectional area and △L is the change in length. In the other hand we can write the young's module by using Bulk and shear modulus, which is

$$E = \frac{9BG}{3B + G} \tag{3.29}$$

G is the shear Module.

Shear modulus: It is also called modulus of rigidity, it is the ratio of the shearing stress to the shearing strain, when a force experiencing parallel to the sample, the sample changing the shape without changing in volume. Shear modulus usually measured by GPa.

$$G = \frac{F/_A}{\triangle x/_h} = \frac{F\ .\ h}{A\ .\ \triangle x} \tag{3.30}$$

G is the shear module, △x is the transverse displacement, $F/_A$ shear stress and $\triangle x/_h$ shear strain.

Similar to Bulk modulus, also Shear modulus calculated with there approaches as given in the following equations.

$$15G_V = (C_{11} + C_{22} + C_{33}) - (C_{12} + C_{23} + C_{31}) + 3(C_{44} + C_{55} + C_{66}) \quad (3.31)$$

$$15/G_R = 4(S_{11} + S_{22} + S_{33}) - 4(S_{12} + S_{23} + S_{31}) + 3(S_{44} + S_{55} + S_{66}) \quad (3.32)$$

$$G_H = (G_V + G_R)/2 \quad (3.33)$$

Poisson’s ratio: It is important to know that the Poisson's effect, which is a measure of how thick or thin a sample becomes perpendicular to the compressive direction, occurs when the sample is enlarged in one direction while the sample's other two opposite directions tend to thin out. It is necessary to know the Poisson's ratio when doing an elastic study of a material. The value of the Poisson’s ratio is around -1 to 0.5. The critical value of it is 0.26. Materials with bigger (smaller) Poisson’s ratio than 0.26 gives that material is elastic (fragile).

$$v = \frac{(3K - 2G)}{(6K + 2G)} \quad (3.34)$$

Zener Anisotropy Factor (A): gives an information about the isotropy property of a material.

$$A = 2\, C_{44} / (C_{11} - C_{12}) \quad (3.35)$$

Debye Temperature (θ_D): The *Debye temperature* is the temperature of a crystal's highest normal mode of vibration.

$$\theta_D = \frac{h}{2\pi k_B}\left(\frac{6\pi^2 n\rho}{M}\right)^{1/3} V_m \quad (3.36)$$

h is Planck constant, *kB* is Boltzman constant, *n* is the number of molecules in a unit cell, *ρ* is density, M is molecular weight and *Vm* is the average velocity of the sound.

3.12. Perovskite Definition

It is named after a Russian mineralogist, Lev Perovskite, given to a complete family of minerals with the same fundamental crystal structure as CaTiO3. The oxide mineral calcium titanate (CaTiO3) was found by Gustav Rose in the Ural Mountains of Russia in 1839. All those materials which have a crystal structure of ABX_3 they are called perovskite crystal structure. The perovskite structures have five atoms in the unit cell (Tejuca and Fierro, 1993; Roque-Malherbe, 2010).

A^{+2} organic or inorganic cation is larger in size than B^{+4} is located at eight corners of the cube. B^{+4} heavy metal cation is located at the center of the cube. X^{-2} anions are located at the six-face centered of the cube, it is usually oxygen or halogens like Chlorine (Cl), Bromine (Br), or Iodine (I). Examples of perovskite materials are BaNiO3, BaTiO3, SrTiO3, GdFeO3, CaTiO3, FeTiO3, MgSiO3 (Tejuca and Fierro, 1993; Roque-Malherbe, 2010).

Perovskites (X=O) have historically been the most investigated because of their exceptional ferroelectric, magnetic, and superconductive characteristics. First halide-based perovskite structure was discovered by Moller in 1958, and the first organic material appeared in halide perovskite by Weber et al in 1978 (Zhou and Wang, 2020).

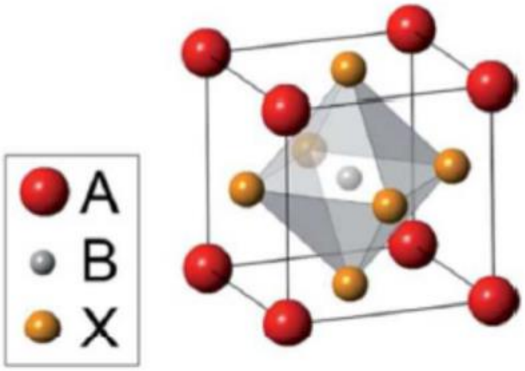

Figure 3.10. ABX_3 perovskite structure (Luo and Daoud, 2015).

The variety of compounds at the properties proven that in the periodic table, approximately 90% of the metal elements are stable and suitable in perovskite type oxide structure (Roque-Malherbe, 2010). Generally, a large number of the perovskite structure are distorted and they depend a very important parameter, a tolerance factor. The perovskite structure is stable if the tolerance factor (t) is in the range of 0.75 to 1 (Tejuca and Fierro, 1993; Roque-Malherbe, 2010).

$$t = \frac{(r_A + r_O)}{\sqrt{2}\,(r_B + r_O)} \tag{3.37}$$

r_A , $r_{B,}$, and r_o is the radius of A, B and Oxygen or halide, respectively (Tejuca and Fierro, 1993).

3.12.1. Properties of perovskite mineral

Perovskite materials have been intensively used in many applications and important areas of solid chemistry, physics, advanced materials due to various structures and configurations. For the reason of the arrangement of perovskite can be easily tuned over a wide range, these materials can be scientifically investigated to make a connection between performance and structure (Tejuca and Fierro, 1993; Fu et al., 2019).

During the 10 years, it is efficiency has increased because of the properties like tunable band gap, high absorption coefficient. These materials are suitable not only for solar cell but also for light emitting diode, for fabrication photodiodes, photodetectors and for different kind of lasers. The combination of novel perovskite materials has been a continuing interest for material scientists focused on catalysis and solid-state chemistry or physics. Furthermore, the mixture of perovskite with other materials is proving to be an effective technique to improve desirable properties and grow new applications (Tejuca and Fierro, 1993), such as sensors, thermoelectric application, battery technology, Fuel cells and especially solid oxide fuel cells, photovoltaics, optoelectronics (Sum and Mathews, 2019).

In addition, the properties of high efficiency, higher stability, high carrier mobility, high absorption coefficient, long charge carrier diffusion length, highly crystalline structure, high absorption coefficient, band gap tuning, low exciting binding energy and facile low temperature solution-based fabrication method are very useful properties for making any kind of solar cells in perovskites which is a reason of using perovskites (Tejuca and Fierro, 1993; Fu et al., 2019).

3.13. The Multi-Particle Problem

A molecule is the small part of a compound that shows all its properties. The Hamiltonian is the total energy operator for a quantum system equation (3.38). We have chosen the Hamiltonian operator because there exists some exact set of eigenfunctions of this operator, which is the solutions to the time-independent, non-relativistic Schrödinger equation and called wave function. Equation (3.39) combines the kinetic and the potential energy terms in the Hamiltonian operator. All nuclei and electrons have kinetic energy. The potential energy includes the coulombic attraction or repulsion of all pairs of charged particles in the molecule (electrons and nuclei), these particles interact via coulomb's law, where the strength of their interactions is governed by the sign of their charges, their magnitude and the inverse of their separation distance.

The purpose of molecular physics is to learn and recognize the structural and physical properties of various molecules. Based on this, we try to derive an understanding of the meanings, responses and properties of molecules in physical, chemical and biological systems. Schrödinger's equation must be solved and the eigenvalues and the eigenvectors of the molecule under investigation obtained in order to calculate the Molecular Hamiltonian (Haken and Wolf, 2004; Sutcliffe and Woolley, 2012).

For the Schrödinger equation of the adiabatic molecule, we can not accurately solve the Schrödinger equation for any system other than hydrogen atoms. The reason is that we have N charged particles, typical atom is composed of a bunch of nuclei and electrons. It means that we have a bunch of particles with N total charge particles, we would choose $\frac{N(N-1)}{2}$ interaction pairs. This is a quadratic number of those and this is known in physics as the many- body problem, it typically for solving any number of particles which is greater than 2, (N>2) it means one electron and one nucleus. Finally in the many-body problem, we can not solve it exactly for any molecular system which has more than two charged particles.

It is the primary goal of the quantum model to explain time-independent Schrodinger's equation in the study of atoms, molecules, and solids (Tinkham and Mckay, 1964). Here, we explain how to determine the electron wave function of a molecule (Haken and Wolf, 2004). We use the Schrödinger equation to calculate the physical properties of such complex systems. In order to determine the physical properties of a system in quantum mechanics, it is necessary to solve the time-independent Schrödinger.

$$\hat{H}\Psi = E\Psi \tag{3.38}$$

The Hamiltonian which describes the energy of the electron in the electrostatic field of the nuclei is given as;

$$\hat{H} = \hat{T}_e + \hat{T}_n + \hat{V}_{ee} + \hat{V}_{nn} + \hat{V}_{en} \tag{3.39}$$

The kinetic energy operator for each electron is:

$$\hat{T}_e = -\sum_{i=1}^{N_e} \frac{\hbar^2}{2m_e}\nabla_i^2 = \sum_{i=1}^{N_e} -\frac{1}{2}\nabla_i^2 \tag{3.40}$$

The kinetic energy operator for each nucleus is:

$$\hat{T}_n = -\sum_{\alpha=1}^{N_n} \frac{\hbar^2}{2M_{\alpha}}\nabla_{\alpha}^2 = \sum_{\alpha=1}^{N_i} -\frac{1}{2}\nabla_{\alpha}^2 \tag{3.41}$$

The potential energy from Coulombic electron-electron repulsion is:

$$\hat{V}_{ee} = \frac{1}{2}\sum_{i=1}^{N_e}\sum_{j=i+1}^{N_e} \frac{e^2}{4\pi\varepsilon_o\left|\vec{r}_i - \vec{r}_j\right|} = \frac{1}{2}\sum_{i\langle j}^{N_e} \frac{1}{\left|\vec{r}_i - \vec{r}_j\right|} \tag{3.42}$$

The potential energy between the electron and nuclei Coulombic attraction is:

$$\widehat{V}_{en} = -\frac{1}{2}\sum_{i=1}^{N_e}\sum_{\alpha=1}^{Nn}\frac{Z_{\alpha}e^{2}}{4\pi\varepsilon_{o}\left|\overrightarrow{r_i}-\overrightarrow{R_\alpha}\right|} = -\frac{1}{2}\sum_{i=1}^{N_e}\sum_{\alpha=1}^{N_n}\frac{Z_{\alpha}}{\left|\overrightarrow{r_i}-\overrightarrow{R_\alpha}\right|} \tag{3.43}$$

The potential energy arising from Coulombic nuclei-nuclei repulsion is:

$$\widehat{V}_{nn} = \frac{1}{2}\sum_{\alpha=1}^{N_n}\sum_{\beta=\alpha+1}^{N_n}\frac{Z_{\alpha}Z_{\beta}e^{2}}{4\pi\varepsilon_{o}\left|\overrightarrow{R_\alpha}-\overrightarrow{R_\beta}\right|} = \frac{1}{2}\sum_{\alpha\langle\beta}^{N_n}\frac{Z_{\alpha}Z_{\beta}}{\left|\overrightarrow{R_\alpha}-\overrightarrow{R_\beta}\right|} \tag{3.44}$$

$$\begin{aligned}\widehat{H} = &-\sum_{i=1}^{N_e}\frac{\hbar^2}{2m_e}\nabla_i^2 - \sum_{\alpha=1}^{N_n}\frac{\hbar^2}{2M_\alpha}\nabla_\alpha^2 + \frac{1}{2}\sum_{i=1}^{N_e}\sum_{j=i+1}^{N_e}\frac{e^2}{4\pi\varepsilon_o\left|\overrightarrow{r_i}-\overrightarrow{r_j}\right|}\\ &+\frac{1}{2}\sum_{\alpha=1}^{N_n}\sum_{\beta=\alpha+1}^{N_n}\frac{Z_\alpha Z_\beta e^2}{4\pi\varepsilon_o\left|\overrightarrow{R_\alpha}-\overrightarrow{R_\beta}\right|} - \frac{1}{2}\sum_{i=1}^{N_e}\sum_{\alpha=1}^{N_n}\frac{Z_\alpha e^2}{4\pi\varepsilon_o\left|\overrightarrow{r_i}-\overrightarrow{R_\alpha}\right|}\end{aligned} \tag{3.45}$$

For simplicity we can write the Hamiltonian equation as;

$$\widehat{H} = -\sum_{i}^{N_e}\frac{1}{2}\nabla_i^2 - \sum_{\alpha}^{N_n}\frac{1}{2M_\alpha}\nabla_\alpha^2 + \frac{1}{2}\sum_{i\langle j}^{N_e}\frac{1}{\left|\overrightarrow{r_i}-\overrightarrow{r_j}\right|} + \frac{1}{2}\sum_{\alpha\langle\beta}^{N_n}\frac{Z_\alpha Z_\beta}{\left|\overrightarrow{R_\alpha}-\overrightarrow{R_\beta}\right|} - \frac{1}{2}\sum_{i}^{N_e}\sum_{\alpha}^{N_n}\frac{Z_\alpha}{\left|\overrightarrow{r_i}-\overrightarrow{R_\alpha}\right|} \tag{3.46}$$

In non-relativistic theories, hydrogen atom is one of the limited cases where Schrödinger’s equation can be solved accurately. It is quite difficult or even impossible to analyze the system for such a large number of electrons and to solve the Schrödinger equation for each electron. However, for other atoms, we must use some approximations, in order to be able to solve the equation. The first of these approaches is the Born-Oppenheimer (1927) approach (Moss, 1973).

3.13.1. Born-Oppenheimer (Adiabatic) approach

The first thing we notice is that the mass of the nucleus is much greater than the mass of the electron. In the hydrogen atom nucleus weight is about 2000 times more than an electron and most nuclei contains more than one particle. Because of that huge mass, a nucleus moves very slowly comparatively to our electrons. So, the set of nuclei is going to move slower comparative to the set of all electrons, because of that, we approximate that the positions of all the nuclei are fixed related to electrons and we can say the kinetic energy of the nucleus is zero $\widehat{T}_n = 0$. It means no motion, no kinetic energy (Kaxiras, 2003; Atkins and Friedman, 2005).

When the Born-Oppenheimer approximation apply to the molecular Hamiltonian, the first thing is the nuclear kinetic energy goes to zero. Additionally nuclear-nuclear repulsion term and $\left|\overrightarrow{R_\alpha} - \overrightarrow{R_\beta}\right|$ is going to be constant. The rest terms such as electron kinetic energy, electron-nuclear attraction, electron-electron repulsion are still difficult, we will solve those all later by the other approximations (Tinkham and Mckay, 1964; Haken and Wolf, 2004).

$$\widehat{H} = \underbrace{-\sum_{\alpha}^{N_n} \frac{1}{2M_\alpha}\nabla_\alpha^2}_{Zero} + \underbrace{\frac{1}{2}\sum_{\alpha\langle\beta}^{N_n} \frac{Z_\alpha Z_\beta}{\left|\overrightarrow{R_\alpha} - \overrightarrow{R_\beta}\right|}}_{Const} \underbrace{-\sum_{i}^{N_e}\frac{1}{2}\nabla_i^2 + \frac{1}{2}\sum_{i\langle j}^{N_e}\frac{1}{\left|\overrightarrow{r_i} - \overrightarrow{r_j}\right|} - \frac{1}{2}\sum_{i}^{N_e}\sum_{\alpha}^{N_n}\frac{Z_\alpha}{\left|\overrightarrow{r_i} - \overrightarrow{R_\alpha}\right|}}_{Difficult} \tag{3.47}$$

$$\widehat{H} = \widehat{V}_{nn} + \widehat{T}_e + \widehat{V}_{ee} + +\widehat{V}_{en} \tag{3.48}$$

$$\widehat{V}_{nn} = \frac{1}{2}\sum_{\alpha\langle\beta}^{N_n}\frac{Z_\alpha Z_\beta}{\left|\overrightarrow{R_\alpha} - \overrightarrow{R_\beta}\right|} = \text{constant} \tag{3.49}$$

$$\widehat{H}_{electron} = -\sum_{i}^{N_e}\frac{1}{2}\nabla_i^2 + \frac{1}{2}\sum_{i\langle j}^{N_e}\frac{1}{\left|\overrightarrow{r_i} - \overrightarrow{r_j}\right|} - \frac{1}{2}\sum_{i}^{N_e}\sum_{\alpha}^{N_n}\frac{Z_\alpha}{\left|\overrightarrow{r_i} - \overrightarrow{R_\alpha}\right|} \tag{3.50}$$

3.13.2. Hartree method and self-consistent field

This approximation describes the movement of one electron interacting with every single atomic nucleus in the system. Interactions with other electrons are not included, which it means that Vee=0. This is considered in the second term representing the coulomb electron-electron interaction (Kohanoff, 2006). For solving time-independent Schrodinger equation for multi-electron atoms or molecules, a new approximation called Hartree approximation, in his first propose method was the Hartree method or Hartree product has emerged that is useful for introduction into the self-consistency field.

$$\Psi_{HP}(x_1,x_2,....,x_N)=\chi_1(x_1)\chi_2(x_2)....\chi_N(x_N) \tag{3.51}$$

$$\Psi_{HP}(x_1,x_2)=\chi_1(x_1)\chi_2(x_2) \tag{3.52}$$

$$\Psi_{HP}(x_2,x_1)=\chi_1(x_1)\chi_2(x_2) \tag{3.53}$$

$$\chi_1(x_2)\chi_2(x_1)=-\chi_1(x_1)\chi_2(x_2) \tag{3.54}$$

$$\widehat{H}_{electron}=-\sum_{i}^{N_e}\frac{1}{2}\nabla_i^2+\frac{1}{2}\sum_{i\langle j}^{N_e}\frac{1}{\left|\overrightarrow{r_i}-\overrightarrow{r_j}\right|}-\frac{1}{2}\sum_{i}^{N_e}\sum_{\alpha}^{N_n}\frac{Z_\alpha}{\left|\overrightarrow{r_i}-\overrightarrow{R_\alpha}\right|} \tag{3.55}$$

$\frac{1}{2}\sum_{i\langle j}^{N_e}\frac{1}{\left|\overrightarrow{r_i}-\overrightarrow{r_j}\right|}$ is the distance calculation depending of pairs of electrons and it is not exactly solvable by the many-body problem in physics and in order to solve it, we need to resort to approximation methods.

$$\widehat{h}_1(i)=\sum_{i}^{N_e}-\frac{1}{2}\nabla_i^2-\frac{1}{2}\sum_{i}^{N_e}\sum_{\alpha}^{N_n}\frac{Z_\alpha}{\left|\overrightarrow{r_i}-\overrightarrow{R_\alpha}\right|} \tag{3.56}$$

$$\widehat{h}_1(i)=\sum_{i}^{N_e}-\frac{1}{2}\nabla_i^2+v_{ext}(R,r_i) \tag{3.57}$$

$$V_{ee}=\frac{1}{2}\sum_{i\langle j}^{N_e}\frac{1}{\left|\overline{r_i}-\overline{r_j}\right|}=\sum_{i\langle j}\upsilon(i,j) \tag{3.58}$$

$$\widehat{H}_{electron}=\sum_{i}h(i)+\sum_{i\langle j}\upsilon(i,j) \tag{3.59}$$

But the problem was that there were many physical parameters that there were didn't understand and unclear behind the physical reason for this method and the electronic component was incomplete. He was failed to satisfy antisymmetric principle. When it comes to swapping out any set of space spin coordinates, fermions should be antisymmetric, i.e., according to the Pauli’s exclusion principle any two electron or any two fermions can not occupy at the same quantum state with the same spin, this means that the sign of the wavefunction changes when two electrons are exchanged (Saue, 2002; Kohanoff, 2006; Sherrill, 2009).

3.13.3. Hartree-Fock method

In 1930, Fock independently pointed out that the Hartree product did not respect the antisymmetric of the particles because of the Pauli’s principle. Later, Hartree-Fock approximation solved the equation of time-independent Schrödinger equation by using a non-linear method. Hartree-Fock theory acted an important character and offers an excellent opening argument for calculations in many-body problems, for electrons, atoms, molecules, and even solids for calculating eigenvalues and eigenfunctions (wave functions). There are a number of electronic structure models that use the Hartree-Fock approximation. According to molecular orbital theory, electron mobility may be described by a single particle function (orbital) independent of the immediate motion of any other electrons (Saue, 2002; Strinati, 2005; Sherrill, 2009).

Fock operation for one electron is

$$\hat{F}(1) = \hat{h}(1) + \hat{V}^{HF}(1) \tag{3.60}$$

$\hat{F}(1)$ is Fock operation for one electron, $\hat{h}(1)$ Core Hamiltonian and $\hat{V}^{HF}(1)$ mean field operator. The mean field operator is going to be the magic of how we deal with the fact of its interactions with all other electrons having to be approximate

$$\hat{V}_i^{HF} = \hat{V}_i^{coul}(x_1) + \hat{V}_i^{exch}(x_1) \tag{3.61}$$

$$\hat{V}_i^{coul}(x_1) = \sum J_{ij}(x_1) \tag{3.62}$$

$$\hat{V}_i^{exch}(x_1) = \sum k_{ij}(x_1) \tag{3.63}$$

$$F(1)\chi_i(x_1) = E_i\chi_i(x_1) \tag{3.64}$$

where χ_i is spin orbital, E_i orbital energy.

$$E = \sum_i h_i + \sum_{i \langle j} J_{ij} - k_{ij} \tag{3.65}$$

J_{ij} is the electrostatic interaction between all pairs of electrons, k_{ij} exchange interaction between all the same spin of electrons. For example, we have a lithium element. It has 3 electrons Figure 3.11 and electron configuration is $1s^2$ $2s^1$.

$$E = J_{11} + 2J_{12} - k_{12} \tag{3.66}$$

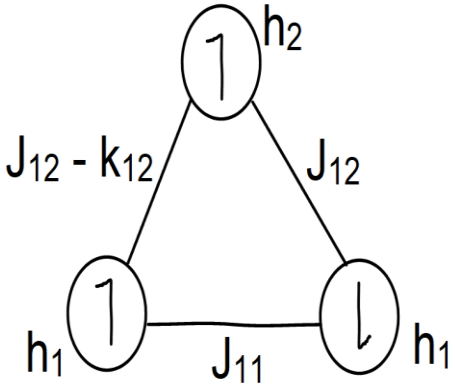

Figure 3.11. Electron quantum configuration of lithium (Li).

3.13.4. Slater determinant and change energy

Slater Determinant satisfy the anti-symmetry requirements of the Pauli’s principle. This Determinant is a proper mechanism to apply the antisymmetric principle for an arbitrary N-electron wave function. Slater Determinant is just a simple way of remembering a rule for how to write down the correct combination of these Hartree product in a way that is properly anti symmetrized and normalized and it save a lot of time to write down the wave function expectation of spin electrons and orbitals.

$$\Psi(\vec{1},\vec{2},\ldots.,\vec{N}) = \frac{1}{\sqrt{N!}}\begin{vmatrix} \chi_1(\vec{1}) & \chi_1(\vec{2}) & \cdots & \chi_1(\vec{N}) \\ \chi_2(\vec{1}) & \chi_2(\vec{2}) & \cdots & \chi_2(\vec{N}) \\ \vdots & \vdots & \ddots & \vdots \\ \chi_N(\vec{1}) & \chi_N(\vec{2}) & \cdots & \chi_N(\vec{N}) \end{vmatrix} \tag{3.67}$$

where $\frac{1}{\sqrt{N!}}$ Is Normalization constant, χ_1 , χ_2 and χ_N are spin orbitals and $(\vec{1},\vec{2},\ldots.,\vec{N})$ are electron coordinates. In a Slater determinant all electrons occupied in (columns) and spin orbitals occupied in (rows) in a molecular system. If the two electrons are in the same orbitals or the coordinates are the same, the nice property of the determinant is any two rows or two columns are equal, the entire determinant is going to zero, it means that the wave function is become zero $\Psi = 0$.

As an example, for Helium (He) element, it has two electrons 1s^2.

$$\Psi(\vec{1},\vec{2}) = \frac{1}{\sqrt{2!}} \begin{vmatrix} \chi_1(\vec{1}) & \chi_1(\vec{2}) \\ \chi_2(\vec{1}) & \chi_2(\vec{2}) \end{vmatrix} \tag{3.68}$$

It means that

$$\Psi(\vec{1},\vec{2}) = \frac{1}{\sqrt{2!}} [\chi_1(\vec{1})\chi_2(\vec{2}) - \chi_1(\vec{2})\chi_2(\vec{1})] \tag{3.69}$$

In the first term $\chi_1(\vec{1})\chi_2(\vec{2})$ says the electron 1 is spin up and electron 2 is spin down, and in the second term, $\chi_1(\vec{2})\chi_2(\vec{1})$ means that electron1 is spin down and electron 2 is spin up. Together, they indicate that is impossible to tell which electron is spin up and which electron is spin down, this is due to indistinguishability of the two electrons (Kohanoff, 2006).

3.13.5. Correlation energy

It is correct that in the Hartree-Fock approximation succeeded to expect in many cases, but when the HF equations have infinite basis sets, the HF limit is defined. Two reasons affect the accuracy of any Hartree-Fock calculations, first is the size of atomic orbitals basis set and the other one is accuracy of the electron repulsion. It means that the HF is not exact because the anti-symmetric wave function is approximated by a single Slater determinant representative under the Hartree-Fock technique for the quantum system. However, it was not possible to define the exact function of Wave as single Slater determinants. The single determinant method did not take coulomb correlation into consideration.

The HF wavefunction did not mention of the correlation effects, it neglected the electron configuration correlation of the system. The instantaneous coulombic interactions between electrons did not take into account. It characterized the electrons as travelling in the average potential field of the other electrons. The great deal of the modern system is describing the electronic structure of the quantum system by using the electron correlation into the interaction of the electrons. Electron correlation is separated into two correlations which are dynamical and static correlation.

Electrons resist each other and they're looking forward to being able to hold each other away. Their motion is however correlated, this correlation which decreases the energy of the system, by reducing the repulsion of electron-electron. This interaction was never reflected in the Hartree-Fock wavefunction and thereby uses the energy which is really extremely high. The Configuration interaction CI technique for achieving correlation energy gives a precise solution to the many-electron problem and it describes many Slater Determinant except a single Slater Determinant which was mentioned in the HF approach.

Electrons' movements are impacted by the existence of all other electrons, which is why correlation energy is defined as the difference between nonrelativistic energy (energy of the ground state) minus the HF limit energy eq (3.7) (Szabo and Ostlund, 1996; Atkins and Friedman, 2005).

$$E_{Corr} = E_{Exact} - E_{HF} \tag{3.70}$$

E_{Corr} is Correlation energy, E_{Exact} is Exact quantum mechanics energy or Ground state energy and E_{HF} is the Hartree-Fock energy. Therefore $E_{HF} \geq E_{Exact}$. The $E_{Corr} \leq 0$ it means that E_{Corr} is negative or equal to zero.

3.13.6. Thomas-Fermi theory and dirac change energy

Another theory is the Thomas-Fermi theory (1927) which has developed for the electronic structure of a many-body system. Thomas-Fermi model was considered as first step of the density functional theory because this method includes the electronic density as a key to solve the problem. Thomas-Fermi model, create the electronic density for an atom as an alternative of using wave function of the Schrodinger equation, because the density has quite enough information to calculate the properties and the ground state energy (Lieb, 2000; Panagiotopoulos, 2020).

$$E = T + V_{Ne} + V_{ee} \tag{3.71}$$

$$E_{TF}[\rho(\vec{x})] = \frac{3}{10}(3\pi^2)^{2/3} \int \rho^{5/3}(\vec{x})\, d^3\vec{x} + \frac{1}{2}\int \frac{\rho(x)\,\rho(y)}{|x-y|}\, d^3x d^3y + \int V_{ext}(x)\rho(x)d^3x \tag{3.72}$$

Where E_{TF} is Thomas-Fermi energy, $\rho(\vec{x})$ energy density of the x direction and V_{ext} is external potential.

This model is called semi-classical because they get both quantum and classical result together. The first term is the quantum result while the other last two term are the classical result.

The exchange energy added by Dirac in 1928, the theory became Thomas-Fermi-Dirac (TFD), but still the theory was inaccurate because the kinetic energy was only an approximation. After that, correlation added to the kinetic energy by Friedrich von Weizsacker which made the TF theory more valuable and upgraded to TFDW system for the massive atoms and huge electrons.

Another point is the bonding between molecules. In 1962, Edward Teller pointed that Thomas-Fermi did not predict the bonding between atoms, so molecules and solids cannot form in this theory (Kumar, 2012; Panagiotopoulos, 2020).

3.13.7. Density functional theory (DFT)

The Thomas-Fermi model had a remarkable advance in the development of approximation methods. This was a significant step to solve the computationally intensive, complex and difficult Schrödinger wave equation for atoms with two or more electrons. It was a good idea especially in the field of atomic physics for developing and wide research area to improve the electronic structure and properties of the materials. The accuracy of the

Thomas- Fermi approach was limited, but it created a new field of research called density functional theory (DFT), which described the quantum mechanics model methodology for the examination of electronic structure in many-body system (Atkins and Friedman, 2005; Kumar, 2012).

In 1964, Hohenberg and Kohn developed and proved another method, which had an important role for dealing the ground state of quantum many-body system is the Density functional theory (DFT) which involved the density of the electrons. And later in 1998 Kohn who was developed the DFT and then developed the computational methods in quantum chemistry shared a Noble prize in chemistry (Kaxiras, 2003; Kohanoff, 2006).

DFT model is more popular than the HF model, the reasons are because in DFT model the electron correlation is less complicated in the field of computational method, and it can count more than 100 molecules which shortens the time (Atkins and Friedman, 2005; Sholl and Steckel, 2009).

3.13.8. Hohenberg-Kohn's theorems

In 1964, Hohenberg and Kohn published two theorems and started the basis for the density functional theory. They approach DFT as an exact theory of the many-body system, it means that everything could be obtained through the electron density (Koch and Holthausen, 2001; Kohanoff, 2006). Fundamentally, the theorems are stating the followings:

The first of the Hohenberg and Kohn, the ground state energy from Schrödinger's equation is a unique function of the electron density. As a result of this configuration, there is a direct correlation between the ground state wavefunction and the electron density.

In the Hamiltonian operator from the Schrödinger equation, we explicitly determine the external potential V_{ext}. Then with this external potential we can calculate the eigen state of the Hamiltonian. Having the eigen state of the Hamiltonian, we can have the ground state, we can obtain the electronic density associated with that ground state. Also, HK say that if we have a ground state electron density, this ground state electron density uniquely determines the external potential. It means with that eigen state, we can calculate everything we want Fig 3.12.

$$\rho_0(r) \Leftrightarrow \hat{H} \tag{3.73}$$

$$\hat{H} = -\frac{\hbar^2}{2m_e}\sum_i \nabla_i^2 + \frac{1}{2}\sum_{i<j}\frac{e^2}{|r_i - r_j|} + \sum_i V_{ext}(r_i) \tag{3.74}$$

$$\hat{H} = \hat{T} + \hat{V}_{ee} + \hat{V}_{ext} \tag{3.75}$$

$$\hat{H} = \hat{F}_{HF} + \hat{V}_{ext} \tag{3.76}$$

$$\hat{F}_{HF} = \hat{T} + \hat{V}_{ee} \tag{3.77}$$

$$\begin{tikzcd}
V_{ext}(r) \arrow[d] & \rho_0(r) \arrow[l, "HK"'] \\
\Psi_i(r) \arrow[r] & \Psi_0(r) \arrow[u]
\end{tikzcd}$$

Figure 3.12. Representation scheme of the Hohenberg and Kohn theorem.

Until now, from the first theorem in the ground state density, we can obtain all the properties of the interest, but the problem is here, it did not say anything about what the functional actually is, that is why the second theorem of the Hohenberg and Kohn is established and defined an significant property of the functional. It state that Shrödinger equation's entire solution has a total electron density that is equal to the energy of the functional (Koch and Holthausen, 2001; Martin, 2004; Sholl and Steckel, 2009).

$$E[\rho(r)] = \int \rho(r)\ V_{ext}(r)dr + F_{HF}[\rho(r)] \tag{3.78}$$

$$F_{HF}[\rho(r)] = \min_{\Psi \rightarrow \rho} < \Psi|T + V_{ee}|\Psi > \tag{3.79}$$

$E[\rho(r)]$ is the energy in ground state density which is taken into account in terms of the HK functional, $F_{HF}[\rho(r)]$ is the Functional of the function of electron density, T is the kinetic energy, V_{ext} is the external potential, $\rho(r)$ is the electron density and Ψ is the wave function.

3.13.9. Kohn-Sham equations

One year later, in 1965 a theorem was published, which is called Kohn-Sham theorem, they described a way to solve the HK theorem. The KS approach is to replace the original difficult interacting particle Hamiltonian with a different one which is solved more easily: which is a non-interacting particle Hamiltonian with an effective potential Vs.

$$\left[-\frac{1}{2}\nabla^2 + V(r) + V_H(r) + V_{XC}(r)\right]\Psi_i(r) = E_i\Psi_i(r) \tag{3.80}$$

$$V(r) = \sum_{i\alpha}^{M}\frac{Z}{r_{i\alpha}} \tag{3.81}$$

$$V_H(r) = \frac{\delta E_H[\rho]}{\delta\rho(r)} = \int\frac{\rho(\grave{r})}{|r-\grave{r}|}d\grave{r} \tag{3.82}$$

$$V_{XC}(r) = \frac{\delta E_{XC}(r)}{\delta\rho(r)} \tag{3.83}$$

$$V_{effective}(r) = V_S(r) = V_H(r) + V_{XC}(r) + V(r) \tag{3.84}$$

From the equation (3.80), the first item in the left-hand side denotes the kinetic energy of the electrons. The second item is significant for the electron and nucleus attraction. The third item is the Hartree potential, because in order to explain the Kohn- and Sham equations, we have to describe the Hartree potential and the last term is the exchange-correlation energy (Atkins and Friedman, 2005; Sholl and Steckel, 2009).

It is clear from Figure 3.13, for the same ground state electron density, we define a non-interacting system having the same electronic density and if we apply the H-K theorem for non-interacting system, according to that ground state electronic density uniquely specify the external potential of each electron which we call the K-S potential.

When we have the K-S potential, we can calculate any eigen states for one particle and one electron eigen state. If we have one particle wave function, we can build the Slater determinant of the N particle system. Once we have that Slater determinant, we can figure out the ground state electronic density.

$$\begin{tikzcd}
V_{ext}(r) \arrow[d] & \rho_0(r) \arrow[l, "\text{HK}"'] \arrow[r, leftrightarrow, "\text{KS}"] & \rho_0(r) \arrow[r, "\text{HK}_0"] & V_{KS}(r) \arrow[d] \\
\Psi_i(r) \arrow[r] & \Psi_0(r) \arrow[u] & \Psi_i = 1, N_e(r) \arrow[u] & \Psi_i(r) \arrow[l]
\end{tikzcd}$$

Figure 3.13. Represent the Kohn and Sham approach which is H-K theorem applied to the non-interacting problems.

Once we have the total Hamiltonian, we could calculate the eigen state. The ground state electronic density of the real system will be the same as the non-interacting ground state electronic density and this ground state electronic density could be obtained from the Slater determinant.

$$\rho_{KS}(r) = 2\sum_{i} \Psi_i^*(r)\Psi_i(r) \tag{3.85}$$

One more point is that, the evaluation of exact kinetic energy functional is difficult due to many-body effect.

The number of research papers published based on DFT follows a nearly exponential growth as a function of the years. It is found out that from the Kohn and Sham approach is very effective approximation which are currently a source of many computations which try to anticipate the characteristics of condensed matter and large molecular systems on the first principle or ab initial basis. LDA and GGA are surprisingly precise, especially noticeable for wide-band systems like semiconductors IV and II-V and metals such as Na & Al and insulators for instance diamonds (Martin, 2004; Sholl and Steckel, 2009).

3.13.10. Local density approximation (LDA)

A simplest approximation that is widely use for the exchange-correlation energy which was proposed by K-S in order to implement their method is called the LDA. This approximation is currently used in different Ab initio calculations.

$$E_{XC}^{LDA}[\rho] = \rho(\vec{r})E_{XC}^{unif}[\rho(\vec{r})]d^3\vec{r} \tag{3.86}$$

E_{XC}^{unif} is the exchange-correlation energy per particle of the homogeneous uniform electron gas with a constant density ρ. Due to LDA we can split the exchange correlation electron gas into two terms, the exchange energy functional and correlation energy functional which are (Atkins and Friedman, 2005; Sholl and Steckel, 2009):

$$E_{XC}^{unif}[\rho(\vec{r})] = E_X^{unif}(\rho) + E_C^{unif}(\rho) \tag{3.87}$$

Exchange energy basically is the average of the electron potential energy, considered as the K-S wave function minus the Hartree energy. But with considering electron gas, with in the K-S model we have this fictious system with non-interacting electrons. The wave function for that system is going to be the Slater determinant, and that Slater determinant is the same as the one we use for H-F model and with this H-F model, we already have calculated the exchange energy. E_C^{unif} cannot be calculated analytically, this quantity has been found numerically.

$$E_X(\rho) = -\frac{3}{4}\left(\frac{3\rho}{\pi}\right)^{1/3} \tag{3.88}$$

There are a lot of information on the performance of the LDA approximation to have different properties of the systems such as electronic structure, band structure, elastic, vibrational properties, density of state, bond length and lattice constants are good enough to compare with the experimental results. The accuracy of the LDA is decreases with varying the constant electron density for many atoms or molecules. Also, there are some concepts that are not well known or found out that LDA is not accurate to calculate in, like binding energy especially in the cohesive energies and Van der Wall interactions could not be properly described (Atkins and Friedman, 2005; Kohanoff, 2006).

3.13.11. Generalized gradient approach (GGA)

Another approximation of the K-S theorem is called the (GGA) which is satisfy the exact properties of the exchange-correlation densities, which are not the uniform electron densities, it is based for slowly varying densities. The exchange- correlation potential of the GGA approximation is (Koch and Holthausen, 2001; Martin, 2004):

$$V_{XC}^{GGA}(r) = V_{XC}[\rho(r), \nabla \rho(r)] \tag{3.89}$$

The exchange-correlation energy of the GGA approximation is:

$$E_{XC}^{GGA} = \int d^3r\, f[\rho(r), \nabla \rho(r)] \tag{3.90}$$

In the GGA approximation is divided into two terms which are:

$$E_{XC}^{GGA} = E_X^{GGA} + E_C^{GGA} \tag{3.91}$$

Furthermore, the GGA approximation in most of the cases is improved and accurate than the LDA approximations such as the binding energies, atomic energies, bond lengths and angles. But in the case of semiconductors the LDA is better described than the GGA except for the binding energies, and in the lattice constants for the noble metals like (Au, Ag and Pt) the GGA is overestimated (Koch and Holthausen, 2001; Kohanoff, 2006).

3.13.12. Pseudopotential method

In order to explore high-lying atomic states, the notion of pseudopotentials was presented by Fermi in 1934. Hellman subsequently advocated the use of pseudopotentials for calculating the energy levels of alkali metals. But it was not taken into account until late 1950s when activities began to increase in the field of condensed matter physics that the significant use of pseudopotential occurred. The major benefit of pseudopotentials is that it is essential to analyze just valence electrons. According to the Fermi, all wave function properties of the electrons near the core are complex and difficult to calculate; the weak potential is meant to be more precise with the wave function. because it faces just with outer electrons (Cohen, 2005; Kohanoff, 2006).

In the pseudopotential method, the electronic structure is divided into 3 categories of states. These are the core states, semi-core states and valence states. The core states participate and involve the chemical bonding activities and it is highly localized because they are close to the nucleus and the radius is small. They are tightly connected to the nucleus and that is called the frozen core states, it means that the core electrons are not important and does not have a role in the chemical bonding. Semi-core states that are states which are localizable and polarizable, it means in some cases that are related to the core states and in different cases that are related with the valence states. The last state is the valence states which are defined as a responsible state for chemical bonding and less tightly bounded with the nucleus (Kohanoff, 2006; Sholl and Steckel, 2009).

$$Z_v = Z - Z_{core} \tag{3.92}$$

The bare coulomb interaction is an interaction that all electrons (core electrons and valence electrons) are participate in this kind of interaction. However, in the pseudopotential there is no more bare coulomb interaction available. It replaced by the screened coulomb potential which means that it replaced with a smooth pseudo wavefunction. The true potential also replaced by a pseudopotential (PS) or effective core potential as seen in Figure 3.14. For computations using pseudopotential in the atoms, establish a minimum energy cut-off in the calculations.

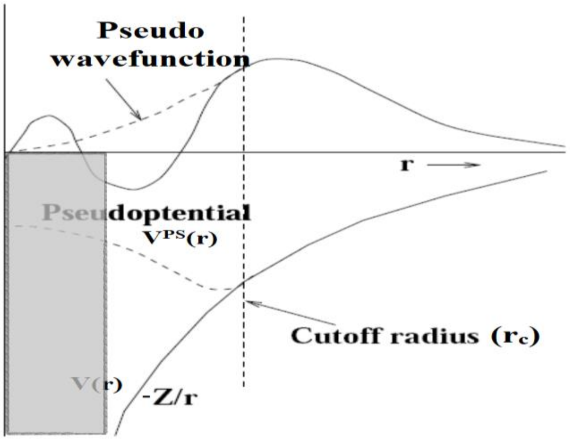

Figure 3.14. schematic illustration of the pseudo wave function, pseudopotential with the all-electron wave function, and all-electron potential.

As it is clear the cut-off radius in the Figure 3.14 is a point at which the pseudo wavefunction and the all-electron wave functions are allied together, it means at and after that point the energy and the electron densities for both of them are the same (Sholl and Steckel, 2009).

4. RESULTS AND DISSCUSION

4.1. $LiPaO_3$ Crystal

The $LiPaO_3$ crystal is a cubic structure. According to its atomic configuration this material is belong to the perovskite cyrstals. The full name of $LiPaO_3$ is Lithium Protactinium Oxide. Space group of this crystal is $Pm\bar{3}m$ (Space group No: 221) and the Point group is $m\bar{3}m$.

In this study we first performed cut-off energy and k-point optimizations. Afterwards volume optimization within two approximations such as GGA and LDA. We calculated the lattice parameters with both approximations. In order to compare all of our results we performed our calculations within both of the approximations.

4.2. Structural Properties of $LiPaO_3$ Crystal

In order to investigate the structural properties of $LiPaO_3$ first of all, we performed cut-of energy optimization in GGA and LDA approximations. We obtained our calculated cut-off energy value as 40 Hartree with both approximatios. Then we did the k-point optimization. For our crystal we found the number of k-points as 35 within 10x10x10 Monkhorst-Pack grid again with both approximations. Afterwards, we performed volume optimization in order to see the relations between the total energy vs pressure and volume also the relation between the volume and the pressure for $LiPaO_3$ crystal. At this step, we calculated the lattice parameters with GGA and LDA approximations. We noticed that the results under both approximations are very close to each other and with the literature.

ABINIT dependes on pseudo-potantial approximation, and uses some types of pseudo-potantials. Here, we used Trouller-Martins pseudo-potantials for both approximations such as GGA and LDA. All those results are given with graphs, tables and detailed explanations thruoghout the thesis.

4.2.1. Cut-off energy

According to Bloch's theorem, the wave function can be written as a summation of discrete plane wave set for a $\vec{k}$ point equation (4.1) which has an infinite number of terms (Kittel, 2005).

$$\psi_{n\vec{k}}(\vec{r})=\sum_{\vec{G}} C_{n,\vec{k}+\vec{G}}\, e^{i(\vec{k}+\vec{G})\vec{r}} \tag{4.1}$$

To handle with this kind of wave set is very difficult. But luckily, it was found that, there is an energy value, after that all calculations with this wave function is very close to each other. So to continue further than this value results a very huge time loss and computer efficiency. So we can finish this summation at a value before infinity, which is called as cut-off energy. This limit value can be obtained by performing cut-off energy optimization. In this optimization, we can see the relation ship with the total energy of a crystal and the cut-off energies. When it is ploted this relationship, it is seen that after a limit value of cut-off energy total energy becomes stable. This value or a little bigger than this value can be chosen as cut-off energy.

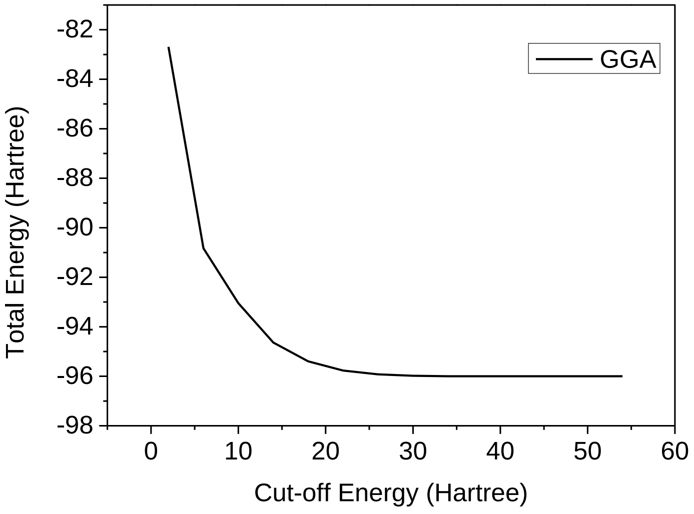

Figure 4.1. The change in total energy with respect to cut-off energy for $LiPaO_3$ under GGA.

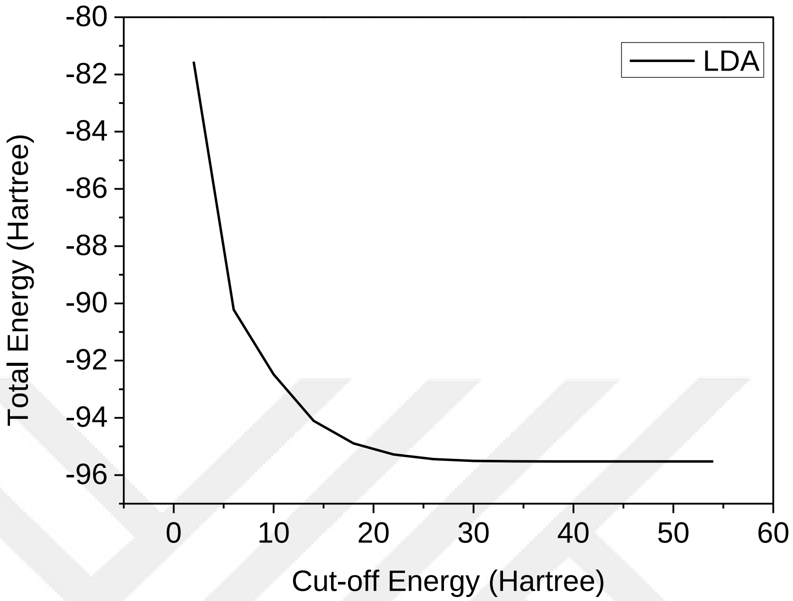

Figure 4.2. The change in total energy with respect to cut-off energy for $LiPaO_3$ under LDA.

In this study cut-off optimization is done for GGA and LDA. We ploted our results in Figure 4.1 and 4.2, and we decided our cut off value as 40 Hartree (1088.45 eV) for both approximations. From Figs. 4.1 and 4.2, it is seen that the total energy value under GGA is -95.96 Hartree (-2611.20 eV) and under LDA is -95.56 Hartree (-2600.32 eV) which are very close to each other.

4.2.2. Number of k-points

In order to do the calculations with Density Functional Theory, we need to take integrals of the wave vectors over the Brillouin zone. However, there is a huge number of k-points in a Brillouin zone. So these calculations are very difficult and time consuming. In order to get rid of that difficulty, Monkhorst and Pack introduced a method by using the symmetry properties of the crystals (Monkhorst-Pack, 1976). They revealed that there are some k-points which has the same symmetrical properties and wave functions with the neighbourhood k-points. So it is enough to consider just that k-point instead of all of them.

So, we can use the k-points with different wave vectors. In order to investigate those k-points, the crystal is divided in to two parts along x, y and z (2x2x2 Monkhorst-Pack grid) directions. Afterwards, the crystal is divided into four, six, eight, etc… parts within 4x4x4, 6x6x6, 8x8x8, etc… Monkhorst-Pack grids, respectivel in order to calculate the number of k-points with different symmetry properties and wave functions. This is called k-point optimization. By increasing the number of grids the number of k-points increases. During this optimization we get the relationship between the number of k-points and the total energy values. We can also obtain the dependence of the total energy and the Monkhorst-Pack grids as given in Figures 4.3 and 4.4, for GGA and LDA approximations, respectively.

YÖK watermark

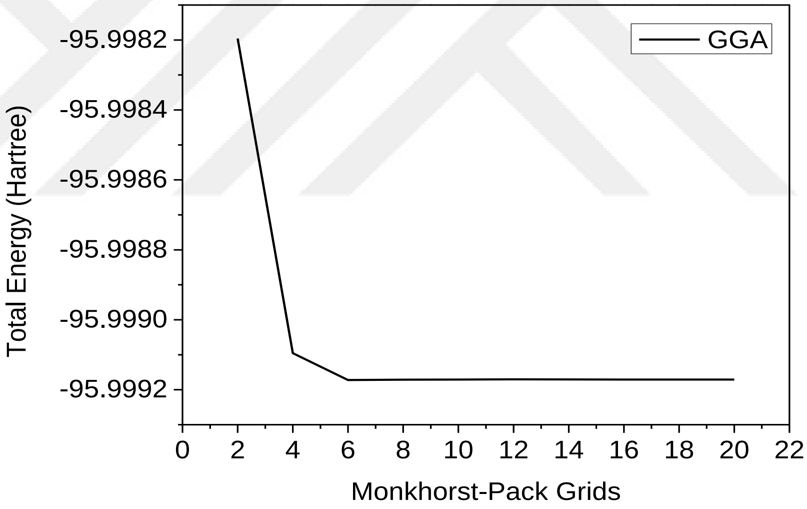

Figure 4.3. Total energy with respect to Monkhorst-Pack grids under GGA approximation for $LiPaO_3$.

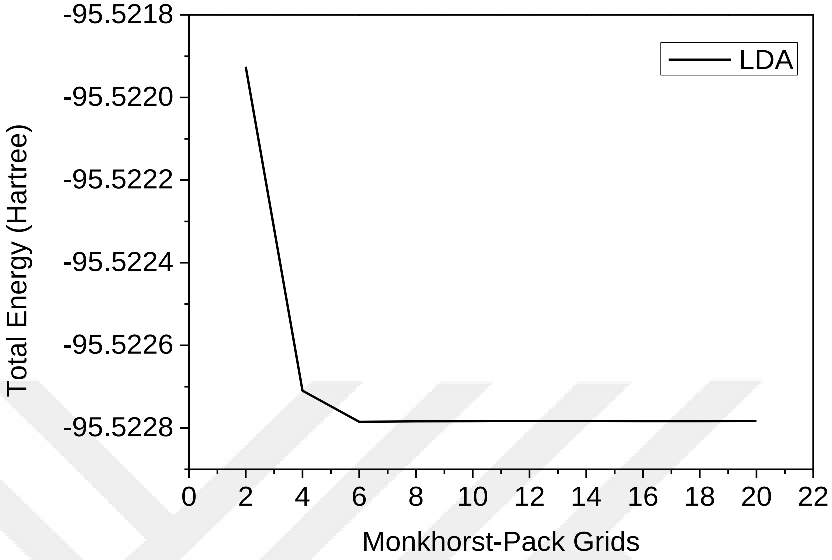

Figure 4.4. Total energy with respect to Monkhorst-Pack grids under LDA approximation for $LiPaO_3$.

YÖK

As seen from the graphs, it is convenient to chose the value of Monkhorst-Pack grids as 10x10x10 for both approximations. For that amount of grids there are 35 k-points.

From the above two figures, it is also noticed that the total energies are very close to both each other and with the results obtained from the cut-off optimizations, that is -95.99 Hartree for GGA and -95.52 for LDA approximations.

4.2.3. Volume optimization

The following step was volume optimization. This optimization gives the calculated lattice parameters, total energy vs volume, total energy vs pressure and pressure vs volume alterations. First of all, we plotted total energy vs volume graphs for GGA Figure 4.5 and for LDA Figure 4.6. When we examine these graphs, we see that there is a minimum point. This point gives the volume value of the decisive $LiPaO_3$ crystal. From this volume values one can calculate the lattice parameters. The calculated lattice parameter is 8.9052 Bohr for GGA and 8.7440 Bohr for LDA, which are very close to the literature value (8.8003 Bohr) . From this point we prefered to continue with GGA approximation to our calculations. The total energy at this point is also the value for the decisive $LiPaO_3$. This total energy values for both approximations are consistent with the values obtained while cut-off energy and k-point optimizations.

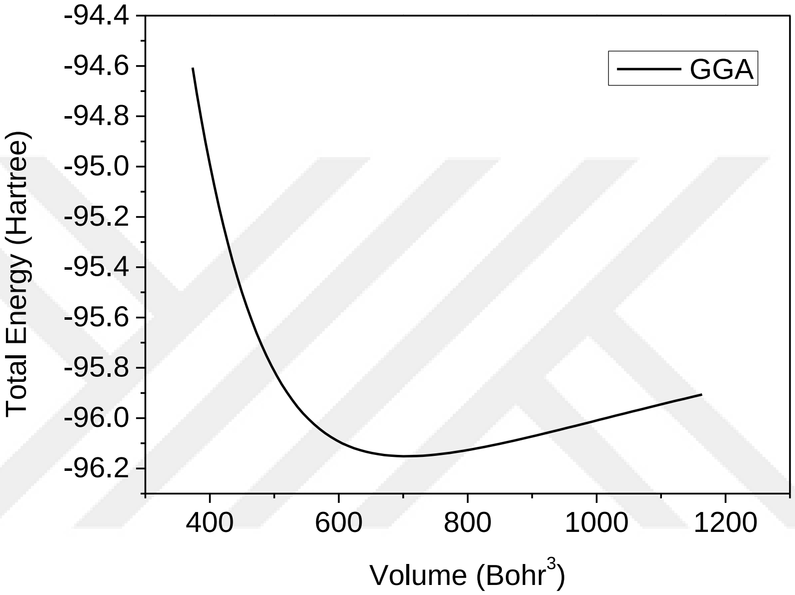

Figure 4.5. Total energy vs. volume graph of $LiPaO_3$ crystal under GGA.

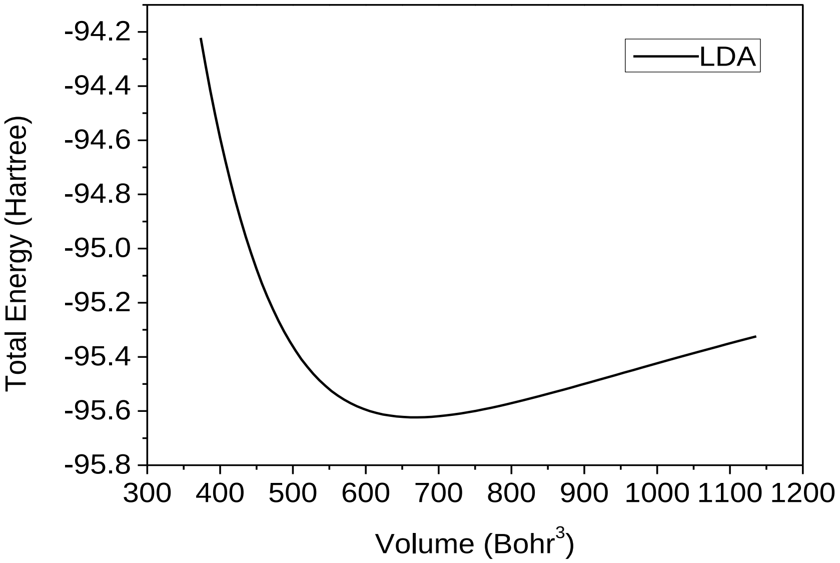

Figure 4.6. Total energy vs. volume graph of $LiPaO_3$ crystal under LDA.

We then plotted the total energy vs pressure graphs for GGA Figure 4.7 and for LDA Figure 4.8. The minimum point of those graphs also give the decisive situation of $LiPaO_3$ crystal. In the ground state the for a decisive crystal the pressure must be equal to zero. This condition is satisfied under both of the approximations for $LiPaO_3$ as seen from Figures. 4.7 and 4.8.

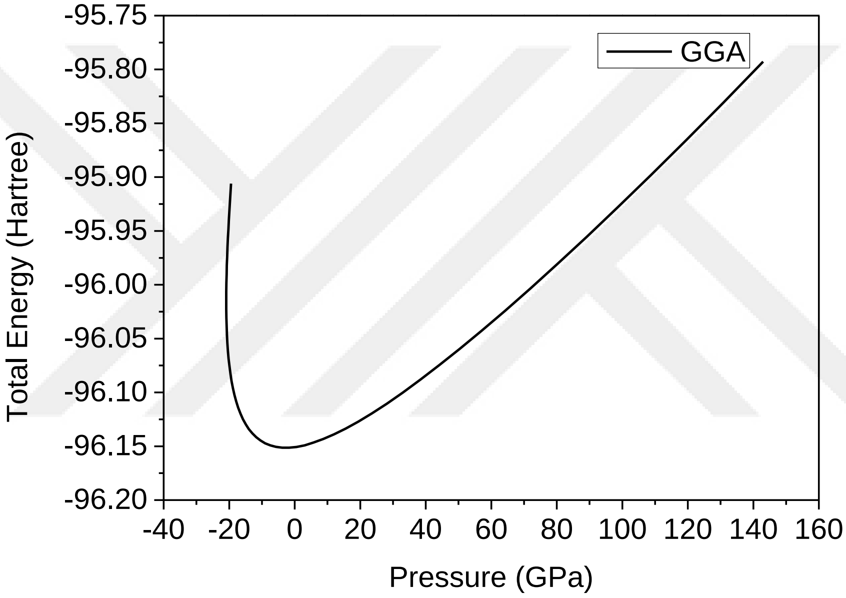

Figure 4.7. Total energy vs. pressure graph of $LiPaO_3$ crystal under GGA.

YÖK watermark

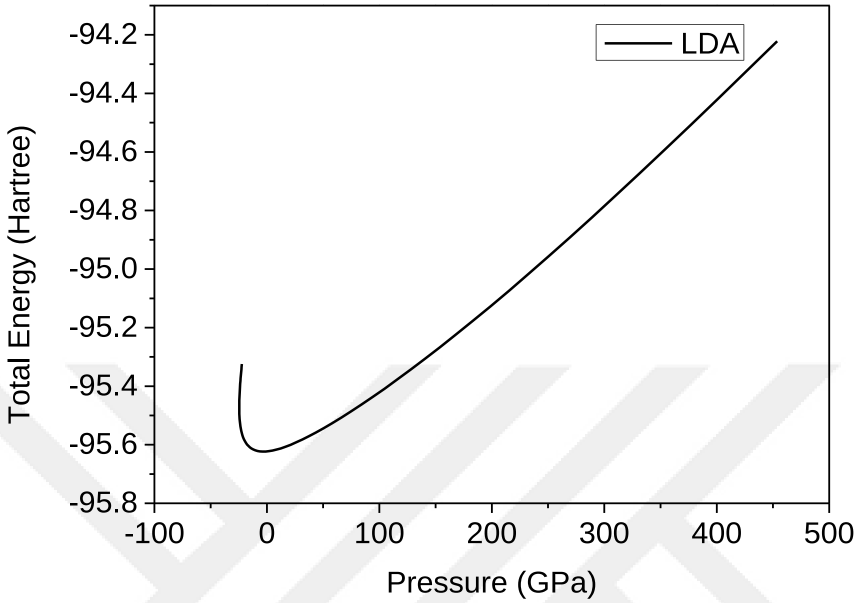

Figure 4.8. Total energy vs. pressure graph of $LiPaO_3$ crystal under LDA.

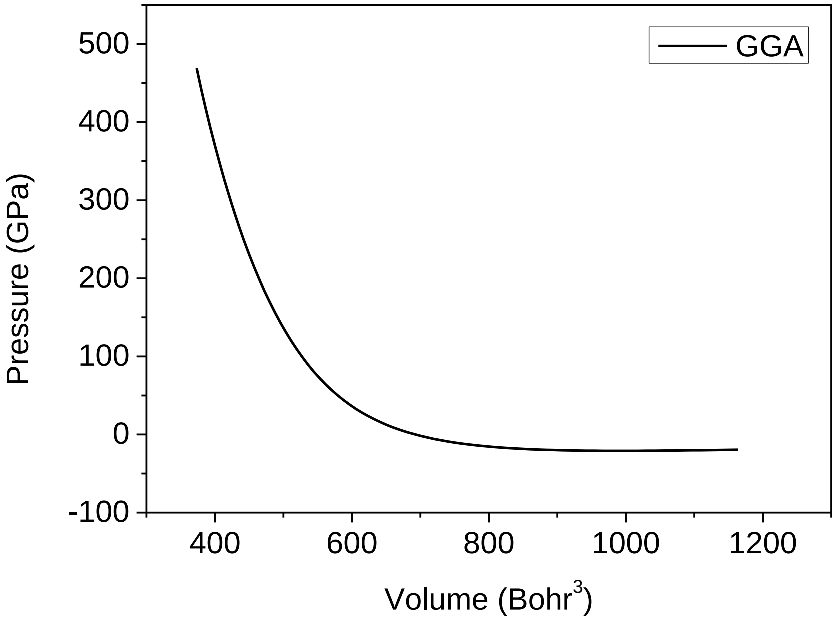

Figure 4.9. Pressure vs. volume graph of $LiPaO_3$ crystal under GGA.

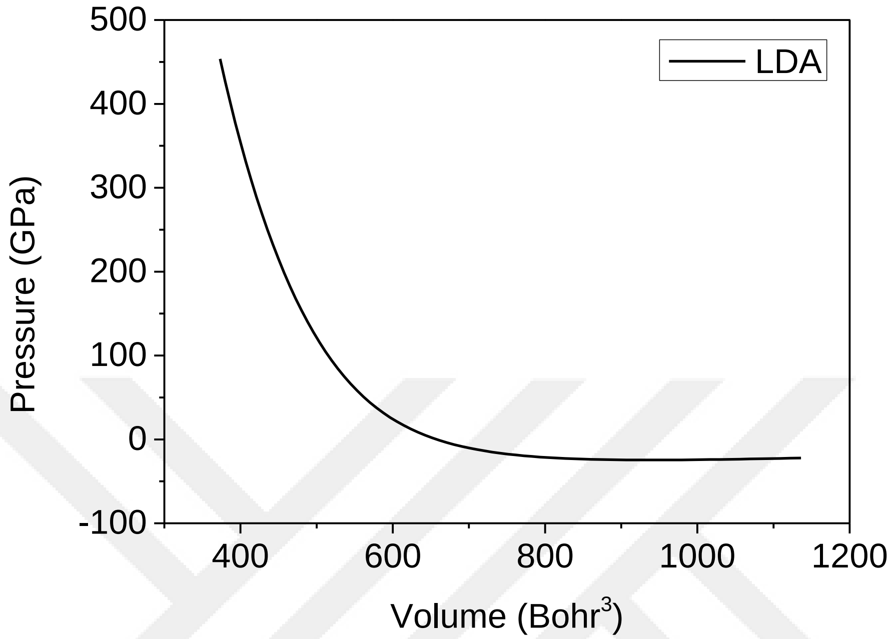

Figure 4.10. Pressure vs. volume graph of $LiPaO_3$ crystal under LDA.

In this part of our study we investigated the pressure and volume relationship. In Figures 4.9 and 4.10, we plotted the pressure vs volume values for GGA and LDA, respectively. It is seen that pressure and volume are inversely relational, as expected.

4.2.4. Lattice parameters of $LiPaO_3$ crystal

The lattice parameters are also obtained from the volume optimization. As given in the previous section, the calculated lattice parameter is 8.9052 Bohr for GGA and 8.7440 Bohr for LDA. We also plotted those graphs and gave in Figure 4.11 for GGA and in Figure 4.12 for LDA. The minimum points show the decisive $LiPaO_3$ crystal.

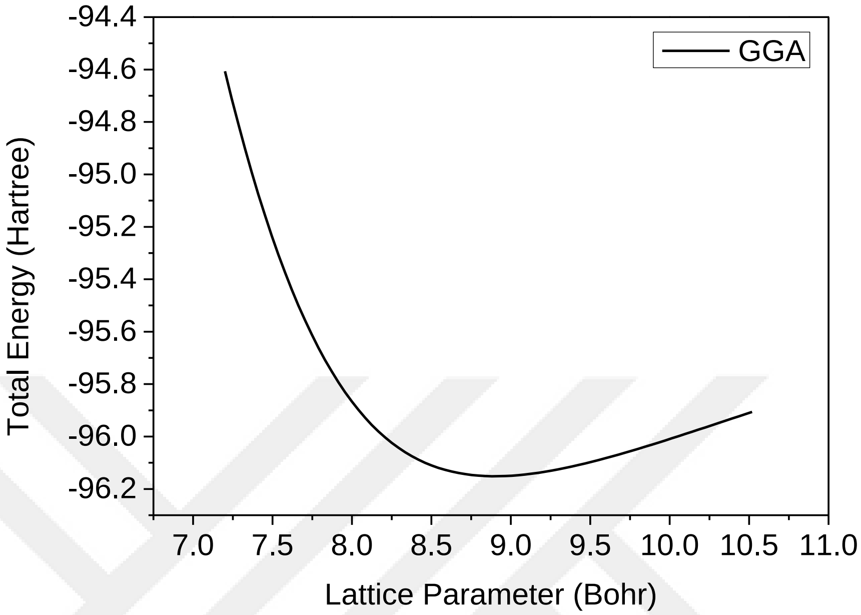

Figure 4.11. Total energy vs. lattice parameter graph of $LiPaO_3$ crystal under GGA.

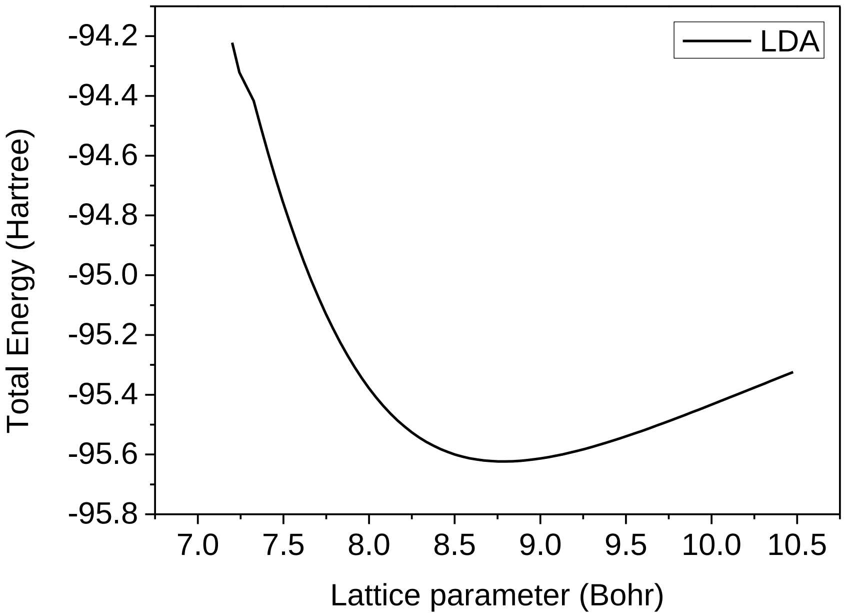

Figure 4.12. Total energy vs. Lattice parameter graph of $LiPaO_3$ crystal under LDA.

4.2.5. Unit cell of $LiPaO_3$ crystal

We focused on the unit cell structure, bonds and the bond lenghts of $LiPaO_3$ crystal by using VESTA computing programme (Momma and Izumi, 2011). The space group of $LiPaO_3$ is $Pm\bar{3}m$ (No:221) and its point group is $m\bar{3}m$. In Figure 4.13 the unit cell of $LiPaO_3$ is given. We also focused on the bonds and bond lengths. In unit cell the bond length between the Pa and O atoms is 4.1001 Bohr, and the bond lenght between Li and O atoms is 3.0684 Bohr.

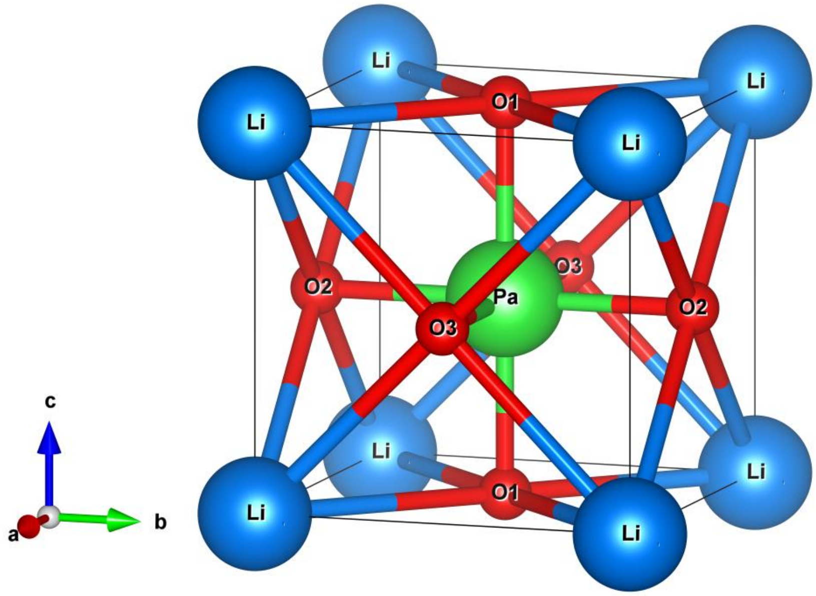

Figure 4.13. The Unit cell of the $LiPaO_3$ crystal (Momma & Izumi, 2011).

4.3. The Electronic Properties of $LiPaO_3$ Crystal

We investigated the electronic structure of $LiPaO_3$ crystal by computing and plotting the electronic band staructure, density of states and partial density of state of this crystal. We plotted the electronic band graph according to $\Gamma - X - M - \Gamma - R - X$ high symmetry points in the 1^{st} Brillouin zone. The density of states and the partial density of state values are given with arbitrary units. We performed the next calculations such as electronic, optic, elastic properties with the GGA approximation.

4.3.1. Electronic band structure

The electronic band structure of $LiPaO_3$ crystal is obtained with GGA Figure 4.14 and LDA Figure 4.15. The graphs obtained with both of the approximations are very close to each other. There are 12 valance bands of the $LiPaO_3$ crystal. In the figures with 9 conduction bands, there are 21 bands. The three of the valence bands are belong to core electrons which around -15 eV energy values. The band gap is 2.10 (2.19) eV with GGA (LDA), so $LiPaO_3$ is semiconductor with a direct transition. The energy of top level of the valence band, filled with the electrons is called as Fermi energy. In Figures 4.14 and 4.15, the Fermi level adjusted as 0 eV and it is shown with horizontal red dashed line.

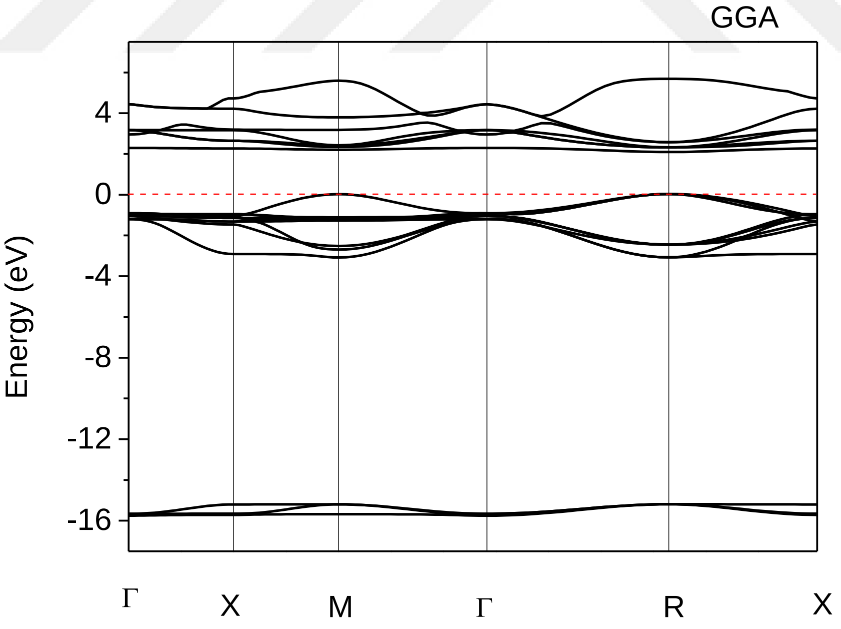

Figure 4.14. Electronic band structure of $LiPaO_3$ under GGA. The red line is the Fermi energy level.

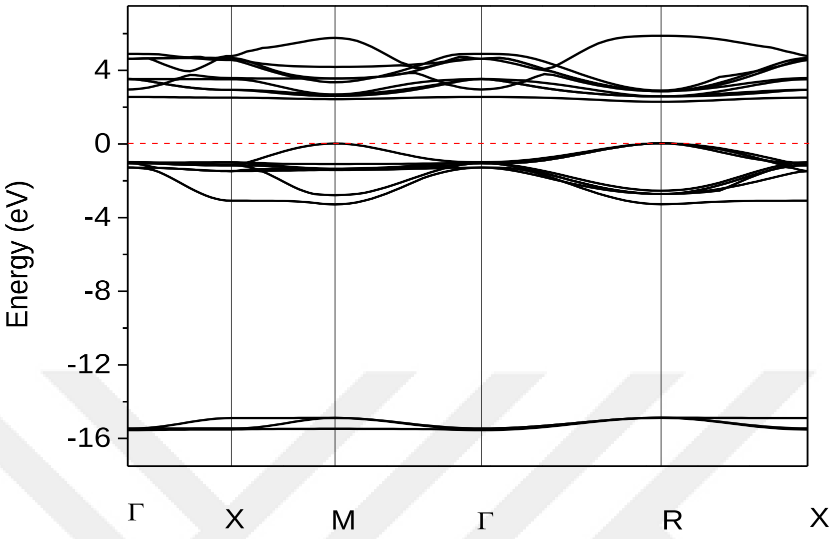

Figure 4.15. Electronic band structure of $LiPaO_3$ under LDA. The red line is the Fermi energy level.

Since the bands around the Fermi level are a little bit mixed, we have given the electron band structures between the -4 and 6 eV values in the following two graphs, namely Figure 4.16 for GGA and Figure 4.17 for LDA in order to investigate more detailed.

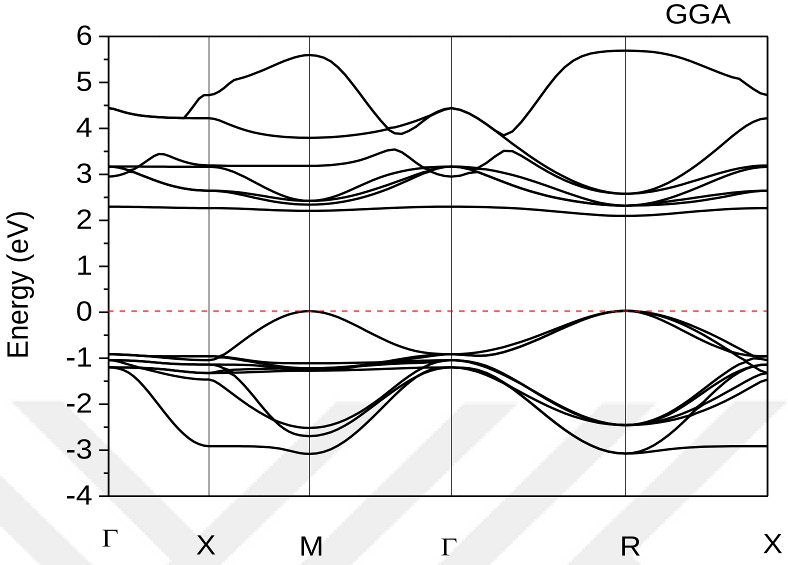

Figure 4.16. Electronic band structure of $LiPaO_3$ between -4 and 6 eV energy values under GGA.

According to Figure 4.16 Figure 4.17 (except for the core electron bands), the minimum energy value of the valence band is -3.09 (-3.27) eV and the maximum energy value of the valence band is matched to 0 (0) eV. The minimum energy value of the conduction band is 2.10 (2.19) eV and the maximum energy of that is 5.67 (5.87) eV for GGA (LDA).

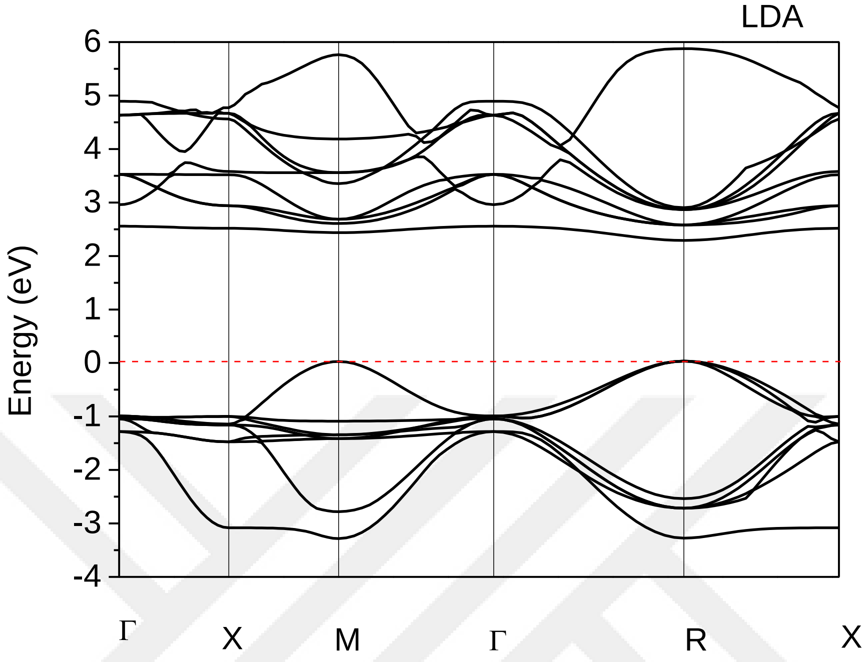

Figure 4.17. Electronic band structure of $LiPaO_3$ between -4 and 6 eV energy values under LDA.

4.3.2. Density of states (DOS)

Afterwards we have calculated and plotted the density of states (DOS) of $LiPaO_3$ crystal for both GGA Figure 4.18 and LDA Figure 4.19 approximations. From Figures 4.18 and 4.19, the contributions of the core electrons, valence and conduction bands are seen clearly. Again the Fermi energy level is matched to 0 eV energy value. The core electron bands are around -15 eV as obtained from electronic band configuration graphs. The minimum and the maximum energy values of the valence and conduction bands are also consistent with the electronic band graphs for both approximations. Also the band gap values can be obtained from density of states graphs, which are consistent with the obtained values in this study.

The density of states are given in arbitrary units and the energy values are given in eV.

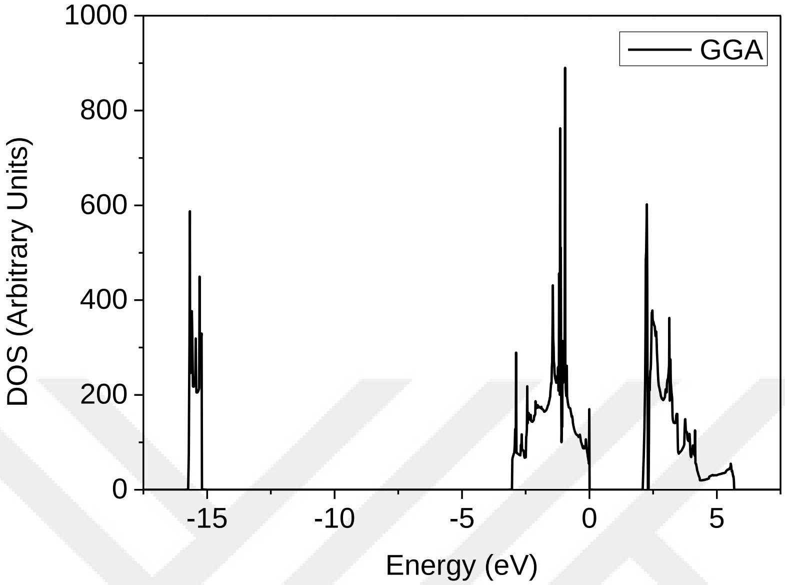

Figure 4.18. Density of states graph of $LiPaO_3$ crystal under GGA.

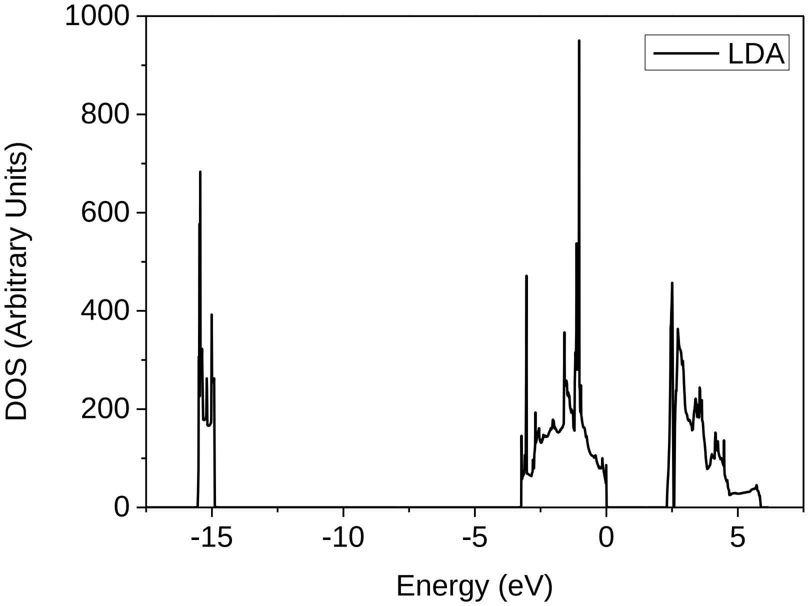

Figure 4.19. Density of states graph of $LiPaO_3$ crystal under LDA.

YÖK

4.3.3. Partial density of states (PDOS)

In the investigation of the electronic properties of the $LiPaO_3$ crystal, we also calculated the partial density of states which are the density of states of each type of the atoms in the crystal. First of all, we focused on the conrtibutions of the Li atoms under GGA and LDA approximations. In Figure 4.20 the partial density of satets graphs under GGA and LDA are given. The both of the graphs are very similar to each other. The main contribution of the Li atom is from conduction bands with mainly s states. There is also slightly contribution with p states in the conduction bands. For Li atoms, it is also noticed that there is a very slightly contribution from the valence bands to the density of states with s and p states.

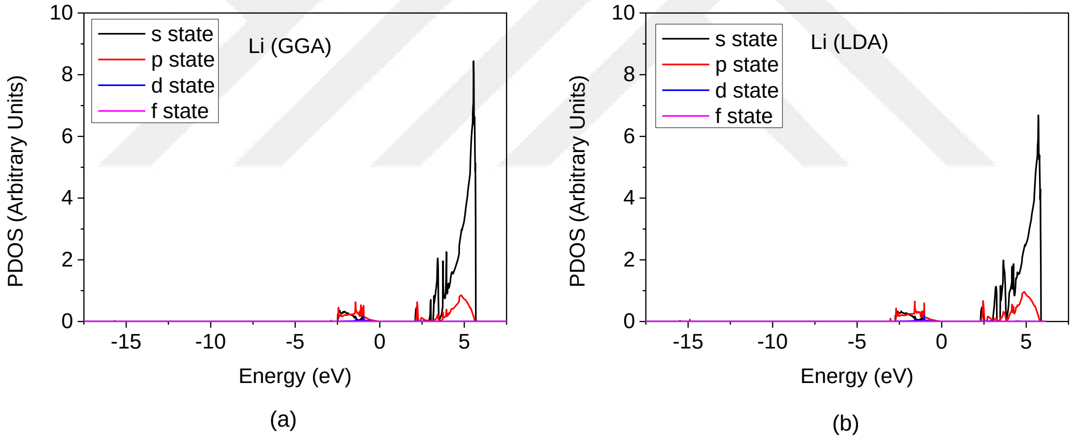

(a)

(b)

Figure 4.20. The partial density of states (PDOS) graph of Li atom under (a) GGA and (b) LDA approximations.

The contribution of Pa atom under GGA and LDA are given in Figure 4.20. From this figure, it is seen that the main contributions for valence and the conductionn bands are from the f states. The contribution from valence is very few but from the conduction bands are very high.

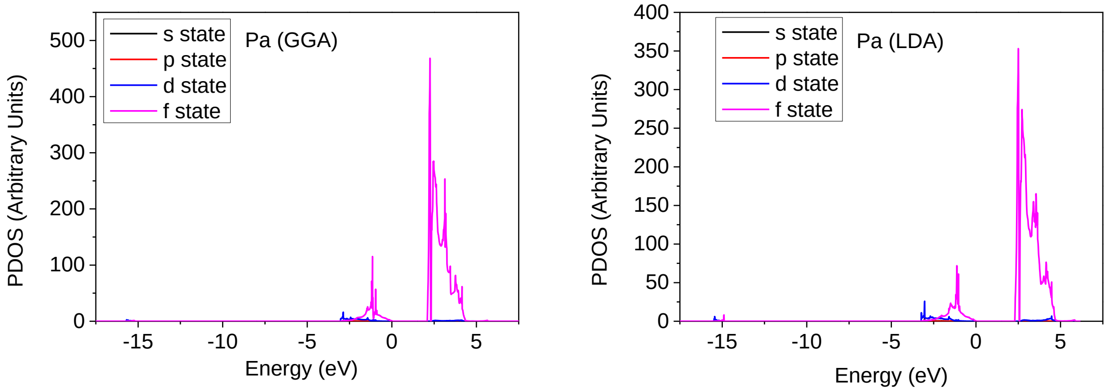

(a)

(b)

Figure 4.21. The partial density of states (PDOS) graph of Pa atom under (a) GGA and (b) LDA approximations.

There are three oxygen atoms in the $LiPaO_3$ crystal. The partial density of states of those O(1), O(2) and O(3) atoms with GGA and LDA approximations can be seen in Figure 4.22. As seen from this figure the characteristic of those atoms are very similar. There are contributions from the core electrons and the valence bands. The contribution of the core electrons are composed mainly from the s states and the contribution of the conduction bands are mainly from the p states.

Also, it is noticed that the addition of the contributions of all these atoms give the density of states for both of the approximations, as given in the previous section.

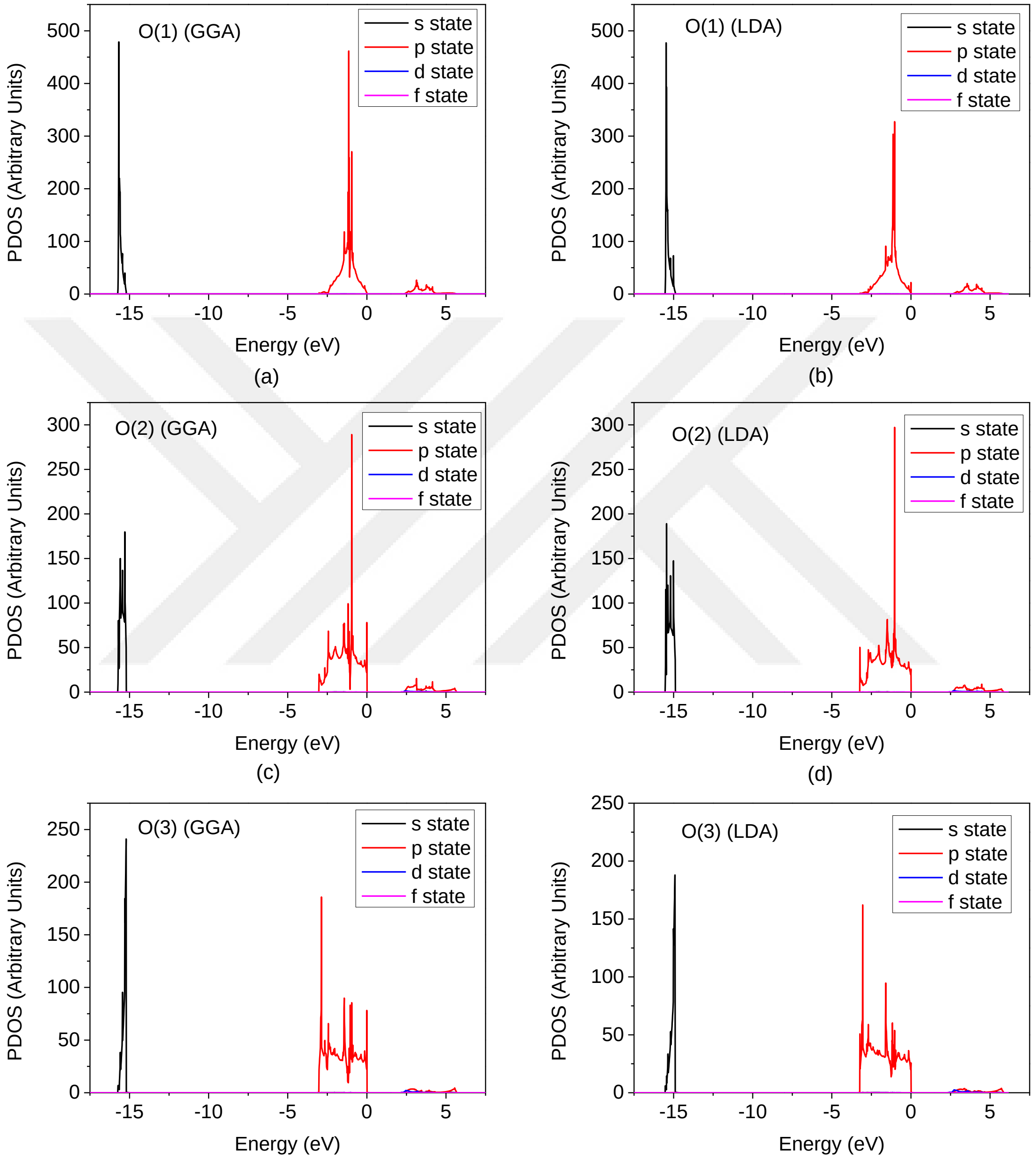

(a) (b) (c) (d) (e) (f)

Figure 4.22. The partial density of states (PDOS) graph of O(1) atom under (a) GGA (b) LDA, O(2) atom under (c) GGA, (d) LDA, O(3) atom under (e)GGA and (f) LDA approximations.

4.4. Optical Properties of $LiPaO_3$ Crystal

In this level of our thesis study we interested in the optical properties of the $LiPaO_3$ crystal. In order to understand the optical properties of a material first of all, we need to calculate the complex dielectric function ($\varepsilon = \varepsilon_1 + i\varepsilon_2$), which is composed of the real (ε_1) and the imaginary (ε_2) parts. The real and the imaginary parts of the dielectric function for GGA (LDA) is given in Figure 4. 23 and Figure 4.24. The negative part of the real component shows that the crystal reflects all of the coming light. The zero values of this component refers to the plasmon excitations. In the imaginary part there are peaks which shows the transitions of electrons from valence to the conduction bands. The static dielectric function is equal to 3.56 (3.51) for GGA (LDA).

The reflectivity (R), refractive index (n), extinction coefficient (k), effective number of electrons (N_{eff}), energy loss functions for surface (L_S) and for volume (L_V) are calculated and given in Figure 4.25 for GGA and in Figure 4.26 for LDA. The value static refractive index is 1.88 for GGA and 1.87 for LDA. L_V gives the energy loss of an electron while passing through the crystal. The peak of L_V gives information about the plasma oscillations. Neff is related with the transition between the bands and for the saturated values there is no transitions.

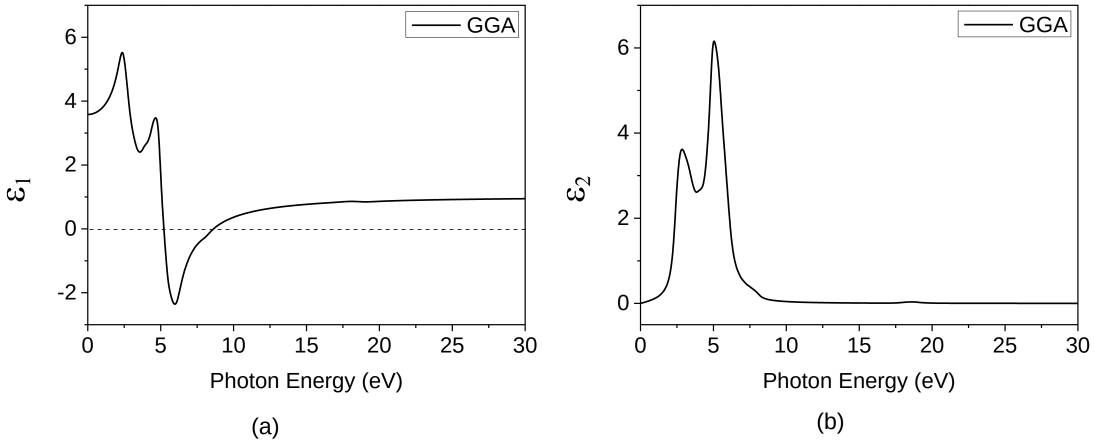

(a)

(b)

Figure 4.23. (a) The real and (b) the imaginal components of complex dielectric function of $LiPaO_3$ crystal under GGA.

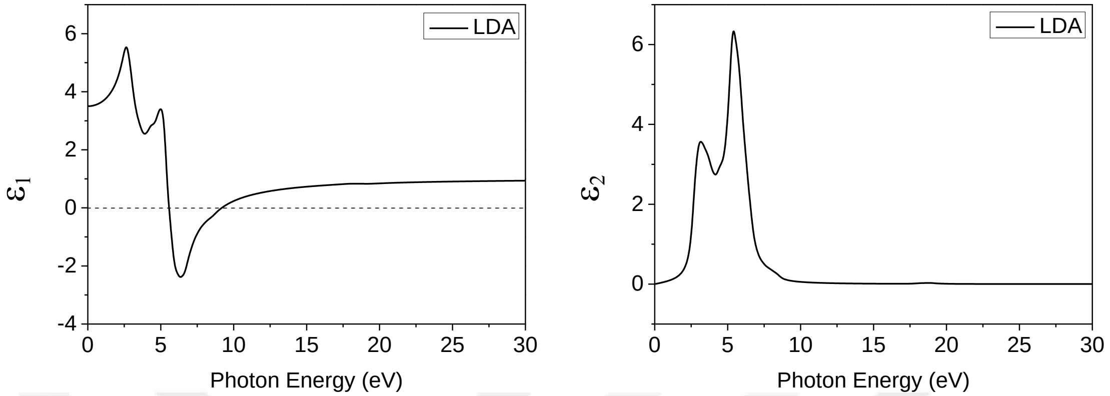

(a) (b)

Figure 4.24. (a) The real and (b) the imaginal components of complex dielectric function of $LiPaO_3$ crystal under LDA.

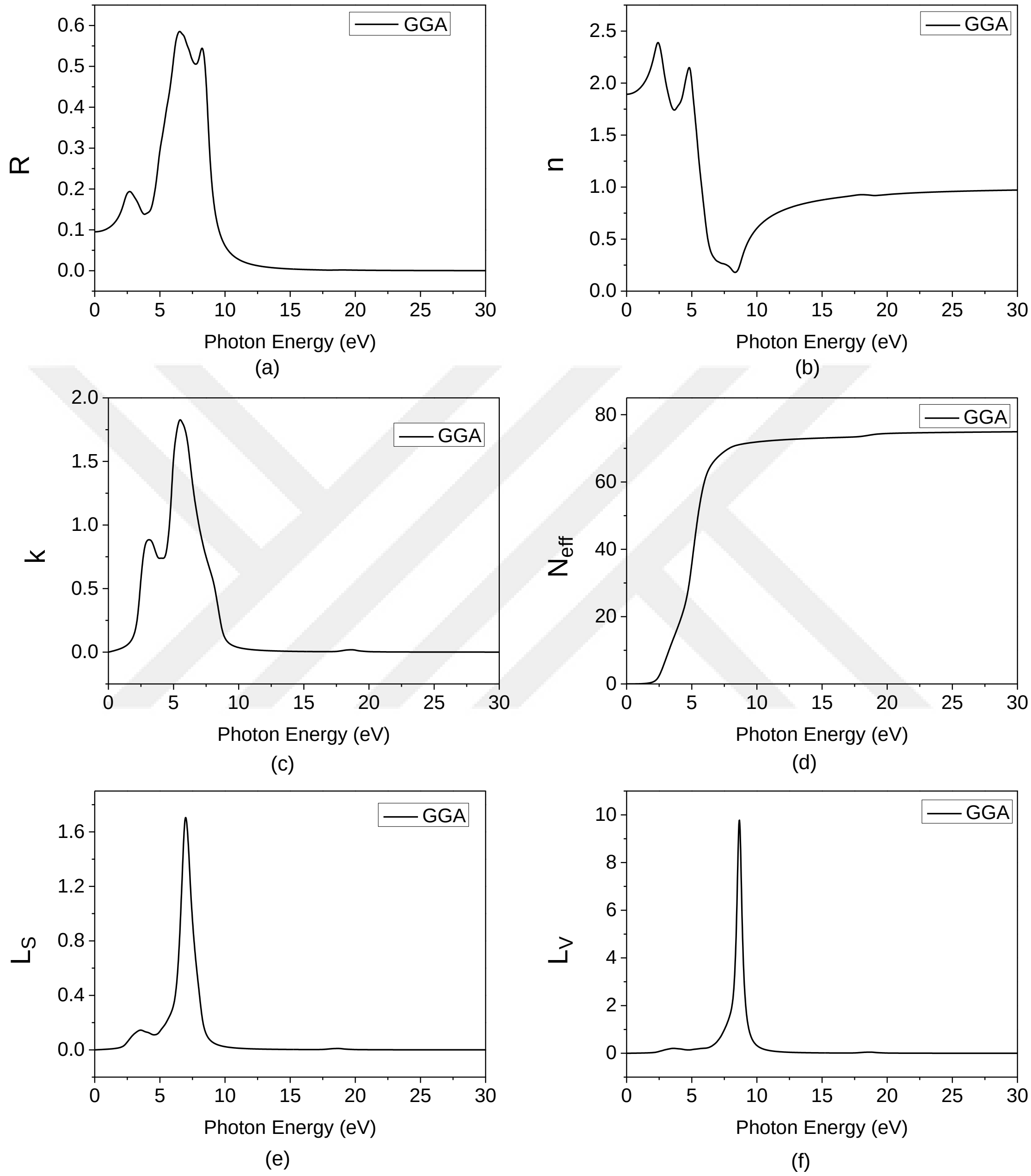
(a) (b) (c) (d) (e) (f)

Figure 4.25. (a) Reflectivity, (b) Refractive index, (c) Extinction coefficient, (d) Effective number of valence electrons per unit cell, (e) Energy loss function for surface and (f) Energy loss function for volume of $LiPaO_3$ crystal under GGA.

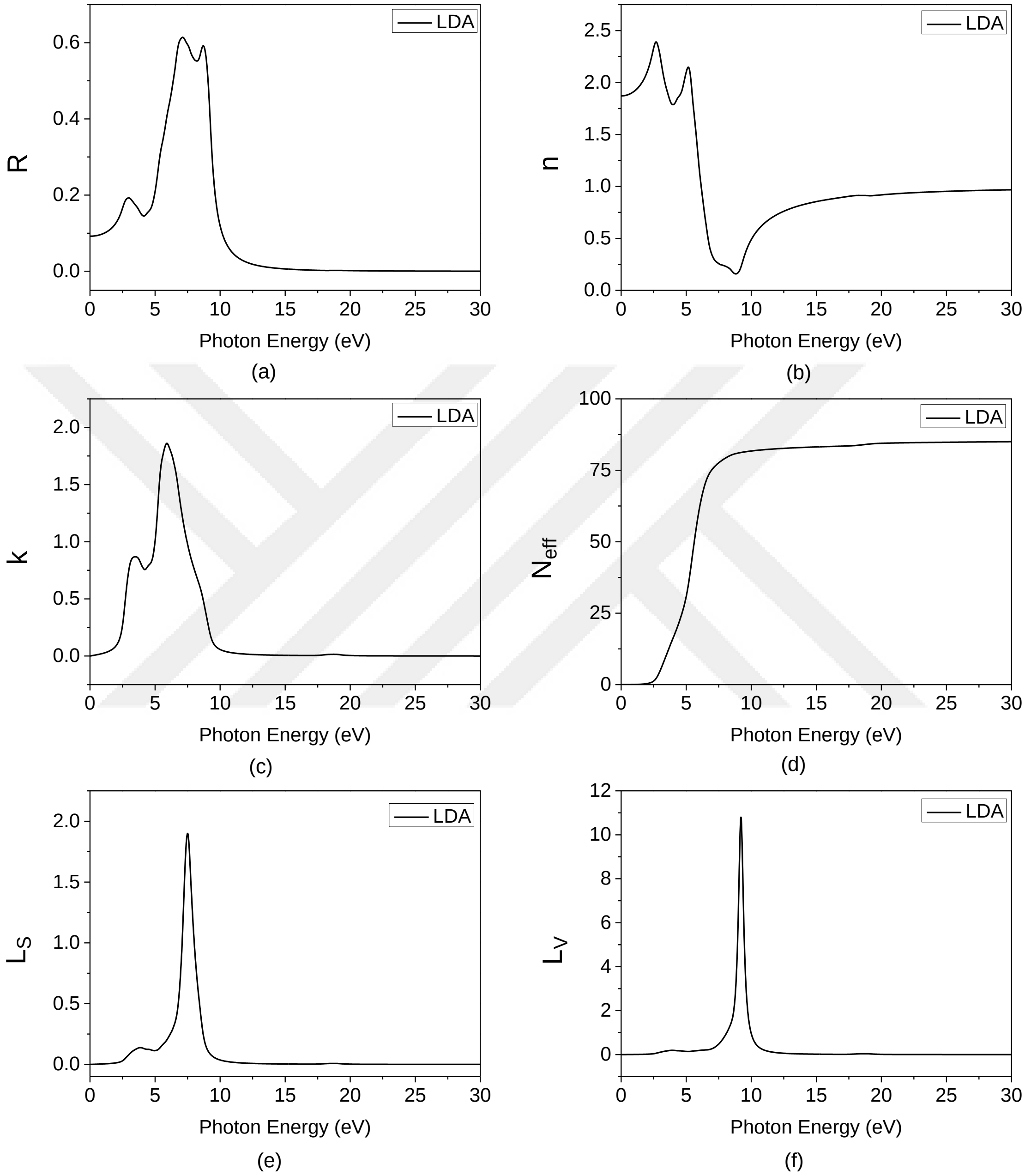

(a) (b) (c) (d) (e) (f)

Figure 4.26. (a) Reflectivity, (b) Refractive index, (c) Extinction coefficient, (d) Effective number of valence electrons per unit cell, (e) Energy loss function for surface and (f) Energy loss function for volume of $LiPaO_3$ crystal under LDA.

4.5. The Elastic Properties of LiPaO3 Crystal

Finally, we examined the elastic properties of the LiPaO$_3$ crystal. The first thing that we did was to calculate the elastic stiffness constants. Elastic stiffness constants are actually rank four tensors as C_{ijkl}, but by using a matrix notation (Nye, 1985) we can convert them to C_{mn}. However C_{mn}'s are not rank two tensors. By using this matrix notation we can reduce the number of the components of these elastic stiffness constants to 36. The 21 of the 36 are independent components. For different crystal structures, there are different number independent elastic stiffness components. The number of independent components of elastic stiffness components are just three for a cubic structure, which are C_{11} $(= C_{22} = C_{33})$, C_{12} $(= C_{13} = C_{21} = C_{23} = C_{31} = C_{32})$ and C_{44} $(= C_{55} = C_{66})$ Table 4.1.

Table 4.1. The calculated elastic stiffness constants of LiPaO$_3$ under GGA and LDA.

Elastic Stiffness Constants	GGA(GPa)	LDA (GPa)
C_{11}	380.72	469.50
C_{12}	27.83	33.81
C_{44}	20.87	20.59

The elastic stiffness constants give many informations of a crystal about its elastic properties. If a crystal obeys the following rules (Mouhat, 2014) which are given in eq (4.1), then this material is said to be mechanically stable. Here B refers to Bulk modulus which is given in Table 4.2. It is clear that with the values given in Table 4.1 this crystal is mechanically stable for GGA and LDA.

$$C_{11} + 2C_{12} > 0,\ C_{44} > 0,\ \ C_{11} - C_{12} > 0\ ,\ \ \ C_{11} > 0 \text{ and } C_{12} < B < C_{11} \qquad (4.1)$$

After the elastic stiffness constants we calculated the Bulk, Shear and Young modulus, and some elastic properties which are given in Table 4.2. The Bulk and the Shear modulus are calculated with three different methods such as Voight, Reuss and Hill methods. The poisson ratio and the flexibility constant gives information about the material if it is elastic of fragile. If the Poisson ratio is bigger that the critical value of 0.26 then this material is elastic. If it is smaller then this value it is a fragile material. Also if the flexibility constant is bigger than 1.75 it is elastic, if it is smaller then it is fragile material. Our Poisson ratio is bigger than 0.26 and flexibility constant is bigger than 1.75, so $LiPaO_3$ is an elastic material.

Debye temperature is related with the thermal conductivity. The Debye temperature values for both approximations show that our material has a thermal conductivity property.

Table 4.2. Some elastic modulus and constants of $LiPaO_3$ crystal under GGA and LDA approximations.

The Elastic Properties	**Symbol (Unit)**	**GGA**	**LDA**
Voigt Bulk Modulus	B_V (GPa)	145.43	179.013
Reuss Bulk Modulus	B_R (GPa)	145.43	179.016
Hill Bulk Modulus	B_H (GPa)	145.43	179.015
Voight Shear Modulus	G_V (GPa)	83.10	99.491
Reuss Shear Modulus	G_R (GPa)	32.31	32.338
Hill Shear Modulus	G_H (GPa)	57.71	65.915
Young Modulus	E (GPa)	152.89	176.127
Poisson Ratio	v (-)	0.33	0.336
Flexibility Constant	$K=B_{VRH}/G_{VRH}$ (-)	2.52	2.716
Debye Temperature	θ_D	132.93	142.282
Zener Anizotropy Factor	A (-)	0.12	0.09

From the Zener anizotropy factor, we can understand the isotropy of that material. If the value of the Zener anisotropy factor is close to 1, that material is said to be isotropic. If that value is close to zero than that material is anisotropic. $LiPaO_3$ is anisotropic because the Zener anisotropy factor values under both approximations are close to zero.

5. CONCLUSION

In this study we investigated the physical properties of $LiPaO_3$ crystal by using the Density Functional Theory within the Generalized Gradient and Localized Density Approximations. We used ABINIT computer programme throughout our study. Additionally, we also used Vesta computer programme for the unit cell sketching, bond and bond lenght calculations.

First of all, we performed the cut-off energy and k-point optimizations. After deciding those values we did volume optimization. Volume optmization gave us the relations between the total energy-volume, total energy-pressure and pressure-volume alterations. Also we calculated the lattice parameter under both approximations. Our calculated lattice parameter values are very close to the value that we obtained from the literature.

In order to understand the structural properties of the $LiPaO_3$ crystal, we plotted the total-energy vs volume, total energy vs. pressure, total energy vs lattice parameter and volume vs. pressure graphs. We also sketched the unit cell structure of $LiPaO_3$ crystal from which the perovskite structure of that crystal can be clearly seen. The bonds and the bond lenghts are also calculated with Vesta programme during the investigation of the structural properties of $LiPaO_3$ crystal.

In the investigation of the electronic properties, calculated and plotted the electronic band structure, density of states and the partial density of states of $LiPaO_3$ under GGA and LDA approximations. From those calculations we noticed that this material is a semiconductor with a direct transition. The density of states graphs are compatible with electronic band structure graphs. The total partial density of states graphs may give the density of states of $LiPaO_3$ crystal.

Afterwards, we investigated the optical properties of $LiPaO_3$ crystal. We calculated the complex dielectric function and some optical properties such as reflectivity, refractive index, extinction coefficient, effective number of valence electrons per unit cell, energy loss function for surface and energy loss function for volume under GGA and LDA approximations. The calculated optical properties are given with figures which are compatible with each other.

Lastly, we focused on the elastic properties of $LiPaO_3$. We calculated the elastic stiffness constants. By the help of these constants we obtained the bulk, Shear, Young modulus and some other elastic constants. We noticed that this crystal is mechanically stable and it is an elastic material.

According to our research there is no previous study about $LiPaO_3$ about the topics that we studied in this work. So we could not compared our results with the literature except fort he lattice parameters. However, we see that our results are consistent with each other throughout all calculations in our thesis study. Because of that we believe that our study will shed light on new studies about $LiPaO_3$ crystal.

REFERENCES

Aharony, A., Entin-Wohlman, O., 2019. ***Introduction to Solid State Physics***. World Scientific Publishing Co. Pte. Ltd, Singapore.

Alajlani, Y., Alaswad, A., Placido, F., Gibson, D., Diyaf, A., 2018. Inorganic thin films materials for solar cell applications. **In *Reference Module in Materials Science and Materials Engineering* Elsevier B.V**, **https://doi.org/10.1016/B978-0-12-803581-8.10355-8.** Date accessed: 17.05.2021.

Atkins, P., Friedman, R., 2005. ***Molecular quantum mechanics***. Fourth edition. Oxford university press, New York, USA.

Azam, S., Ifran, M., Abbas, Z., Rani, M., Saleem, T., Younus, A., Akhtar, N., Liaqat, B., Shabbir, M., Al-Sehemi, A.G., 2019. ***DFT study of the electronic and optical properties of ternary chalcogenides AlX_2Te_4***. Materials research express, **6** (11): 116314.

Balachandran, P, V., Emery, A, A., Gubematis, J, E., Lookman, T., Wolverton, Ch., Zunger, A., 2018. Predictions of new ABO_3 perovskite compounds by combinig machine learning and density functional theory. ***Physics Review Materials, 2***(4): 043802.

Beer, M.De., Maina, J.W., 2008. ***Some fundamental definitions of the elastic parameters for homogeneous isotropic linear elastic materials in pavement design and analysis***. 7-11 July 2008, Pretoria, South Africa. 282-293.

Benmhidi, H., Rached, H., Rached, D., Benkabou, M., 2016. Ab initio Study of Electronic Structure, Elastic and Transport properties of Fluoroperovskite $LiBeF_3$. ***Journal of Electronic Materials***, **46** (4): 2205-2210.

Cabuk, S., 2010. first principles study of the electronic, linear and nonlinear optical properties of Li(Nb, Ta)O_3. ***International Journal of Modern Physics B***, **24** (32): 6277-6290.

Canadell, E., Doublet, M.L., Iung, CH., 2012. ***Orbital Approach to the Electronic Structure of Solids***. Oxford University Press, New York, USA.

Cleland, A.N., 2003. ***Foundations of nano mechanics from solid state theory to device applications***. Springer-Verlag, Berlin, Germany.

Cohen, M.L., 2005. ***Electronic structure calculations: Plane-wave methods. Volume one of Encyclopedia of Condensed matter physics***. Elsevier academic press, 1:561-569.

Cullity, B.D., 1956. ***Elements of X-ray Diffraction***. Addison-Wesley Publishing Company, INC, US.

Devlal, K., 2020. Solid State Physics: Crystal structure. ***https://www.uou.ac.in/lecturenotes/science/MSCPHY17/Solid%20state%20physics%20by%20Dr.%20kamal%20Devlal.pdf.*** Date accessed: 22.04.2021.

Doitpoms, 2021. ***https://www.doitpoms.ac.uk/tlplib/brillouin_zones/contents.php.*** Department of Materials Science & Metallurgy, University of Cambridge. Date accessed: 28.05.2021.

Douglas, B.E., Ho, Sh., 2006. ***Structure and Chemistry of Crystalline Solids***. Springer Science+Business Media, INC, New York, USA.

Electronic correlation, 2021. ***https://en.wikipedia.org/wiki/Electronic_correlation.*** Date accessed: 10.07.2021.

Enderlein, R., Horing, N., 1997. ***Fundamentals of semiconductor physics and devices***. Word scientific publishing Co. Pte. Ltd, London, UK.

Erum, N., Iqbal, M., 2017. First principles investigation of Protactinium-based oxide-perovskites for flexible opto-electronic devices. ***Chinese Physics***, **26** (4): 047102.

Fu, K., Ho-Baillie, A.W.Y., Mulmudi, H.K., Trang, Ph.Thi.Thu., 2019. ***Perovskite solar cells technology and practices***. Apple Academic Press INC, Florida, USA.

Galsin, J.S., 2019. ***An Introduction to theory Solid state physics***. Academic press, Elsevier INC, London, UK.

Grenier, B., Ballou, R., 2012. ***Crystallography: Symmetry groups and group representations***. EPJ Web of Conferences, 22: 00006.

Grundmann, M., 2016. ***The physics of semiconductors: an introduction including nanophysics and applications***. Third edition. Springer international Publishing AG, Switzerland.

Hahn, Th., 2002. ***International Tables for Crystallography Volume A: Space-Group Symmetry***. Fifth edition. International Union of Crystallography, springer, Netherland.

Haken, H., Wolf, H.Ch., 2004. ***Molecular physics and elements of quantum chemistry***. Second edition. Springer-Verlag, Berlin, Germany.

Hammond, CH., 2015. ***The basics of crystallography and diffraction***. Fourth edition. Oxford university press, Oxford, UK.

Hartree-Fock method, 2021. ***https://en.wikipedia.org/wiki/Hartree%E2%80%93Fock_method.*** Date accessed: 01.07.2021.

Hoffmann, F., 2020. ***Introduction to crystallography***. Springer Nature Switzerland AG, Cham, Switzerland.

Jain, A., Ong, Sh, P., Hautier, G., Chen, W., Richards, W, D., Dacek, S., Cholia, Sh., Gunter D., Skinner, D., Ceder, G., Persson, K, A., 2013. Commentary: The material Project: A material genonme approach to accelerating materials innovation. ***APL Materials,*** **1** (1): 011002.

Javid, M., Khan, Z., Mehmood, Z., Nabi, A., Hussain, F., Imran, M., Nadeem, M., Anjum, N., 2018. Structural, electronic and optical properties of $LiNbO_3$ using GGA-PBE and TB-mBJ functional: A DFT study. ***International Journal of Modern Physics B***, **32** (14): 1850168.

Jia, K., Gang, B., 2018. Electronic Structure and Optical properties of $LiBiO_3$ Doped with V, Nb and Ta. ***Journal of Wuhan University of Technology-Mater. Sci. Ed.***, **33** (4): 863-870.

Kasap, S., 2006. ***Principles of electronic materials and devices***. Third Edition. McGraw-Hill companies, INC, New York, US.

Kaxiras, E., 2003. ***Atomic and Electronic Structure of Solids***. Cambridge University Press, Cambridge, UK.

Kazmerski, L., 1980. ***Polycrystalline and Amorphous Thin Films and Devices***. Academic Press, INC, New York, US.

Khan, W., Azam, S., Shah, F.A., Goumri-Said, S., 2015. DFT and modified becke Johanson (mBJ) potential investigations of the optoelectronic properties of $SnGa_4Q_7$ (Q= S, Se) compounds: Transparent materials for large energy conversion. ***Solid State Sciences,*** **48**: 244-250.

Khandy, SH., Islam, I., Gupta, D., Laref, A., 2018. Electronic structure, mechanical and thermodynamic properties of $BaPaO_3$ under pressure. ***Journal of Molecular Modeling***, **24**: 131.

Kittle, Ch., 2005. ***Introduction to Solid State Physics***. Eight edition. John Wiley & Sons, INC., US.

Klug, H.P., Alexander, L.E., 1974. ***X-ray Diffraction properties for Polycrystalline and Amorphous Materials***. Second edition. Jojn Wiley & Sons, INC, New York, USA.

Koch, W., Holthausen, M.C., 2001. ***A chemist's guide to Density Functional Theory***. Second edition. Wiley-Vch Verlag, New York, USA.

Kohanoff, J., 2006. ***Electronic structure calculations for solids and molecules: theory and computational methods***. Cambridge university press, Cambridge, UK.

Kumar, A., 2012. ***A brief introduction to Thomas-Fermi model in partial differential equations. Department of mathematics and statistics***. McGill university, Montreal, QC.

Lal, M., Kapila, Sh., 2017. Structural, electronic, optical and mechanical properties of $BaPaO_3$ and $BaUO_3$ cubic perovskite. ***International Journal of Pure and Applied Physics***, **13** (1): 67-76.

Li, Sh. S., 1993. ***Semiconductor Physical Electronics***. Plenum press, New York, N.Y, US.

Li, X., Dan, Y., Dong, R., Cao, Zh., Niu, Ch., Song, Y., Li, Sh., Hu., J., 2019. Computational Screening of new Perovskite Materials using Transfer learning and deep learning. ***Applied sciences, 9***(24): 5510.

LibreTexts, 2021.Symmetry elements, the Identity symmetry ***https://chem.libretexts.org/Courses/Pacific_Union_College/Quantum_Chemistry/12%3A_Group_Theory__The_Exploitation_of_Symmetry/12.02%3A_Symmetry_Elements.*** Date accessed, 01.06.2021.

Lieb, E.H., 2000. ***A brief review of Thomas-Fermi theory. Department of physics and mathematics***. Princeton university, Princeton, New Jersey. (64)

Lucarini, V., Saarinen, J.J., Peiponen, K.E., Vartiainen, E.M., 2005. ***Kramers-Kronig relations in optical materials research***. Springer-Verlag, Berlin, Germany.

Luo, Sh., Daoud, W.A., 2015. Recent progress in organic-inorganic halide perovskite solar cells: mechanisms and materials design. ***Journal of Materials Chemistry A,*** **3** (17): 8992-9010.

Lyuksyutov, I., Naumovets, A.G., Pokrovsky, V., 1992. ***Two-Dimensional crystals***. Academic press, INC, San Diego, US.

Martin, R.M., 2004. ***Electronic structure basic theory and practical methods***. Cambridge University press, Cambridge, UK.

Mello, U.T., Cavalcanti, P.R., 2020. A point creation strategy for Mesh Generation using crystal lattices as Templates. ResearchGate publication, 2434940.

Momma, K., Izumi, F., 2011. Vesta 3 for three-dimensional visualization of crystal, volumetric and Morphology data. ***Journal of Applied Crystallography,*** **44** (6): 1272-1276.

Monkhorst, H, J., Pack, J, D., 1976. Special points for Brillouin-zone integrations. ***Physical Review B,*** **13** (12): 5188.

Moss, R.E., 1973. ***Advanced molecular quantum mechanics***. Chapman and hall, London, UK.

Mouhat, F., Coudert, F, X., 2014. Necessary and sufficient Elastic stability conditions in various crystal systems. ***Physics review B,*** **90** (22): 224104.

Myers, H., 2009. ***Introductory Solid-State Physics***. Second Edition. Taylor & Francis Ltd, London, UK.

Nasir, S., Hussein, M.Z., Zainal, Z., Yusof, N.A., Zobir, S.A.M., Alibe, I.M., 2018. Potential valorization of by-product materials from oil palm: a review of alternative and sustainable Carbon sources for Carbon-based Nanomaterials synthesis. ***Peer-Reviewed Review Article, Bioresources,*** **14** (1).

Nye, J, F., 1985. ***Physical properties of Crystals: Their Representation by Tensors and Matrices***. Oxford University press, United States. Chapter 8.

Ott-Borchardt, W., 1995. ***Crystallography***. Second edition. Springer-Verlag, Berlin, Germany.

Oura, K., Lifshits, V.G., Saranim, A, A., Zotov, A.V., Katayama, M., 2003. ***An introduction surface science***. Springer-Verlag, Berlin, Germany.

Panagiotakopoulos, Th.E., 2020. ***Thomas-Fermi model***. University of Florida, USA.

Rahman, Md., Rubel, M., Rashid, Md., Alam, M., Hossain, Kh., Hossain, Md., Khatun, A., Hossain, Md., Islam, A.K.M., Kolima, S., Kumada, N., 2019. Mechanical, electronic, optical, and thermodynamic properties of orthorhombic $LiCuBiO_4$ crystal: a first-principles study. ***Journal of Materials Research and Technology***, **8** (5): 3783-3794.

Rajeswari, M.R. ***density-based methods Thomas-Fermi***. Department of Biochemistry, India Institute of Medical Sciences, New Delhi.

Razeghi, M., 2002. ***Fundamentals of solid-state engineering***. Kluwer Academic publishers, New York, USA.

Reventos, M.M, Rius, J., Amigo, J.M., 2012. Mineralogy and geology: the role of crystallography since the discovery of X-ray diffraction in 1912. Revista de ia Sociedad Geologica de Espana, 25 (3-4): 133-143.

Rioult, M., 2015. ***Hematite-based epitaxial tin films as photoanodes for solar water splitting*** (Doctoral thesis in Physics). University of Paris-Saclay, France.

Roldan, R., Chirolli, L., Prada, E., Silva-Guillen, J.A., San-Jose, P., Guinea, F., 2017. ***Theory of 2D crystals: graphene and beyond***. Chemistry society revies, 46 (15): 4387-4399.

Roque-Malherbe, R.M.A., 2010. ***The physical chemistry of materials***. CRC Press Taylor & Francis group, USA.

Rosa, R.G.T. ***The Hartree-Fock method***. Institute of Physics of São Carlos, University of São Paulo.

Saue, T., 2002. ***Post Dirac-Hartree-Fock methods-properties***. Chapter 7. Theoretical and computational chemistry, 11, p 332-400, https://doi.org/10.1016/S1380-7323(02)80033-4.

Sherrill, C., 2009. ***An introduction to Hartree-Fock molecular orbital theory***. Semantic scholar, Corpus ID 6783299.

Sholl, D.S., Steckel, J.A., 2009. ***density functional theory: A practical introduction***. John Wiley & Sons, INC, New Jersey, Canada.

Singleton, J., 2001. ***Band theory and electronic properties of solids***. Oxford university press, New York, USA.

Singleton, J., 2001. ***Band theory and electronic properties of solids***. Oxford University Press, New York, USA.

Slola-Valim, M., 2015. ***Static and dynamic elastic properties, the cause of the difference and conversion methods-case study***. National research institute, Nafta-Gaz, (11):816-826, DOI: 10.18668/NG2015.11.02.

Solyom, J., 2007. ***Fundamentals of the physics of solids: Volume I- Structure and Dynamics***. Springer-Verlag, Berlin, German.

Stenzel, O., 2016. ***The physics of thin film optical spectra: An introduction***. Second edition. Springer international Publishing, Switzerland, 44.

Strinati, G.C., 2005. ***Hartree and Hartree-Fock methods in electronic structure***. Materials science and materials engineering, p 311-318, *https://doi.org/10.1016/B0-12-369401-9/00443*-5.

Su, K., Xu, X., Lai G., Hu, S., Zhu, W., Tang, J., Chen, X., 2021. First-principles investigation of the elastic, photocatalytic and ferroelectric properties of $LiNbO_3$ type $LiSbO_3$ under high pressure. ***Materials Today Communications***, 27: 103406.

Sum, T.Ch., Mathews, N., 2019. ***Halide perovskites: photovoltaics, light emitting devices and beyond***. Wiley-VCh, Weinheim, Germany.

Sutcliffe, B.T., Woolley, R.G., 2012. On the quantum theory of molecules. ***The Journal of Chemical Physics,*** **137** (22).

Symmetry otterbein, 2021. Symmetry operations and examples. ***http://faculty.otterbein.edu/djohnston/sym/tutorial/identity.html#.*** Date accessed: 01.06.2021.

Szabo, A., Ostlund, N.S., 1996. ***Modern quantum chemistry: introduction to advanced electronic structure theory***. Dover publications, INC, New York, USA.

Szwacki, N.G., Szwacka, T., 2010. ***Basic elements of crystallography***. Pan Stanford Publishing Pte. Ltd, Temasek Boulevard, Singapore.

Tejuca, L.G., Fierro, J.L.G., 1993. ***Properties and applications of perovskite-type oxides***. Marcel Dekker, New York, USA.

Thomas-Fermi Model, 2021. ***https://en.wikipedia.org/wiki/Thomas%E2%80%93Fermi_model.*** Date accessed: 25.07.2021.

Tilley, R., 2006. ***Crystals and crystal structures***. Wiley, J., Ltd, S., England, UK.

Tinkham, M., McKay, G., 1964. ***Group theory and quantum mechanics***. McGraw-Hill book company, New York, USA.

Tsymbal, E.T., 2021. Physics 927, section 5: Lattice vibrations. ***http://physics.unl.edu/tsymbal/teaching/SSP-927/index.shtml.*** Date accessed: 20.04.2021.

Vainshtein, B.K., Fridkin, V.M., Indenbom, V.L., 2000. ***Modern Crystallography Volume 2: Structure of Crystals***. Third edition. Springer-Verlag, Berlin, Germany.

Valence and conduction bands, 2021. Semiconductor band structure. ***https://en.wikipedia.org/wiki/Valence_and_conduction_bands***. Date accessed: 15.06.2021.

Van Troeye, B., Gillet, Y., Ponce, S., Gonze, X., 2014. First-principles characterization of the electronic and optical properties of hexagonal $LiIO_3$. ***Optical Materials***, **36** (9): 1494-1501.

Vasileska, D., Goodnick, S.M., 2006. ***Computational electronics***. Morgan & Claypool Publishers, 1 (1):1-216.

Wang, K., Li, D., Fei, Z., Ma, X., Zeng, X., 2019. Discovery of a new crystal structure of $LiBeF_3$ and its thermodynamic and optical properties. ***Computational Materials Science***, **169**: 109077.

Wang, W.H., 2012. The elastic properties, elastic models and elastic perspectives of metallic glasses. ***Progress in Materials Science,*** **57** (3):487-656.

Waseda, Y., Matsubara, E., Shinoda, K., 2011. ***X-ray Diffraction Crystallography***. Springer-Verlag, Berlin, Germany.

Zhou, W., Zhao, Z., 2016. electronic structures of efficient M BiO_3 (M = Li, Na, K, Ag) photocatalyst. ***Chinese Physics B***, **25** (3): 037102.

Zhou, Ye., Wang, Yan., 2020. ***Perovskite quantum dots: Synthesis, properties and applications***. Springer Nature Singapore, springer series in materials science, Singapore, 303.

EXTENDED TURKISH SUMMARY
(GENİŞLETİLMİŞ TÜRKÇE ÖZET)

$LiPaO_3$ BİLEŞİĞİNİN BAZI FİZİKSEL ÖZELLİKLERİ: BİR TEMEL İLKELER ÇALIŞMASI

HUSSEIN, Khalat Ezzulddin
Yüksek Lisans Tezi, Fizik Anabilim Dalı
Tez Danışmanı: Doç. Dr. Emel KİLİT DOĞAN

ÖZ

Bu tez çalışmasında $LiPaO_3$ kristalinin yapısal, elektronik, optik ve elastik özellikleri Yoğunluk Fonksiyoneli Teorisi ile Genelleştirilmiş Gradyent ve Yerel Yoğunluk Yaklaşımları altında incelenmiştir. Tüm hesaplamalar için ABINIT bilgisayar programı kullanılmıştır. ABINIT'e ek olarak kristalin birim hücresinin çizimi, bağ yapısı ve bağ uzunluklarının incelenmesinde Vesta programı kullanılmıştır.

İlk olarak, yapılacak tüm optimizasyonlarda kullanılmak üzere kesme enerjisi ve k-noktaları optimizasyonu yapılmış, böylece tüm hesaplamalarda kullanılacak kesme enerjisi ve k-noktaları sayısı belirlenmiştir. Ardından hacim optimizasyonu yapılarak, kararlı kristalin toplam enerjisine karşılık hacim ve basınç değişimleri elde edilmiş. Bunların yanında kristalin hacim basınç değişimi ve teorik örgü parametresi hesaplanmıştır. Yapısal özelliklerin incelenmesinde son olarak, $LiPaO_3$ kristalinin birim hücresi çizdirilmiş, bağ yapısı ve uzunlukları hesaplanmıştır.

$LiPaO_3$ kristalinin elektronik özelliklerin anlaşılabilmesi için elektronik band yapısı, durum yoğunluğu ve kısmı durum yoğunlukları grafikleri hesaplanmış ve çizdirilmiştir. Tüm bu grafikler her iki yaklaşım altında çizdirilmiş ve çıkan sonuçların birbirine oldukça yakın oldukları görülmüştür. $LiPaO_3$ kristalinin direk geçişe sahip bir yarıiletken olduğu ve yasak band aralığının GGA yaklaşımı altında 2.10 eV, LDA yaklaşımı altında ise 2.19 eV elde edilmiştir.

Ardından $LiPaO_3$ kristalinin optik özellikleri çalışılmıştır. Bu kapsamda ilk olarak kompleks dielektrik fonksiyonu her iki yaklaşım altında elde edilmiştir. Kompleks dielektrik fonksiyonun gerçek ve sanal bileşenleri hesaplanmış ve grafikleri çizdirilmiştir. Ardından bu değerler kullanılarak, yansıtma, kırılma indisi, sönüm katsayısı, birim hücre başına etkin

değerlik elektron sayısı, yüzey için enerji kayıp fonksiyonu ve hacim için enerji kayıp fonksiyonu hesaplanmıştır. Tüm bu optik özellikler hem GGA hem de LDA yaklaşımları altında hesaplanmış ve grafikleri çizdirilmiştir. Tüm optik özelliklerin de elektronik ve yapısal özelliklerde elde edilen sonuçlarda olduğu gibi kendi içlerinde oldukça tutarlı oldukları görülmüştür.

Son olarak ise $LiPaO_3$ kristalinin elastik özellikleri incelenmiş ve ortaya konmuştur. Bu bağlamda ilk olarak elastik sertlik katsayıları hesaplanmış ve ardından da bu değerler kullanılarak, Bulk, Shear ve Young modülleri ile, Poisson oranı, esneklik katsayısı, Debye sıcaklığı ve Zener anisotropi katsayısı hesaplanmıştır. Tüm bu hesaplamalar sonucu, incelenen kristalin mekanik olarak kararlı oldupu ve esmek yapıya sahip bir malzeme olduğu bulunmuşur.

Yaptığımız kapsamlı literatür çalışmasına göre $LiPaO_3$ kristali üzerine yapılmış benzer çalışmaların hiç olmadığı, yapısal, elektronik, optik ve elastik özelliklerinin daha önce hiç incelenmediği görülmüştür. Bu nedenle yaptığımız bu tez çalışmasının $LiPaO_3$ kristali ile ilgili gelecekte yapılacak çalışmalara ışık tutacağı kanaatindeyiz.

Anahtar kelimeler: ABINIT, Durum yoğunluğu, Elastik özellikler, Elektronik özellikler, $LiPaO_3$, Kısmi durum yoğunluğu, Optik özellikler, Yoğunluk fonksiyoneli teorisi.

1. MATERYAL VE YÖNTEM

Gerek doğada var olan gerekse yapay olarak üretilmiş olsun, malzemelerin fiziksel özelliklerinin anlaşılması, onların uygulama alanları bakımından oldukça önemlidir. Bir malzemenin fiziksel özelliklerinin anlaşılabilmesi için zamandan bağımsız Schrödinger denkleminin çözülebilmesi gereklidir. Bu denklem tek elektron için çözülebilir ancak incelenen malzemelerde oldukça çok sayıda elektron vardır. Bu sebeple bu denklem çözülemez hale gelir. Bu nedene geçmişten günümüze bir takım yaklaşımlar yapılmış be bu "çok parçacık problemine" çözümler aranmıştır. İlk olarak Born-Oppeinheimer, ardından Hartree ve son olarak da Hartree-Fock değişkeni eektron ve electron dalga fonksiyonu olarak alıp çözümler üretmişler ancak tam çözüm sağlayamamışlardır. Ardından Thomas-Fermi değişkeni electron yerine electron yoğunluğu alarak önemli bir aşama kaydetmiştir ve zamandan bağımsız Schrödinger denkleminin çözümünde oldukça önemli bir ilerleme kaydetmiştir. Ardından Hohenberg ve Kohn iki teorem üretip çözümleri üzerinde çalışarak ilk defa Yoğunluk Fonksiyoneli Teoreimini temellerini atmışlardır. Ardından Kohn ve Sham zamandan bağımsız Schrödinger denklemi yerine kendi denklemlerini koyarak yaptıkları çözümler Yoğunluk Fonksiyoneli Teoreimini tam olarak ortaya koymuş ve çok parçacık problemine çözüm bulmuşlardır.

Günümüzde Yoğunluk Fonksiyoneli Teoremine dayalı olarak hesap yapan birçok program vardır. Siesta, Quantum Espresso, Abinit, Wien2k bunlardan sadece birkaçıdır. Biz bu çalışmada ABINIT programını kullandık. ABINIT 1997 yılında Xavier GONZE ve arkadaşları tarafından başlatılan ve birçok farklı grupların uluslararası işbirliği ile gelişime açık olarak oluşturulan bir yazılım projesidir. ABINIT, yoğunluk fonksiyonel hesaplarını düzlemsel dalga ve pseudo potansiyeller kullanarak yapar (Gonze ve ark., 2002). ABINIT'in geliştirilmesinin yanında öğretilmesi için de çevrimiçi eğitimler verilmektedir (www.abinit.org.)

ABINIT Kohn –Sham denklemlerini iteratif yöntemlerle çözerek malzemelerin fiziksel özelliklerini hesaplayıp ortaya koyabilen bir programdır. Bunun yanında bu çalışmada birim hücrenini çizilmesi, bağ yapılarının anlaşılması ve bağ uzunluklarının hesaplanması için VESTA (Momma, K., & Izumi, 2011) bilgisayar programı da kullanılmıştır. Bu program da yine Yoğunluk Fonksiyoneli teorisi ile çalışan programlarda uyum içinde çalışabilmektedir.

2. BULGULAR VE TARTIŞMA

2.1. $LiPaO_3$ Kristali

The $LiPaO_3$ kristali kübük yapıda olup perovskit sınıfında yer almaktadır. $LiPaO_3$ kristalinin uzun adı Lityum Protaktinyum Oksit'tir. Uzay grubu $Pm\bar{3}m$ (No: 221) ve nokta grubu ise $m\bar{3}m$ 'dir.

2.2. $LiPaO_3$ kristalinin Yapısal Özellikleri

$LiPaO_3$ kristalinin yapısal özelliklerini araştırmak için ilk olarak kesme enerjisi ardından da k-noktaları optimizasyonları yapılmıştır. Kesme enerjisi ve k-noktaları değerleri saptandıktan sonra, hacim optimizasyonu yapılarak örgü parametreleri değerleri elde edilmiştir.

2.2.1. Kesme enerjisi

Denklemlerin çözümünde kullanılan dalga fonksiyonları Bloch teoremine göre sonsuz terimin toplamından oluşur. Bu durum hesaplamaları imkansız hale getirir. Bu nedenle bu toplamı sonsuz yerine daha küçük bir değerde sonlandırabilmeliyiz. Toplam enerjinin kinetik enerjiye bağlı grafiği çizdirildiğinde belirli bir değerde kararlı kristalin toplam enerji değerine ulaşıldığı görülmüştür. Bu değer kesme enerjisi değerine karşılık gelir. Kesme enerjisinden ne kadar büyük değer seçilirse işlem biraz daha zaman alır. Ancak sonuçta ciddi bir fark oluşmaz. Bu nedenle işlemleri daha kısa sürede tamamlamak ve daha az bilgisayar gücüne ihtiyaç duymak için kesme enerjisi değeri saptanmalıdır. Bu çalışmada aşağıdaki grafikler sonucu her iki yaklaşım altında da kesme enerjisi değeri 30 Hartree olarak saptanmıştır.

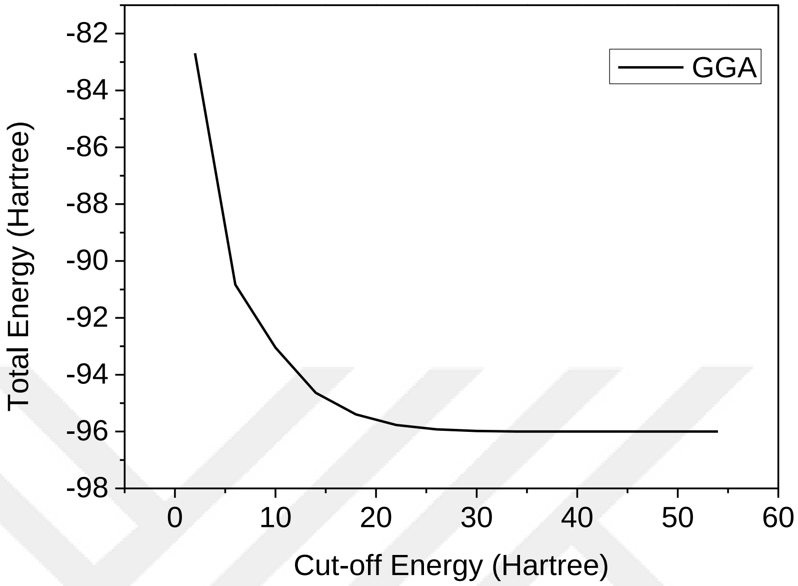

Şekil 2.1. Toplam enerjinin kesme enerjisine göre GGA yaklaşımı altındaki değişimi.

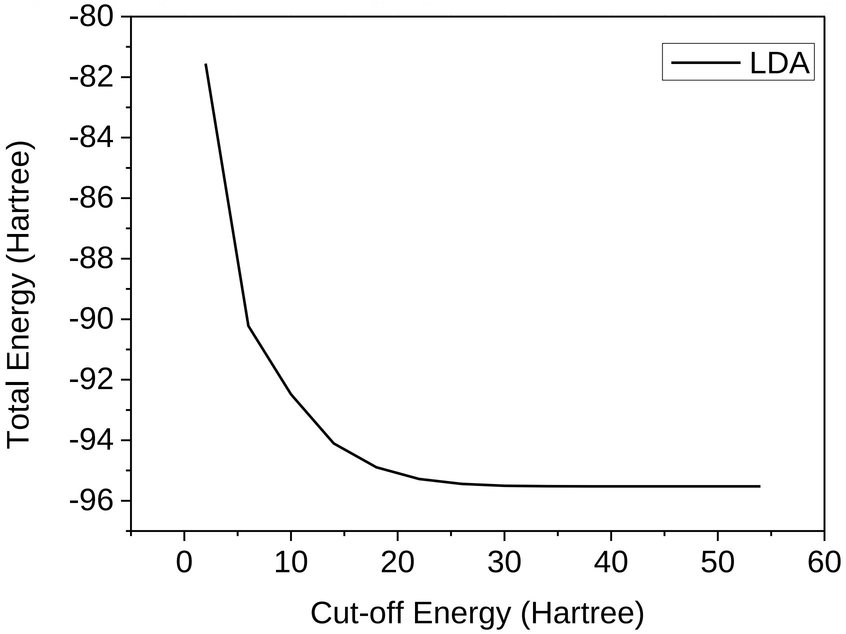

Şekil 2.2. Toplam enerjinin kesme enerjisine göre LDA yaklaşımı altındaki değişimi.

2.2.2. K-noktalarının sayısı

Yine yapılan hesaplamalarda k-noktaları üzerinden integraller alınmaktadır. Milyonlarca k-noktası olduğu için yine bu durum hesaplamaları içinden çıkılmaz bir hale getirmektedir. Bu nedenle Monkhorst ve Pack (Monkhorst-Pack, 1976) kristallerin simetri özelliklerinden yararlanarak bir metod geliştirmişlerdir. Bu metoda göre tüm k-noktalarını hesaba katmak yerine farklı simetri özelliklerine sahip k noktaları saptanıp onları işleme almak oldukça kolaylık sağlar. Çünkü bir k noktası yakın konşuluğundaki diğerleriyle aynı özelliklere sahiptir bunların tektek hesaplanması yerine içlerinden bir tanesi temsilci gibi seçilip kullanıldığında ve sadece bu şekilde farklı özelliktekiler ele alındığında işlemler oldukça kolaylaşır. Bunun için öncelikle birim hücre x, y ve doğrultularında eşit parçalara ayrılır. Bu parçalar ne karad çok olursa hesaplama daha hassas olur ancak bir yerden sonra arttırmanın bir yararı olmayacağından uygun bir bölümleme yapılmalıdır.

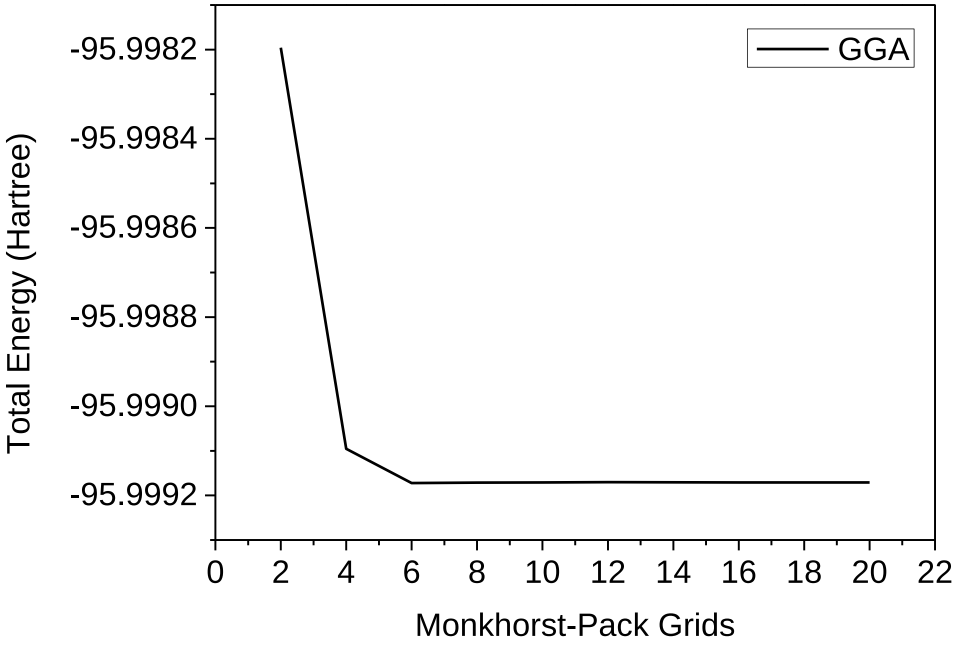

Şekil 2.3. Toplam enerjiye karşılık Monkhorst-Pack bölümlemeleri (GGA yaklaşımı altında).

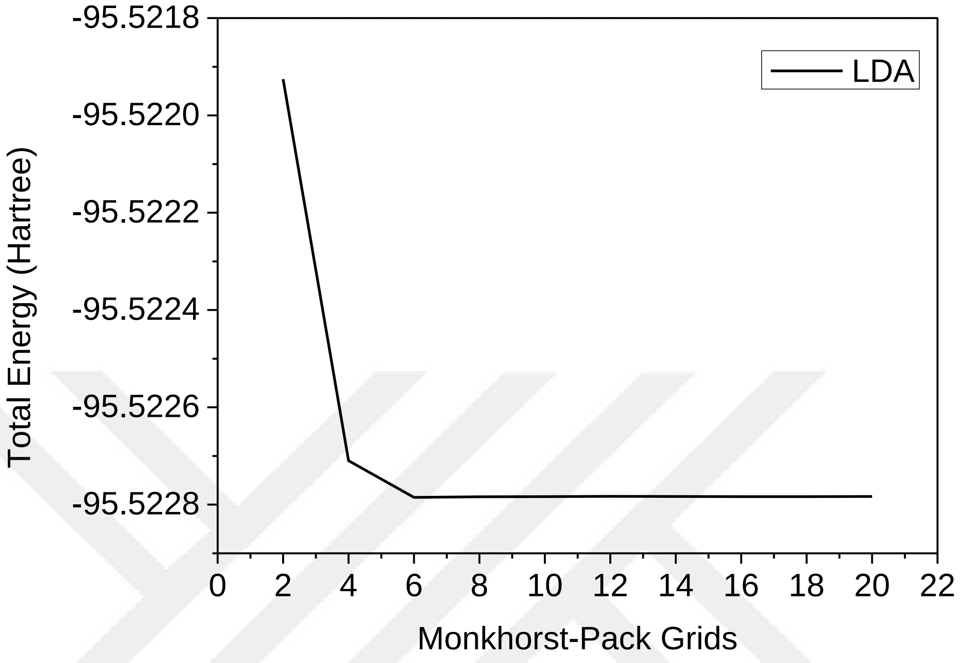

Şekil 2.4. Toplam enerjiye karşılık Monkhorst-Pack bölümlemeleri (LDA yaklaşımı altında).

Bu çalışmada 10x10x10 Monkhorst-Pack bölümlemesi ile 35 k nokratı hesaba katılmıştır.

2.2.3. Hacim optimizasyonu

Hacim optimizasyonu ile $LiPaO_3$ kristalinin kararlı durumdaki toplam enerjisi ve örgü parametreleri bulunmuştur. Ayrıca bu kristalin toplam enerjiye karşılık hacim ve basınç değişimleri ile basınca karşılık hacim değişimleri her iki yaklaşım altında elde edilmiştir.

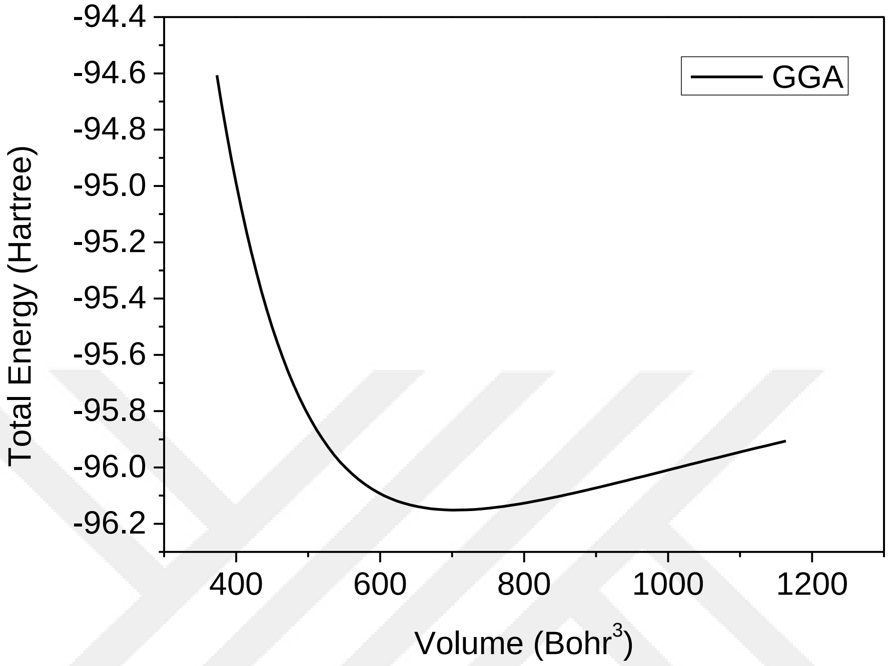

Şekil 2.5. $LiPaO_3$ kristalinin GGA yaklaşımı altında toplam enerjiye karşılık hacim grafiği.

Toplam enerjiye karşılık hacim grafiklerinin minimum noktası kristalin kararlı durumuna karşılık gelir.

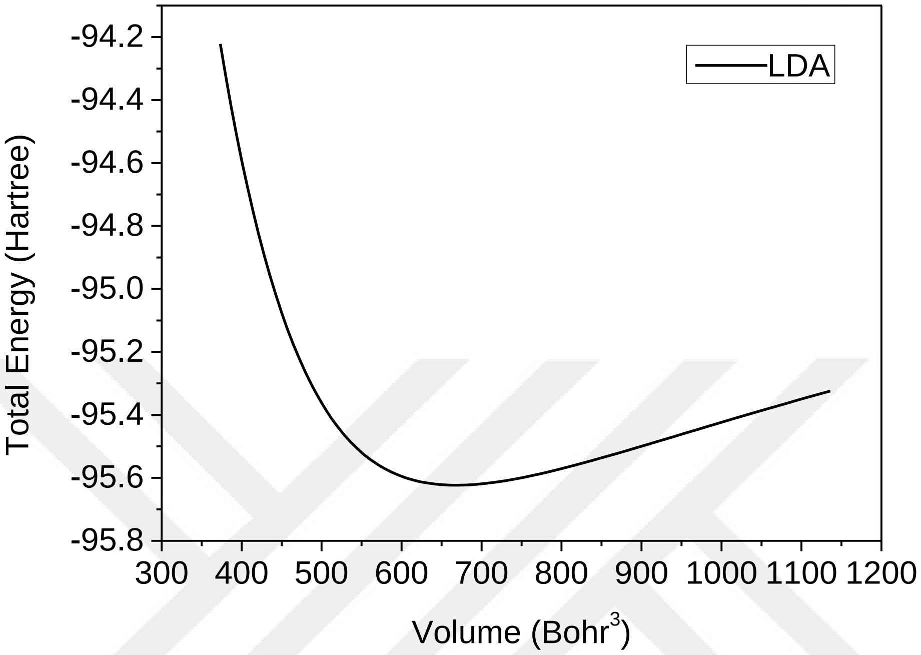

Şekil 2.6. LiPaO$_3$ kristalinin LDA yaklaşımı altında toplam enerjiye karşılık hacim grafiği.

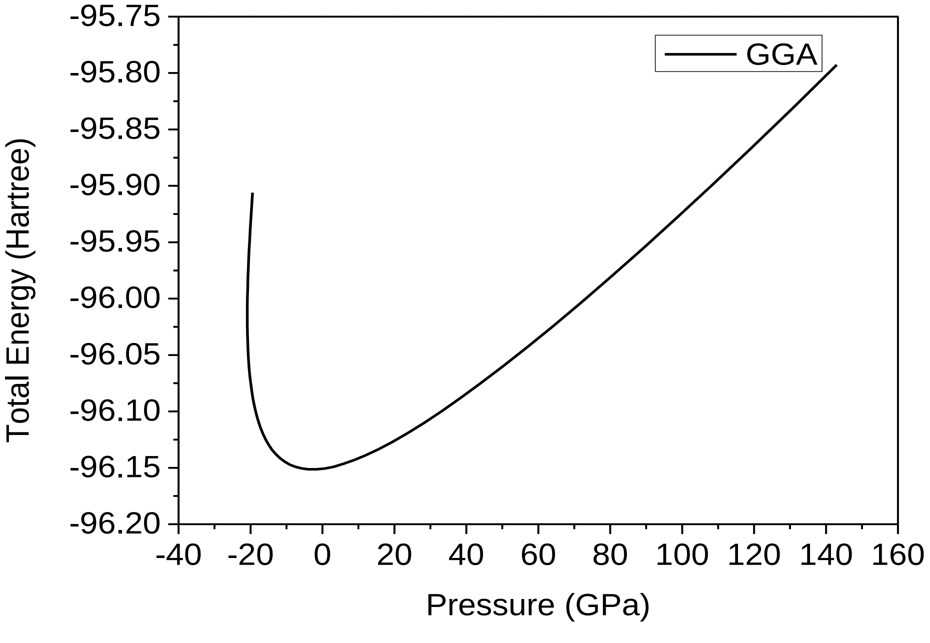

Şekil 2.7. LiPaO$_3$ kristalinin GGA yaklaşımı altında toplam enerjiye karşılık basınç grafiği.

YÖK watermark

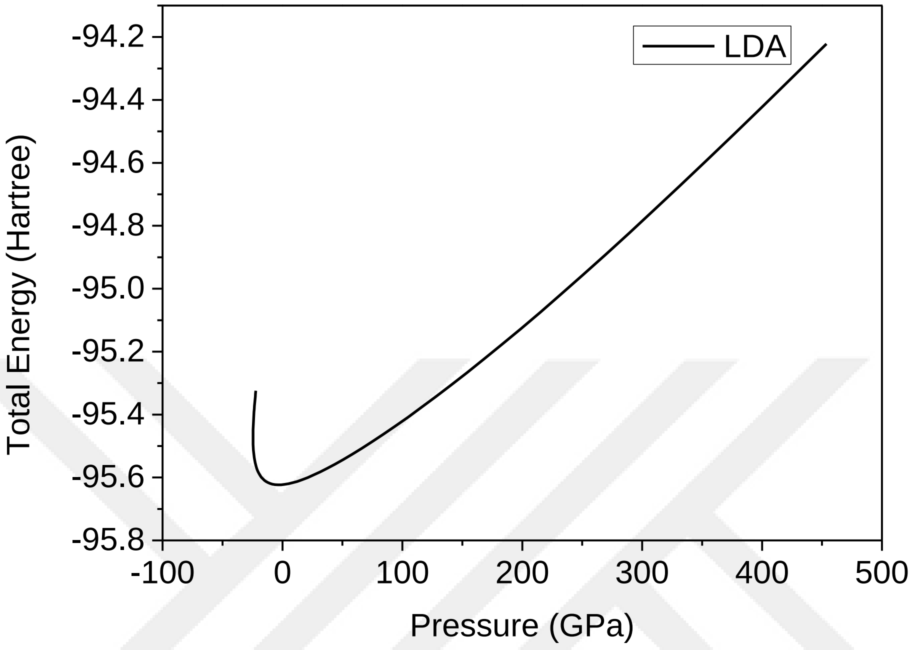

Şekil 2.8. $LiPaO_3$ kristalinin LDA yaklaşımı altında toplam enerjiye karşılık basınç grafiği.

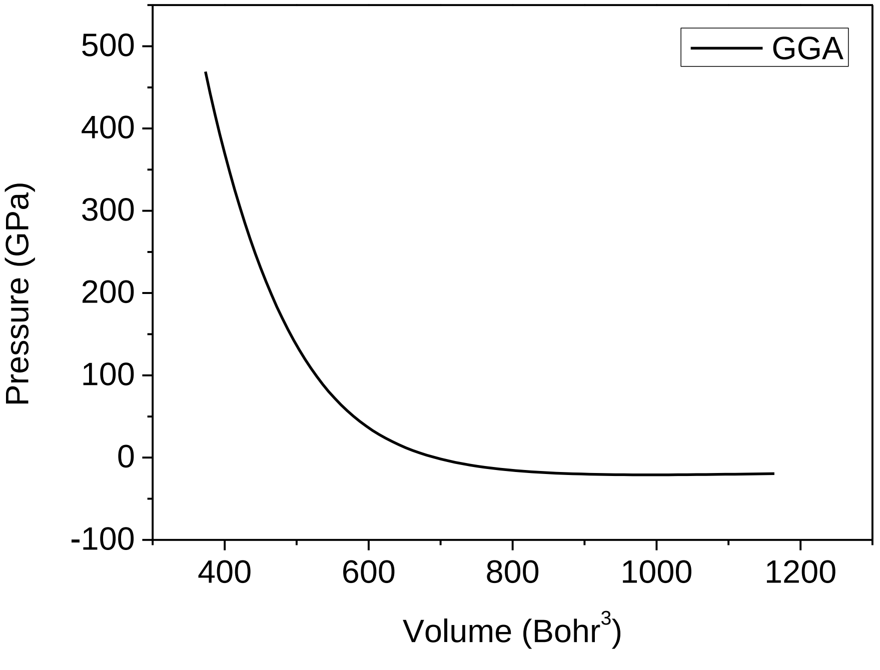

Şekil 2.9. $LiPaO_3$ kristalinin GGA yaklaşımı altında basınca karşılık hacim grafiği.

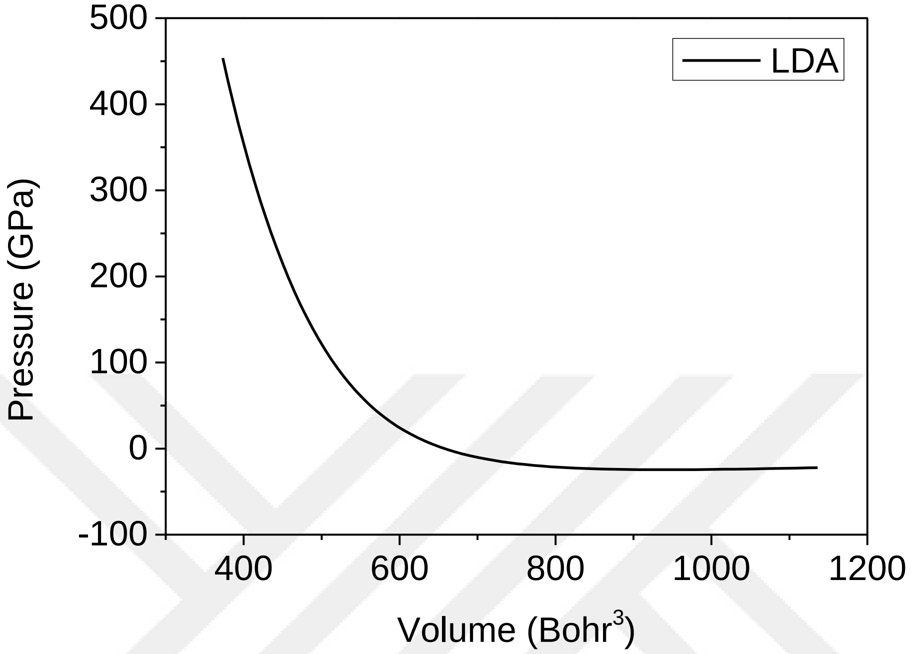

Şekil 2.10. $LiPaO_3$ kristalinin LDA yaklaşımı altında basınca karşılık hacim grafiği.

Basınca karşılık hacim grafiklerinden bu iki niceliğin ters orantılı olduğu görülmüştür.

2.2.4. $LiPaO_3$ kristalinin örgü parametreleri

Bu çalışmada hacim optimizasyonu ile hesaplanan örgü parametresi GGA yaklaşımı altında 8.9052 Bohr ve LDA yaklaşımı altında ise 8.7440 Bohr bulunmuştur. Literatürdeki örgü parametresi değeri ise 8.8003 Bohr'dur.

Aşağıda toplam enerjiye karşılık örgü parametreleri grafikleri hem GGA hem de LDA yaklaşımları altında verilmiştir.

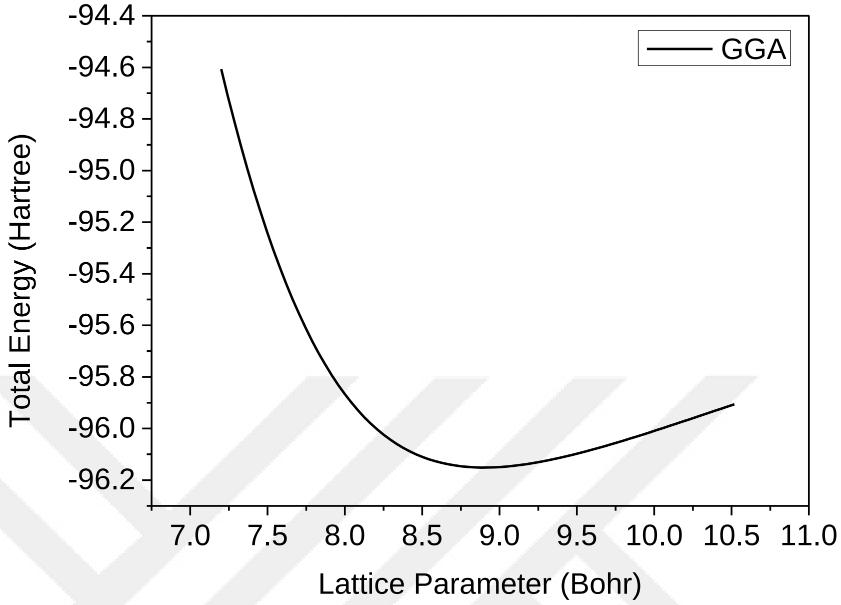

Şekil 2.11. $LiPaO_3$ kristalinin GGA yaklaşımı altında taplam enerjiye karşılık örgü parametresi.

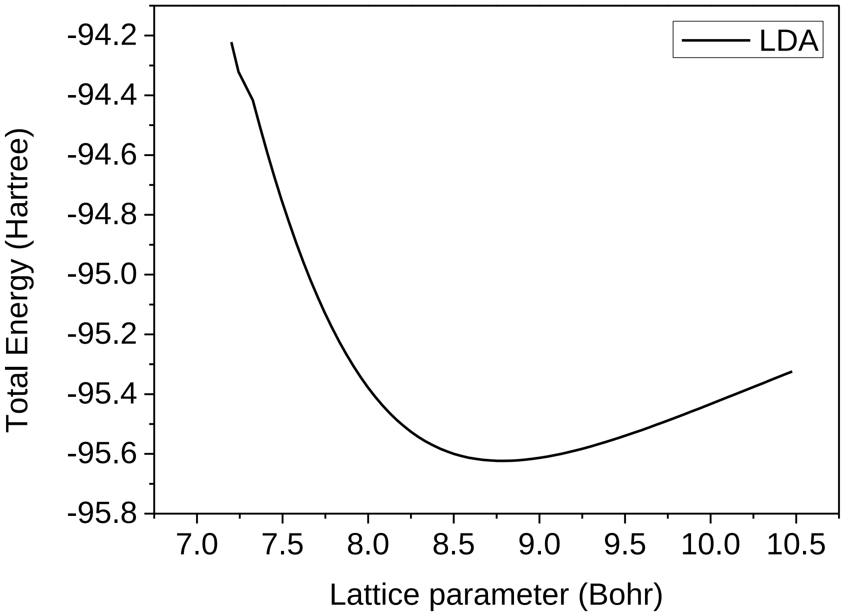

Şekil 2.12. $LiPaO_3$ kristalinin GGA yaklaşımı altında taplam enerjiye karşılık örgü parametresi.

2.3. $LiPaO_3$ Kristalinin Elektronik Özellikleri

Burada $LiPaO_3$ kristalinin elektronik özelliklerini hesapladık. Bunun için elektronik band yapısını $\Gamma - X - M - \Gamma - R - X$ yüksek simetri noktalarına göre elde ettik. Ardından durum yoğunlukları ve kısmi durum yoğunluklarını her iki yaklaşım altında elde ettik.

2.3.1. Elektronik band yapısı

$LiPaO_3$ kristalinin elektronik band yapısını GGA ve LDA yaklaşımları altında hesaplayıp grafiklerini çizdirdik. Bu grafiklerden yasak band aralığı GGA için 2.10 eV LDA için ise 2.19 eV olarak bulundu. $LiPaO_3$ kristalinin doğrudan geçişe sahip bir yarıiletken olduğu görülmüştür.

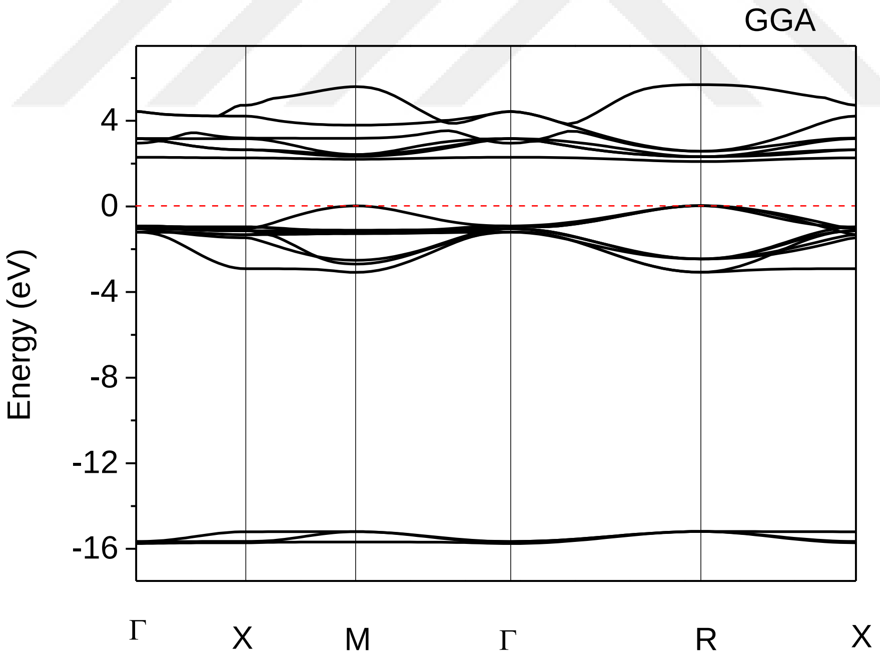

Şekil 2.13. $LiPaO_3$ kristalinin GGA yaklaşımı altındaki elektronik band yapısı grafiği.

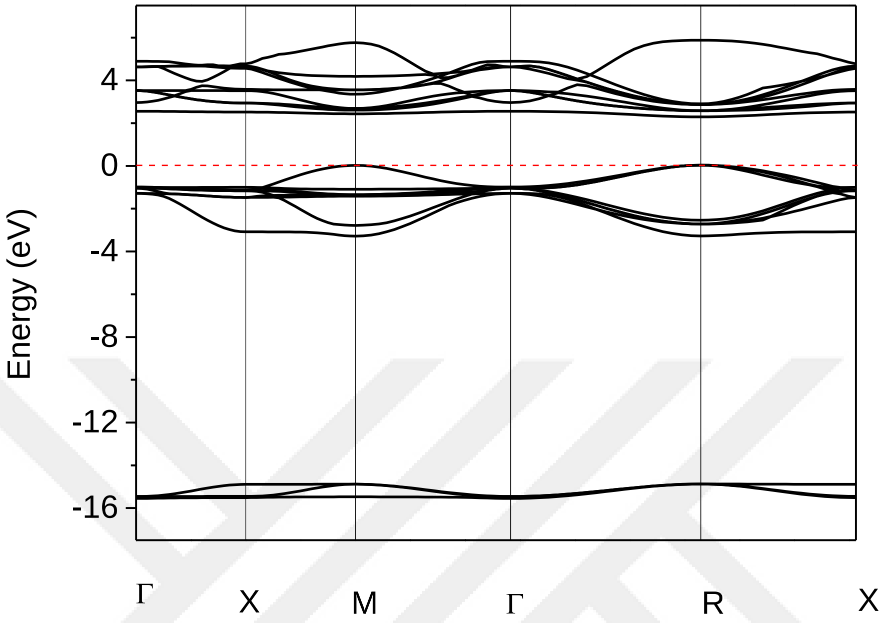

Şekil 2.14. $LiPaO_3$ kristalinin LDA yaklaşımı altındaki elektronik band yapısı grafiği.

Band grafiklerindeki enerji aralığı oldukça fazla olduğundan ve kor elektronlara ait band değerlerinin oldukça düşük enerji değerine sahip olmalarından dolayı iletim ve değerlik bandları bu grafiklerde yeterince net görülemediği için, aşağıdaki grafiklerde elektronik band grafikleri her iki yaklaşım için -4 ile 6 eV değer aralığında gösterilmektedir.

[watermark]

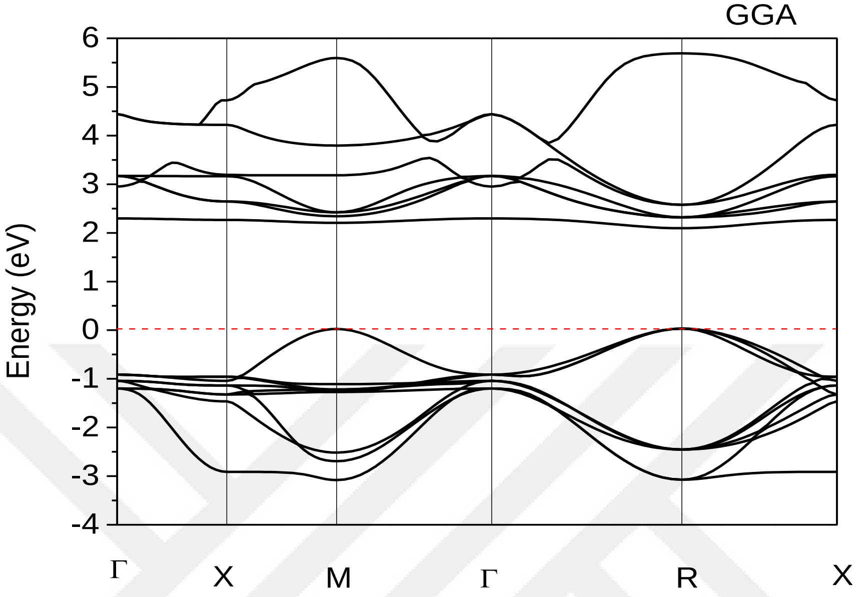

Şekil 2.15. LiPaO$_3$ kristalinin GGA yaklaşımı altındaki elektronik band yapısının -4 ile 6 eV aralığındaki grafiği.

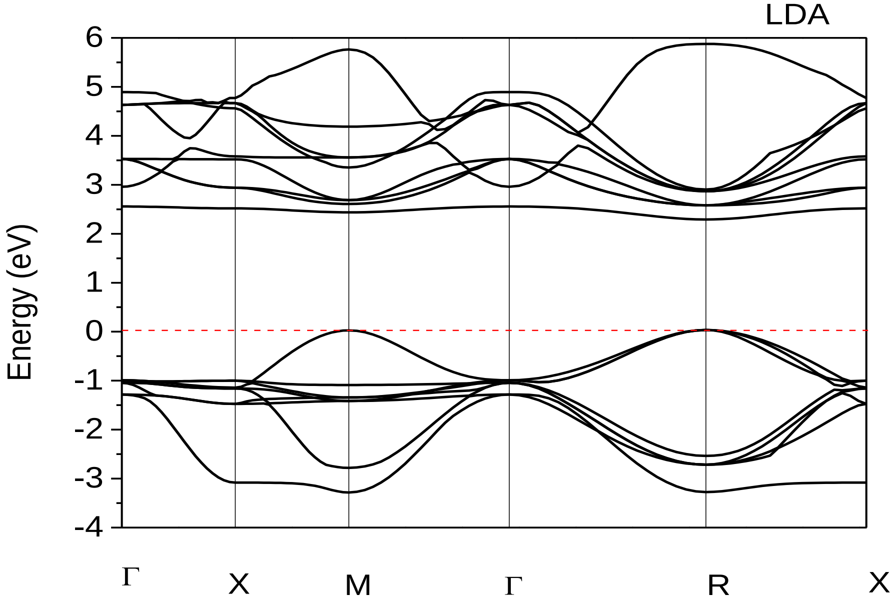

Şekil 2.16. LiPaO$_3$ kristalinin LDA yaklaşımı altındaki elektronik band yapısının -4 ile 6 eV aralığındaki grafiği.

2.3.2. Durum yoğunlukları (DOS)

Ardından $LiPaO_3$ kristaline ait durum yoğunlukları her iki yaklaşım için hesaplanmış ve aşağıda verildiği gibi çizdirilmiştir. Bu grafiklerin elektronik band yapısı grafikleri ile uyum içinde oldukları görülmektedir.

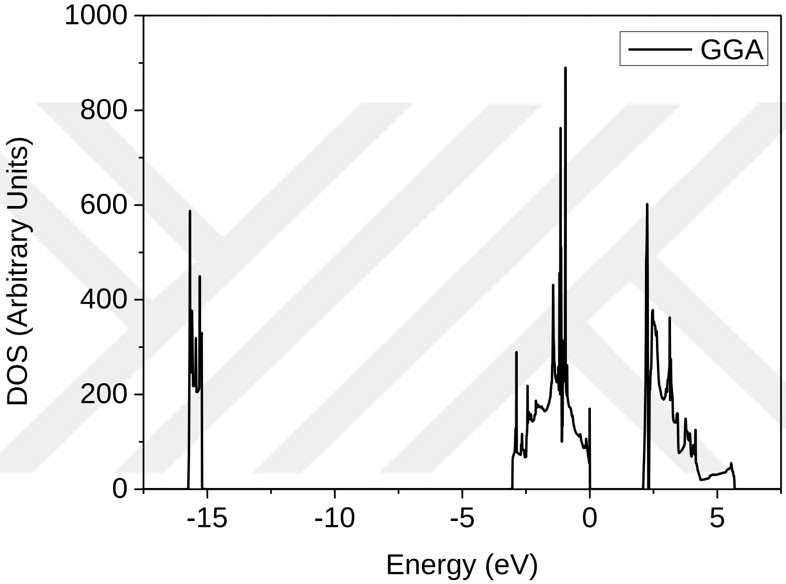

Şekil 2.17. $LiPaO_3$ kristalinin GGA yakalşımı altındaki durum yoğunluğu grafiği.

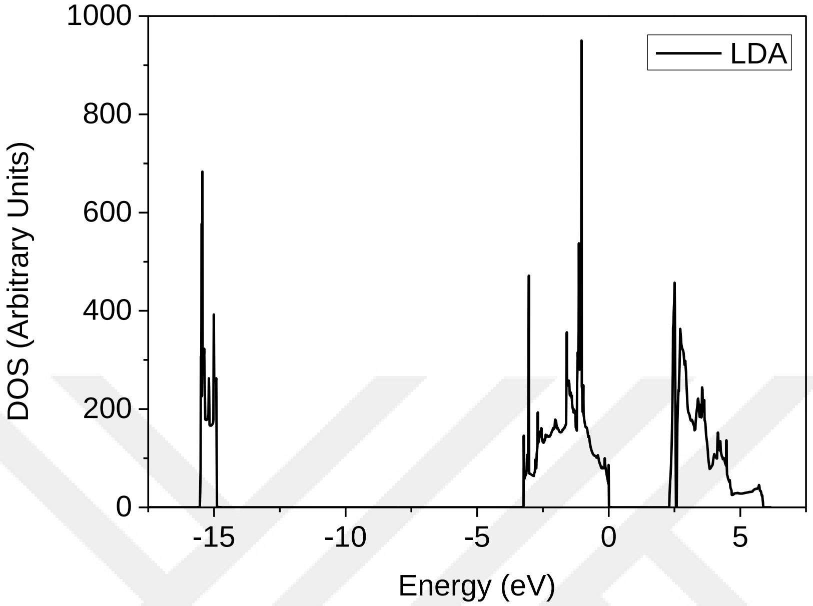

Şekil 2.18. $LiPaO_3$ kristalinin LDA yakalşımı altındaki durum yoğunluğu grafiği.

2.3.3. Kısmi durum yoğunlukları (PDOS)

$LiPaO_3$ kristalini meydana getiren farklı atom gruplarının durum yoğunluğuna katkısına kısmi durum yoğunlukları denir. Burada Li, Pa, O(1), O(2) ve O(3) atomlarının ayrı ayrı kısmi, durum yoğunlukları her iki yaklaşım içinde hesaplanmıştır.

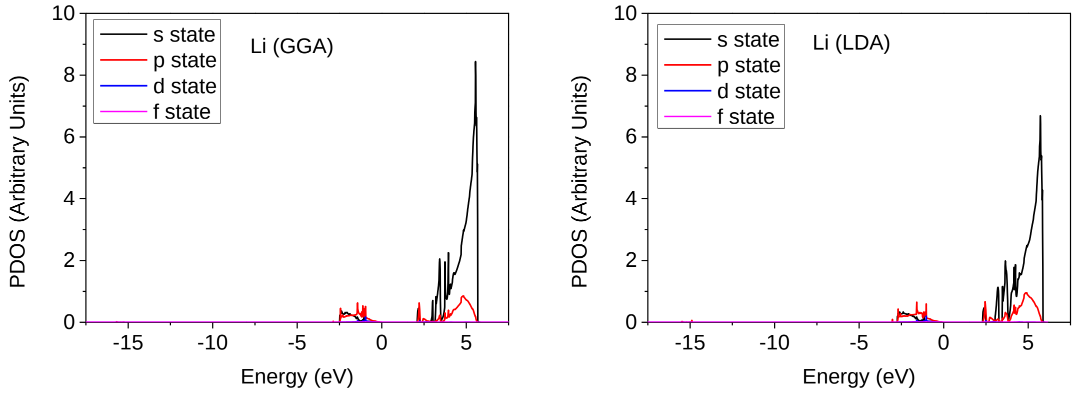

(a) (b)

Şekil 2.19. Li atomunun (a) GGA ve (b) LDA altındaki kısmi durum yoğunlukları.

Li atomunun katkısı ağırlıklı olarak iletim bandından s durumu ile gelmektedir.

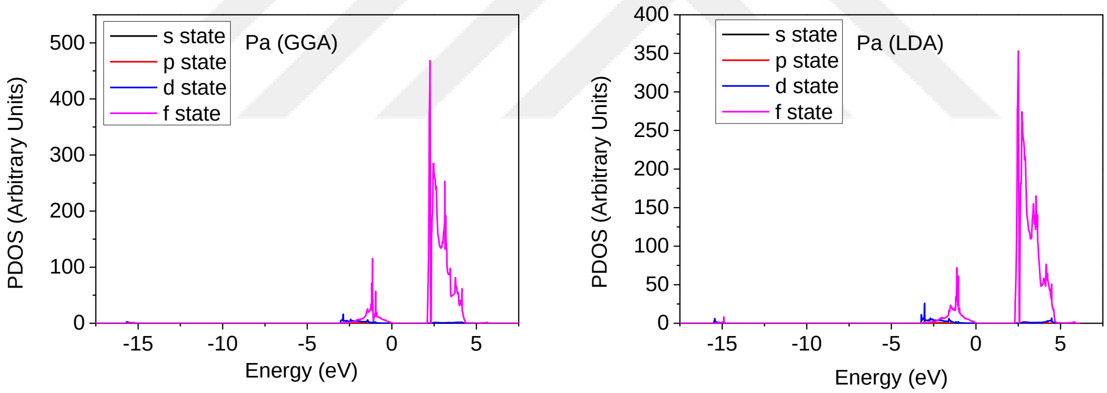

(a) (b)

Şekil 2.20. Pa atomunun (a) GGA ve (b) LDA altındaki kısmi durum yoğunlukları.

Pa atomunun katkısı ise ağırlıklı olarak iletim bandından olmasının yanında değerlik bandına da az da olsa katkısı bulunmaktadır. Tüm bu katkılar f durumu tarafından gelmektedir.

O(1) O(2) ve O(3) atomlarından gelen katkılar hemen hemen benzerdir. Kor elektronlardan gelen katkı s durumundan, iletim bandından gelen katkı ise p durumundan oluşmaktadır.

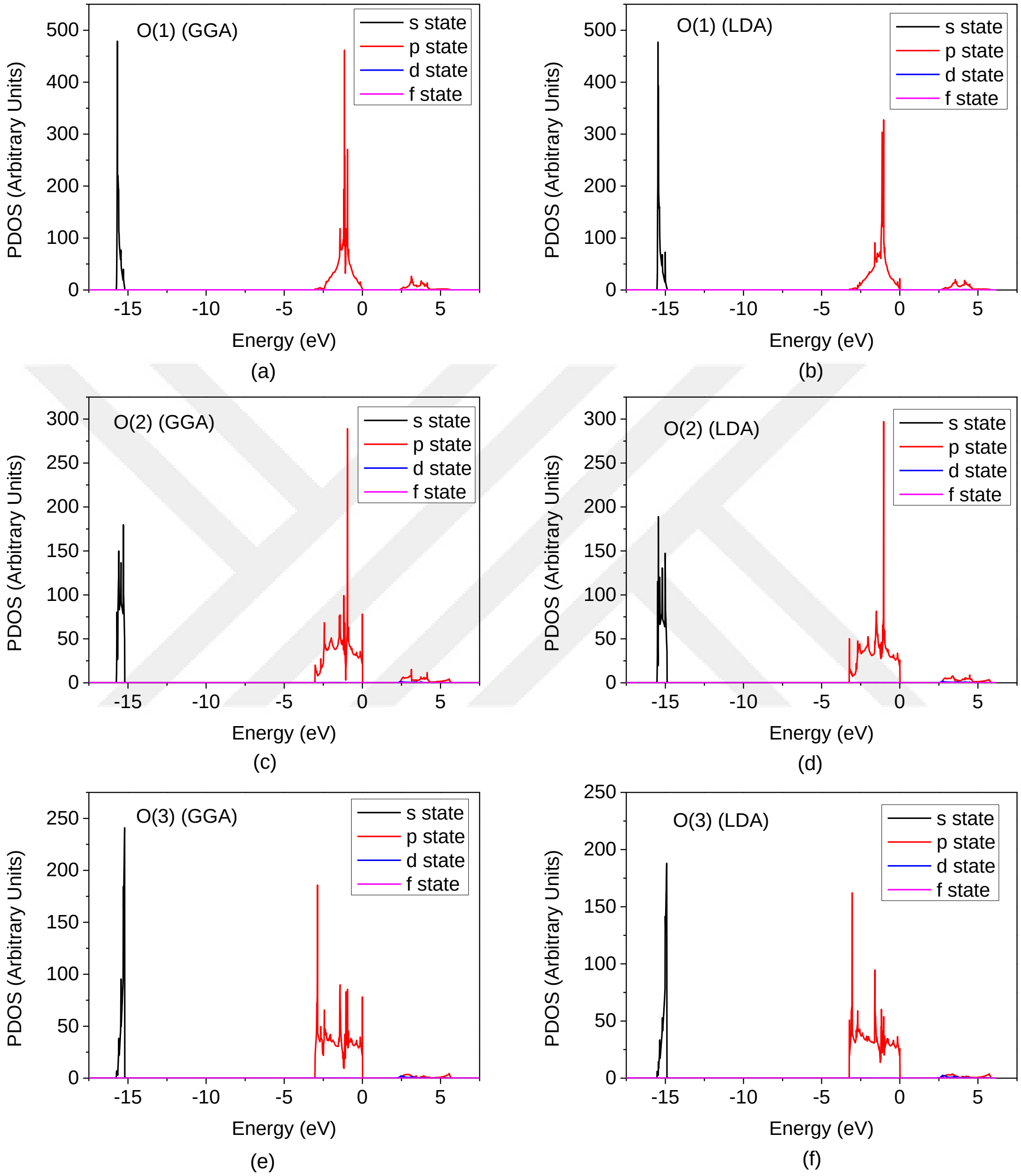

Şekil 2.21. O(1), O(2) ve O(3) atomlarının GGA ve LDA altındaki kısmi durum yoğunlukları.

2.4. LiPaO$_3$ Kristalinin Optik Özellikleri

Çalışmanın bu aşamasında ilk olarak kompleks dielektrik fonksiyonu, bu fonksiyonun reel ve sanal bileşenleri GGA ve LDA yaklaşımları altında hesaplanmıştır.

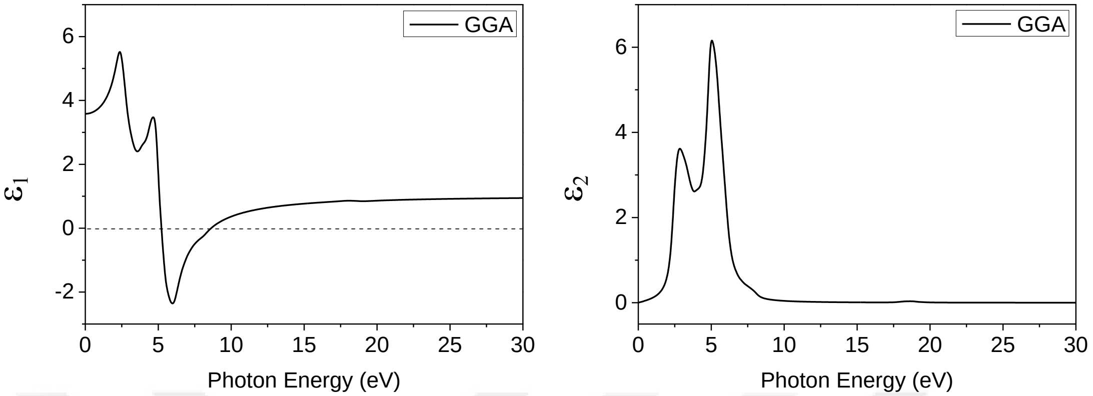

(a)

(b)

Şekil 2.22. LiPaO$_3$ kristalinin kompleks dielektrik fonksiyonunun GGA yaklaşımdaki (a) reel ve (b) sanal bileşenleri.

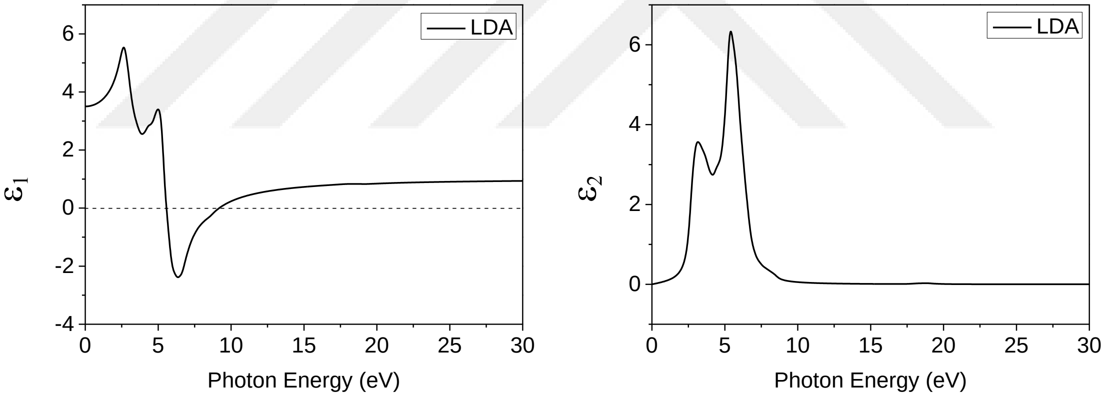

(a)

(b)

Şekil 2.23. LiPaO$_3$ kristalinin kompleks dielektrik fonksiyonunun LDA yaklaşımdaki (a) reel ve (b) sanal bileşenleri.

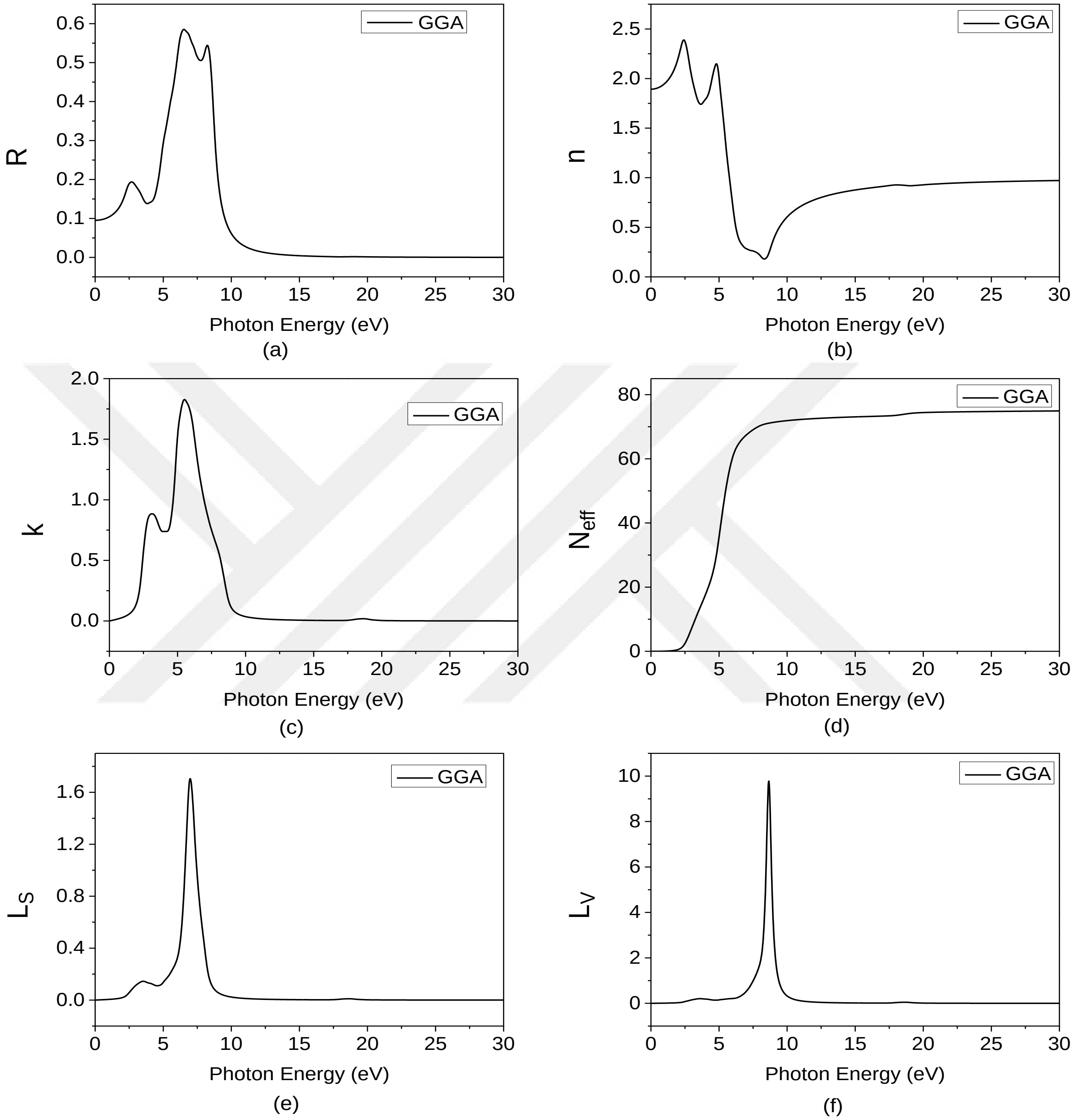

Şekil 2.24. $LiPaO_3$ kristalinin GGA yaklaşımı altındaki (a) Yansıtma, (b) Kırılma indisi, (c) Sönüm katsayısı, (d) Birim hücre başına etkin değerlik elektron sayısı, (e) Yüzey için enerji kayıp fonksiyonu ve (f) Hacim için enerji kayıp fonksiyonu.

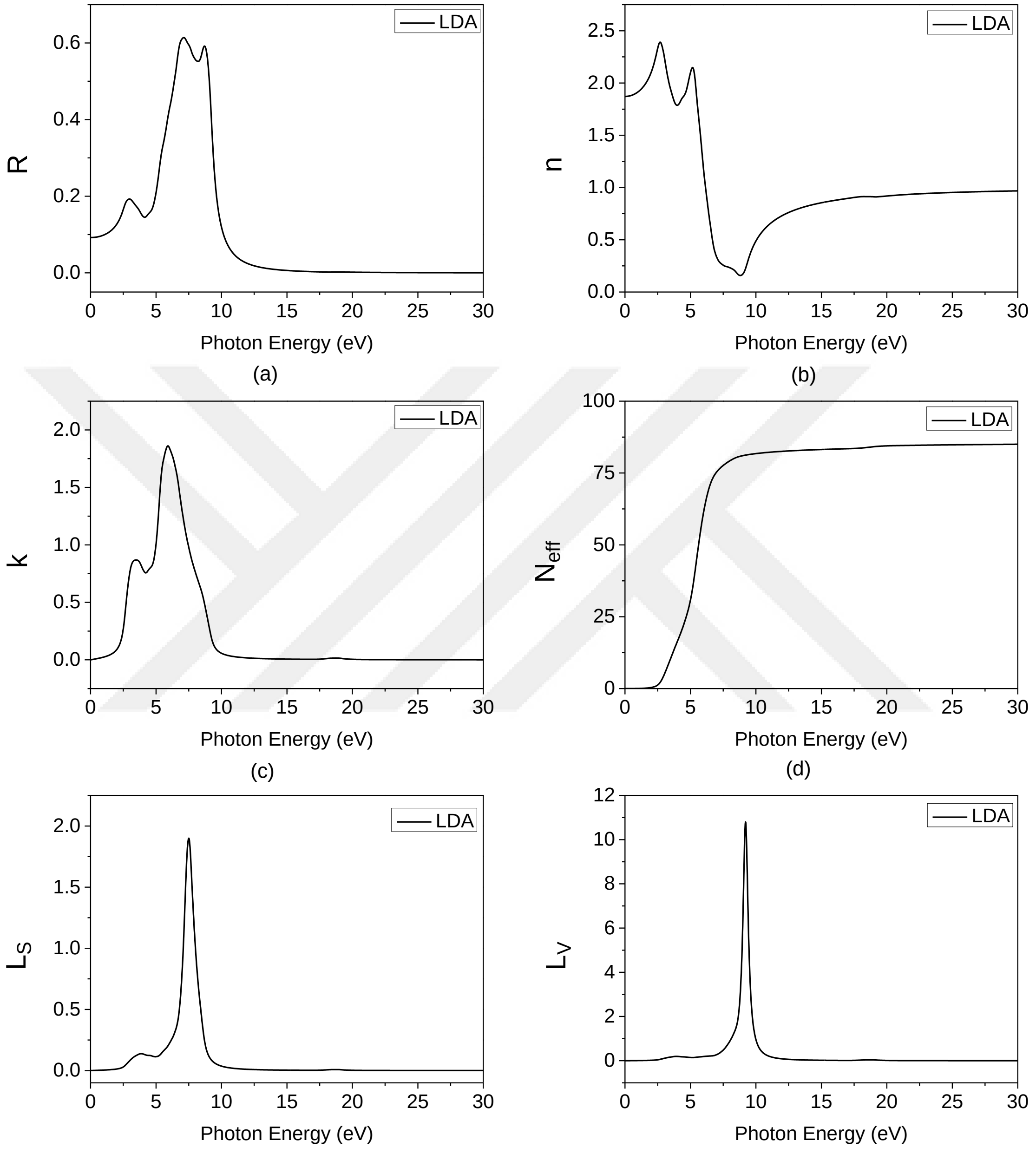

(a) (b) (c) (d) (e) (f)

Şekil 2.25. LiPaO_3 kristalinin LDA yaklaşımı altındaki (a) Yansıtma, (b) Kırılma indisi, (c) Sönüm katsayısı, (d) Birim hücre başına etkin değerlik elektron sayısı, (e) Yüzey için enerji kayıp fonksiyonu ve (f) Hacim için enerji kayıp fonksiyonu.

2.5. $LiPaO_3$ Kristalinin Elastik Özellikleri

Burada ilk olarak $LiPaO_3$ kristalinin elastik sertlik katsayılarını hesapladık. Elastik sertlik katsayıları aslında rankı 4 olan tensörlerdir (C_{ijkl}) ama matris notasyonu (Nye, 1985) kullanarak bu değerleri iki indise indirgeyebiliriz (C_{mn}). Ancak C_{mn} değerleri bu halleriyle rankı iki olan tensör değildirler. Sadece ilk durumda 81 tane bileşenden 36 bileşene indirgenmişlerdir. Bu 36 bileşenden 21 tanesi bağımsız bileşendir. Bazı kristal sınıflarında bu sayı simetri özelliklerine bağlı olarak daha da düşer. Kübik yapıda bu sayı sadece üçtür ve bunlar C_{11} $(= C_{22} = C_{33})$, C_{12} $(= C_{13} = C_{21} = C_{23} = C_{31} = C_{32})$ ve C_{44} $(= C_{55} = C_{66})$ dir (Çizelge 2.1).

Çizelge 2.1. $LiPaO_3$ kristalinin GGA ve LDA yaklaşımları altında elastik sertlik katsayıları.

Elastik Sertlik Katsayıları	GGA (GPa)	LDA (GPa)
C_{11}	380.72	469.50
C_{12}	27.83	33.81
C_{44}	20.87	20.59

Çizelge 2.2. $LiPaO_3$ kristalinin GGA ve LDa yaklaşımları altındaki bazı elastic özellikleri.

Elastik Özellikler	Sembol (Birim)	GGA	LDA
Voigt Bulk Modülü	B_V (GPa)	145.43	179.013
Reuss Bulk Modülü	B_R (GPa)	145.43	179.016
Hill Bulk Modülü	B_H (GPa)	145.43	179.015
Voight Shear Modülü	G_V (GPa)	83.10	99.491
Reuss Shear Mdülü	G_R (GPa)	32.31	32.338
Hill Shear Modülü	G_H (GPa)	57.71	65.915
Young Modülü	E (GPa)	152.89	176.127
Poisson Oranı	ν (-)	0.33	0.336
Esneklik Sabiti	$K=B_{VRH}/G_{VRH}$ (-)	2.52	2.716
Debye Sıcaklığı	θ_D	132.93	142.282
Zener Anizotropi Faktörü	A (-)	0.12	0.09

Elastik sertlik katsayılarını kullanarak, Bulk, Shear ve Young modülleri ile Poisson oranı, esneklik katsayısı, Debye sıcaklığı ve Zener anizotropi faktörü GGA ve LDA yaklaşımları altında hesaplanmıştır. Elde edilen sonuçlar ışığında $LiPaO_3$ kristalinin mekanik olarak kararlı olduğu ve esnek bir yapıya sahip olduğu anlaşılmıştır.

3. SONUÇ

Bu çalışmada, $LiPaO_3$ kristalinin fiziksel özelliklerini Genelleştirilmiş Gradyan ve Yerel Yoğunluk Yaklaşımları altında Yoğunluk Fonksiyonel Teorisini kullanarak araştırdık. Çalışmamız boyunca ABINIT bilgisayar programını kullandık. Ayrıca birim hücre çizimi, bağ ve bağ uzunluğu hesaplamaları için Vesta bilgisayar programı kullanılmıştır.

Öncelikle kesme enerjisi ve k noktası optimizasyonlarını gerçekleştirdik. Bu değerlere karar verdikten sonra hacim optimizasyonu yaptık. Hacim optimizasyonu bize toplam enerji-hacim, toplam enerji-basınç ve basınç-hacim değişiklikleri arasındaki ilişkileri verdi. Ayrıca örgü parametresini her iki yaklaşımda da hesapladık. Hesaplanan örgü parametre değerlerimiz literatürden elde ettiğimiz değere çok yakındır.

$LiPaO_3$ kristalinin yapısal özelliklerini anlamak için toplam enerji - hacim, toplam enerji - basınç, toplam enerji - örgü parametresi ve hacim - basınç grafiklerini çizdik. Ayrıca, bu kristalin perovskit yapısının açıkça görülebildiği $LiPaO_3$ kristalinin birim hücre yapısını da çizdik. $LiPaO_3$ kristalinin yapısal özellikleri araştırılırken, bağlar ve bağ uzunlukları da Vesta programı ile hesaplanmıştır.

Elektronik özelliklerinin araştırılmasında, GGA ve LDA yaklaşımları altında $LiPaO_3$ kristalinin elektronik bant yapısı, durum yoğunluğu ve kısmi durum yoğunlukları hesaplanmış ve çizilmiştir. Bu hesaplamalardan, bu malzemenin doğrudan geçişli bir yarı iletken olduğu görülmüştür. Durum yoğunluğu grafikleri, elektronik bant yapısı grafikleriyle uyumludur. Kısmi durum yoğunlukları grafiklerinin toplamı, $LiPaO_3$ kristalinin durumlarının yoğunluğunu vermektedir.

Daha sonra $LiPaO_3$ kristalinin optik özelliklerini araştırdık. Kompleks dielektrik fonksiyonu ve yansıma, kırılma indisi, sönüm katsayısı, birim hücre başına etkin değerlik elektron sayısı, yüzey için enerji kaybı fonksiyonu ve hacim için enerji kaybı fonksiyonu gibi bazı optik özellikleri GGA ve LDA yaklaşımları altında hesapladık. Hesaplanan optik özellikler birbiriyle uyumlu sonuçlar vermiştir.

Son olarak $LiPaO_3$'ün elastik özelliklerine odaklandık. Elastik sertlik sabitlerini hesapladık. Bu sabitlerin yardımıyla Bulk, Shear, Young modülü ve diğer bazı elastik sabitleri elde ettik. Bu kristalin mekanik olarak kararlı olduğunu ve elastik bir malzeme olduğunu fark ettik.

Araştırmamıza göre bu çalışmada incelediğimiz konular hakkında LiPaO$_3$ hakkında daha önce yapılmış bir çalışma bulunmamaktadır. Bu nedenle sonuçlarımızı örgü parametreleri dışında literatürle karşılaştıramadık. Ancak tez çalışmamızda yaptığımız tüm hesaplamalarda sonuçlarımızın birbiriyle uyumlu olduğunu görmekteyiz. Bu nedenle çalışmamızın LiPaO$_3$ kristali ile ilgili yeni çalışmalara ışık tutacağına inanıyoruz.

CURRICULUM VITAE

She completed her Secondary and High School in Halabja Province, to complete her Bachelor degree moved to Koya city to continue her study to achieve Bachelor degree in the field of physics at Koya University, Faculty Science & Health, Department of Physics, then she got Bachelor degree in 2016. Now she is a master student at Van Yuzuncu Yil University, Institute of Natural and Applied Science, Physics Depatment.

About the language skills, she knows Kurdish (Mother Tongue), English, Turkish and Arabic. Finally, about her program qualifications, she knows Microsot office (Word, Excel and Power Point), Origion 8.5, Grapher 9, Matlab, Abinit, Vesta, Mathcad and Photoshop.

VAN YUZUNCU YIL UNIVERSITY
THE INSTITUTE OF NATURAL AND APPLIED SCIENCES
THESIS ORIGINALITY REPORT

Date:27/06/2022

Thesis Title: **SOME PHYSICAL PROPERTIES OF $LiPaO_3$ COMPOUND: AN AB INITIO STUDY**

The title of the mentioned thesis, above having total 115 pages with cover page, introduction, main parts and conclusion, has been checked for originality by Turnitin computer program on the date of 27/06/2022 and its detected similar rate was 13 % according to the following specified filtering

Originality report rules:

- Excluding the Materials and Methods
- Excluding the Bibliography,
- Excluding the publications obtained from the thesis,
- Excluding the text parts less than 7 words (Limit match size to 7 words)

I read the Thesis Originality Report Guidelines of Van Yuzuncu Yil University for Obtaining and Using Similarity Rate for the thesis, and I declare the accuracy of the information I have given above and my thesis does not contain any plagiarism; otherwise I accept legal responsibility for any dispute arising in situations which are likely to be detected.

Sincerely yours,

27/06/2022

Name and Surname: Khalat Ezzulddin HUSSEIN

Student ID#: 19910001158

Deparment: Physics

Program: M. Sc. ☐ Ph.D. ☐

APPROVAL OF SUPERVISOR
SUITABLE

APPROVAL OF THE INSTITUTE
SUITABLE

Doç. Dr. Emel KİLİT DOĞAN

Prof. Dr. Harun AKKUŞ